

**Remote Frequency Conversion Using  
SOA and EAM for 60 GHz Bi-  
Directional Radio-on-Fiber Systems**

**Jun-Hyuk Seo**

**The Graduate School**

**Yonsei University**

**Department of Electrical and Electronic Engineering**

# **Remote Frequency Conversion Using SOA and EAM for 60 GHz Bi- Directional Radio-on-Fiber Systems**

A Dissertation

Submitted to the Department of Electrical and Electronic Engineering  
and the Graduate School of Yonsei University in partial fulfillment of  
the requirements for the degree of Doctor of Philosophy

**Jun-Hyuk Seo**

**June 2006**

This certifies that the dissertation of **Jun-Hyuk Seo** is approved.

---

Thesis Supervisor: **Woo-Young Choi**

---

**Sang-Kook Han**

---

**Ilgu Yun**

---

**Young Min Jhon**

---

**Dong-Soo Shin**

**The Graduate School**

**Yonsei University**

**June 2006**

# Tables of Contents

<i>Tables of Contents</i> .....	<i>i</i>
<i>List of Figures and Tables</i> .....	<i>iii</i>
<i>Abstract</i> .....	<i>ix</i>
<b>1. Introduction</b> .....	<b>1</b>
1-1. Why 60 GHz?.....	1
1-2. Radio-on-Fiber Systems for 60 GHz systems .....	5
1-3. Bi-Directional RoF Link.....	11
1-4. Outline .....	14
<b>2. Remote Frequency Up-Conversion Using SOA-PD Configuration</b> .....	<b>16</b>
<b>2-1. Operation Principle of Frequency Up-Conversion</b> .....	<b>16</b>
2-1-1. Optical LO and IF signal generation .....	18
2-1-2. Cross-gain modulation (XGM) of SOA.....	22
2-1-3. Frequency up-conversion at a PD .....	26
2-1-4. Frequency up-conversion experiment .....	29
<b>2-2. Simulation of Frequency Up-Conversion Using a Transfer Matrix Method</b> .....	<b>32</b>
2-2-1. SOA Modeling using TMM.....	33
2-2-2. Simulation results of SOA gain characteristics.....	39
2-2-3. Simulation results of frequency up-conversion.....	44
<b>2-3. Gigabit Data Transmission using SOA-PD Frequency Up-Converter at 60 GHz band</b> .....	<b>48</b>
2-3-1. Measurement of SOA XGM frequency response .....	49
2-3-2. Data transmission experiments and results .....	52
<b>3. Remote Frequency Down-Conversion Using EAM</b> .....	<b>61</b>
<b>3-1. Uplink RoF Systems for Bi-Directional Data Transmission</b> .....	<b>61</b>

<b>3-2. Operation Principle of EAM Frequency Down-Conversion</b>	<b>65</b>
3-2-1. Characteristics of EAM	65
3-2-2. Optoelectronic frequency down-conversion in EAM	70
<b>3-3. Conversion Efficiency of EAM Frequency Down-Conversion</b>	<b>74</b>
3-3-1. Experimental setup and conversion efficiency definition	74
3-3-2. Down-conversion efficiency results	79
<b>3-4. 60 GHz Uplink RoF Systems using Frequency Down-Conversion</b>	<b>83</b>
3-4-1. Experimental setup and results for 60-GHz data transmission	83
<b>4. Remote Frequency Up/Down-Conversion using Cascade SOA-EAM Configuration</b>	<b>91</b>
4-1. Bi-directional RoF systems	91
4-2. Operation Principles of Frequency Converters	93
4-2-1. Frequency up-conversion for downlink transmission	93
4-2-2. Frequency down-conversion for uplink transmission	98
4-3. Conversion Efficiency Characteristics of SOA-EAM Frequency Converters	103
4-3-1. Conversion efficiency definition	103
4-3-2. Measurement results of conversion efficiency	106
4-4. 60 GHz Bi-Directional RoF Systems using SOA-EAM Configuration	112
4-4-1. Experimental setup and data transmission results	112
<b>5. Summary</b>	<b>124</b>
<b>References</b>	<b>128</b>
<b>Publication Lists</b>	<b>137</b>

## List of Figures and Tables

Figure 1-1. Status of license-free 60 GHz-bands in several countries. ...	2
Figure 1-2. Directivity comparison among ISM band carrier signals. ...	3
Figure 1-3. Wireless applications using 60 GHz signals. ....	4
Figure 1-4. Simple bi-directional RoF system configuration. ....	5
Figure 1-5. Schematic of dispersion-induced signal fading problems in intensity modulated millimeter-wave signal transmission. ....	7
Figure 1-6. Dispersion compensators for optical millimeter-wave signal transmission without signal penalty. ....	8
Figure 1-7. Simple bi-directional RoF link based on remote frequency conversion technique. ....	10
Figure 1-8. RoF downlink system configuration based on optoelectronic frequency up-conversion using HPT. ....	10
Figure 1-9. Bi-directional millimeter-wave RoF link using EAM. ....	12
Figure 1-10. Bi-directional RoF systems using remote frequency conversion based on a cascaded SOA-EAM configuration proposed in this dissertation. ....	13
Figure 2-1. Base station of downlink RoF systems based on remote frequency up-conversion and photonic frequency up-converter. ....	17
Figure 2-2. Schematic of photonic frequency up-conversion based on SOA-PD configuration. ....	17
Figure 2-3. Optical LO generation using DSB-SC method, and optical IF generation using direct laser diode modulation. ....	21
Figure 2-4. Stimulated processes in a two level system. ....	23
Figure 2-5. Process of optical IF signal modulation in optical LO signals by SOA XGM. Below is a simple operation principle of XGM. ....	25
Figure 2-6. Frequency up-conversion by the signal beating process in PD. ....	27

Figure 2-7. Experimental setup to verify optical frequency up-conversion at 25 GHz band. LD : Laser Diode, EDFA : Erbium-Doped Fiber Amplifier, RF-SA : RF-Spectrum Analyzer, PC : Polarization Controller.....	29
Figure 2-8. RF Spectrum measured before SOA (a), and after SOA (b). .....	31
Figure 2-9. Schematic of SOA model based on time-dependent TMM. .....	33
Figure 2-10. (a) Field model in unit SOA, (b) Field propagation and reflection model in different refractive index layers.....	35
Figure 2-11. Optical gain of SOA as a function of output optical power with different SOA injection currents.....	42
Figure 2-12. Optical gain of SOA as a function of SOA injection current. .....	42
Figure 2-13. Material gain of SOA (a) and optical gain of SOA (b) as a function of input signal wavelength with different SOA injection currents.....	43
Figure 2-14. Schematic of frequency up-conversion efficiency.....	44
Figure 2-15. Frequency up-conversion efficiency as a function of SOA input optical LO powers.....	47
Figure 2-16. Frequency up-conversion efficiency and SOA gain as a function of input optical IF wavelengths. ....	47
Figure 2-17. Measurement setup for SOA XGM frequency response. OBPF: Optical Band Pass Filter, TLS: Tunable Laser Source.....	51
Figure 2-18. Frequency response for SOA XGM for a -12 dBm SOA input pump signal power.....	51
Figure 2-19. Experimental setup for 1.244 Gbit/s 63 GHz RoF downlink data transmission. LPF: LowPass Filter.....	54
Figure 2-20. Optical spectrum of downlink optical LO and data signals before SOA (a) and after SOA (b). ....	55

Figure 2-21. RF spectrum of frequency up-converted 63 GHz data signals (a) and demodulated baseband signals (b). Resolution bandwidth for both spectra is 1 MHz. ....	56
Figure 2-22. Dependence of BERs performance on SOA input optical baseband signal power.....	58
Figure 2-23. Dependence of BER performance on SOA input LO signal power.....	59
Figure 3-1. Uplink RoF system configurations. (a) direct RF transmission systems, (b) IF/Baseband Feeder systems.....	62
Figure 3-2. Uplink millimeter-wave RoF systems based on EAM.....	63
Figure 3-3. Remote frequency down-conversion RoF uplink systems using EAM. ....	64
Figure 3-4. Operation principle schematic of multiple quantum-well EAM.....	66
Figure 3-5. Experimental setup to measure optical transmission and absorption characteristics of EAM. ....	67
Figure 3-6. Optical transmission (a) and photodetection characteristics (b) of EAM as a function of applied voltage at different input wavelength conditions. ....	69
Figure 3-7. Schematic of optoelectronic frequency down-conversion for uplink RoF systems.....	72
Figure 3-8. RF spectrum of frequency down-converted signals (a) and RF and LO signals after photodetection of optical IF signals.....	73
Figure 3-9. Experimental setup to measure frequency down-conversion efficiency. EOM : Electrooptic Modulator.....	76
Figure 3-10. Optical spectrum measured before EAM (a) and after optical filtering of optical LO signals (b). ....	77
Figure 3-11. RF spectrum of uplink IF signals (a) and RF signals (b) after photodetection of optical IF signals. ....	78
Figure 3-12. Frequency down-conversion efficiency as a function of EAM bias condition. ....	81

Figure 3-13. Frequency down-conversion efficiency as a function of EAM input optical LO power. ....	81
Figure 3-14. Frequency down-conversion efficiency as a function of EAM input optical IF power (a) and wavelength (b).....	82
Figure 3-15. $S_{11}$ parameter characteristics at the input port of 60 GHz narrow-band packaged EAM.....	84
Figure 3-16. Experimental setup for 60 GHz frequency down-conversion and uplink data transmission. BPF : Bandpass Filter.	85
Figure 3-17. Frequency down-converted 500 MHz IF signal spectrum. Resolution bandwidth is 10 kHz .....	86
Figure 3-18. (a) 10 Mbps QPSK modulated signal spectrum at 60 GHz, (b) frequency down-converted QPSK modulated signal spectrum at 500 MHz. Resolution bandwidth is 100 kHz. ....	89
Figure 3-19. Eye diagram of demodulated 10 Mbps QPSK signals at 500 MHz. ....	90
Figure 4-1. Proposed bi-directional RoF system configuration adopting a photonic mixer at a base station. ....	92
Figure 4-2. Schematic for frequency up-conversion processes and experimental setup used for verification.....	94
Figure 4-3. RF spectra for downlink frequency up-conversion: (a) IF signals without SOA, (b) frequency up-converted signals. The resolution bandwidth was 300 kHz for (a) and 100 kHz for (b). A 17 dB gain electrical amplifier was used for (b). ....	96
Figure 4-4. Normalized signal amplitude of frequency up-converted signals and calculated results of double-sideband signal transmission at 60 GHz band. The measured up-converted signal power is normalized to the power at back-to-back conditions. ...	97
Figure 4-5. Schematics for frequency down-conversion processes and experimental setup used for verification.....	100
Figure 4-6. RF spectra for uplink frequency down-conversion: (a) RF signals measured at the central station, (b) frequency down-converted signals measured at the central station. The resolution	

bandwidth was 1 kHz for both. A 17 dB gain electrical amplifier was used for (a), and a 20 dB gain electrical amplifier was used for (b). .....	101
Figure 4-7. Normalized signal amplitude of frequency down-converted signals and calculated results of double-sideband signal transmission at 60 GHz band. The measured down-converted signal power is normalized to the power at back-to-back conditions.....	102
Figure 4-8. Schematic of frequency up-conversion efficiency (a) and frequency down-conversion efficiency.....	105
Figure 4-9. Dependence of frequency conversion efficiency ( $\eta_{up}$ and $\eta_{down}$ ) on EAM bias conditions. ....	108
Figure 4-10. Frequency up-conversion efficiency ( $\eta_{up}$ ) (a), and frequency down-conversion efficiency ( $\eta_{down}$ ) (b) as a function of optical LO signal power. Optical LO power was measured in front of SOA.....	110
Figure 4-11. Frequency conversion efficiencies as a function of SOA input optical IF signal power. ....	111
Figure 4-12. Frequency conversion efficiencies as a function of SOA input optical IF wavelength. ....	111
Figure 4-13. Experimental setup for 60 GHz bi-directional RoF systems. ....	114
Figure 4-14. Optical spectra of downlink signals (a) and uplink signals (b). ....	115
Figure 4-15. RF spectrum of frequency up-converted data signals....	118
Figure 4-16. Constellation and Eye diagram of demodulated downlink 5 Msymbol/s QPSK (a) and 16QAM data signals.....	119
Figure 4-17. RF spectrum of the frequency down-converted uplink signals.....	120
Figure 4-18. Constellation and Eye diagram of demodulated uplink 5 Msymbol/s QPSK (a) and 16QAM data signals.....	121

Figure 4-19. Measured EVMs as a function of SOA input optical IF signal power for downlink and uplink.....	123
Figure 4-20. Measured EVMs as a function of optical IF signal wavelength for downlink and uplink.....	123
Table 2-1. SOA simulation parameters. ....	41

## Abstract

Photonic frequency converters based on semiconductor optical amplifier (SOA) and electroabsorption modulator (EAM) for cost-effective and practical 60 GHz Radio-on-Fiber (RoF) systems are investigated, and 60 GHz RoF systems are realized through these photonic frequency converters. In RoF systems, these frequency converters are applied as a remote frequency converter to mitigate dispersion-induced signal fading problems. They also help to simplify base station architectures. Each frequency up- and down-conversion technique is proposed and analyzed separately, and then a new photonic mixer combining two schemes is introduced for bi-directional RoF link design.

The frequency up-conversion method for downlink data transmission uses cross-gain modulation of SOA and square-law characteristics of photodetector. In this scheme, both 60 GHz local oscillator (LO) signals and intermediate frequency (IF) signals are optically transmitted from a central station to base stations. The SOA large signal simulation model using transfer matrix method is applied to show the basic operation characteristics of SOA. Based on this simulation model, the frequency up-conversion processes are clarified, and frequency up-conversion efficiency is estimated as functions of SOA input optical LO powers and optical IF wavelengths at 60 GHz band. The gigahertz operation bandwidth of the frequency up-

converter is verified experimentally at different input optical powers, and ASK 1.244 Gbit/s downlink data transmission systems are successfully demonstrated at 60 GHz band for the first time. For uplink RoF data transmission, frequency down-conversion method using EAM nonlinearity is proposed. It also uses optical LO and optical IF signals delivered from the central station, and frequency down-converted signals are optically transmitted back to the central station. The internal conversion efficiency definition is suggested for this frequency down-converter to exclude other optical effects in RoF links. The conversion efficiency is measured at 30 GHz band as functions of EAM biases, EAM input optical LO and IF powers, and optical IF wavelengths. The uplink RoF link employing this frequency down-converter is also realized at 60 GHz band, and error-free 5 Msymbol/s QPSK data is transmitted. For bi-directional RoF links, two concepts of frequency conversion are integrated to one cascaded SOA and EAM configuration performing both frequency up- and down-conversion with optically provided LO and IF signals. The frequency conversion efficiency is also defined for the proposed frequency converter, and measured at 60 GHz band as functions of EAM biases, SOA input optical LO and IF powers, and optical IF wavelengths. The dispersion insensitive bi-directional signal transmission is also proved by comparing measured uplink and downlink signal power using a proposed frequency converter with calculated 60 GHz signal power transmitted in the form of optical double sideband. Finally, 60 GHz bi-

directional RoF links are demonstrated successfully. 5 Msymbol/s QPSK and 16QAM data signals are delivered in the form of optical IF signals bi-directionally, and frequency up- and down-conversion occur at the base station. The system performances are evaluated through the measured error vector magnitudes as functions of SOA input optical IF powers and wavelengths.

**KEYWORDS:** photonic mixer, optical/optoelectronic frequency converter, semiconductor optical amplifier, electroabsorption modulator, photodetector, microwave photonics, radio-on-fiber system, fiber-optic/millimeter-wave data transmission, broadband wireless system

# 1. Introduction

## 1-1. Why 60 GHz?

With the help of wireless technology development, we are using cell phones anywhere in the world, having wireless LAN services in many hot spots, and watching television programs in public places through the digital media broadcasting receivers. Moreover, the prevailing wireless systems are evolving to the so-called triple play systems providing voice, data, and video services at the same time. To realize such systems, high bandwidth efficient modulation techniques or broad bandwidth systems using high frequency carriers are inevitable. Current wireless LAN and broadcasting systems using several GHz or sub-GHz carriers are focusing on increasing bandwidth efficiency. However, the required data rate for future wireless systems should be beyond gigabits per second, so that carriers containing enough bandwidth for such gigabit data transmission are necessary. Under such demands, millimeter-wave-band systems are being actively investigated, and especially, 60 GHz systems become the most popular millimeter-wave systems [1-6].

60 GHz carriers initially have enough bandwidth for gigabit data transmission, but the more important reason for attracting interests is that many countries are opening 60 GHz band as a license-free band [1-4]. Fig. 1-1 shows present status of license-free bands at 60 GHz for several countries [4]. As shown in the figure, several gigahertz

bandwidths are opened at 60 GHz band, which means bandwidth efficiency is not an important part and how to use such wide bandwidth becomes more important issues. In addition, 60 GHz signals have other physical characteristics benefiting to wireless systems.

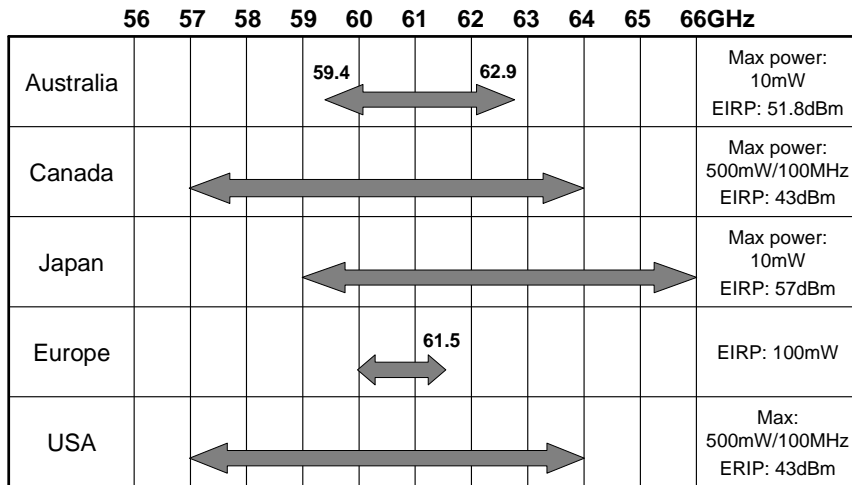


Figure 1-1. Status of license-free 60 GHz-bands in several countries.

Because the oxygen-absorption loss of 60 GHz signals is 10-15 dB/km [7], they can be used for short range communications and indoor wireless systems requiring less interference among users. Moreover, such high absorption characteristics can be applied to frequency reuse in wireless systems having lots of cells [1-3]. The high directivity of 60 GHz signals is another useful characteristic to increase wireless link gain, to decrease signal interferences, and to mitigate inter-symbol-interferences caused by multi-path fading [5]. Fig. 1-2 shows the

schematic comparison of directivity for some ISM (Industrial, Scientific, and Medical) band frequency signals, and the notably high directivity of 60 GHz signals can be observed. Short wavelength of 60 GHz signals compared with other present wireless carriers can be also useful to design small system components [1-6].



Figure 1-2. Directivity comparison among ISM band carrier signals.

The most popular application of 60 GHz is wireless personal area networks, which are currently under standard discussion at the IEEE 802.15.3c working group [4-5]. Very high data rate beyond 2 Gbit/s is allowed to this system for high-speed internet access, streaming content download, real-time streaming, and wireless data bus for cable replacement. For future broadband indoor wireless LAN systems, 60 GHz is considered as a strong candidate, and Europe is leading the system development mixing 5 GHz band wireless LAN services with 60 GHz systems supplying higher data rate [3, 5]. The European IST project BroadWay is suggesting this concept [5]. Free space Gigabit

Ethernet services (1.244 Gbit/s) using 60 GHz signals are also investigated, and applications mixed with free space fiber-optic systems are being developed [2, 5]. In Japan, 60 GHz technologies for wireless home network systems, especially, the wireless video Home-Link system including wireless 1394 applications are examined [5]. Besides these wireless applications, 60 GHz can be used for high resolution imaging and sensors, and astronomical observation using very large arrayed radio telescopes [8-9]. In the Atacama plateau, Chile, tens of arrayed radio astronomical observatories using 60 GHz are being established.

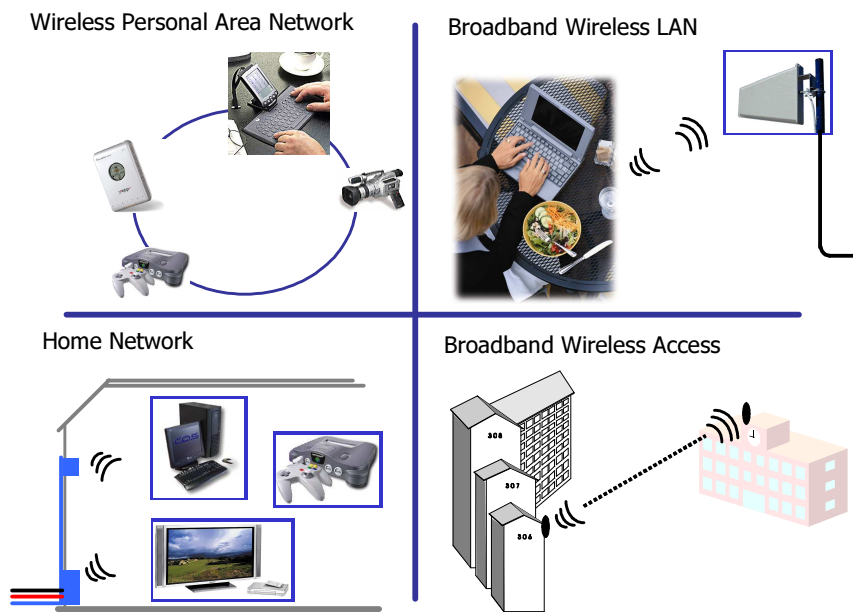


Figure 1-3. Wireless applications using 60 GHz signals.

## 1-2. Radio-on-Fiber Systems for 60 GHz systems

60 GHz is a promising candidate for future broadband wireless communication systems. However, there are some problems to realize 60 GHz systems in the near future. As stated above, the free-space propagation loss of 60 GHz is very high, so that a lot of base stations covering small-sized cells are required to implement systems. Moreover, high speed millimeter-wave devices based on compound semiconductors are very expensive and high frequency component designs and packages are also difficult. Therefore, the deployment cost of 60 GHz systems will be very high and simple and cost-effective base station design becomes important. As one solution, Radio-on-Fiber (RoF) technologies are attracting much attention [9-13].

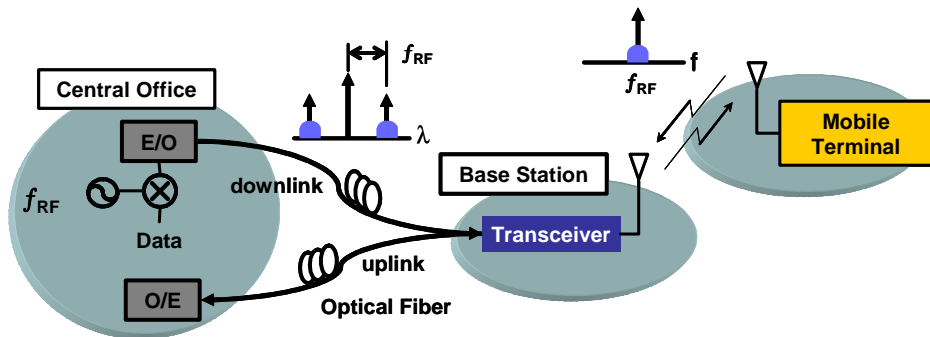


Figure 1-4. Simple bi-directional RoF system configuration.

Fig. 1-4 shows the schematic of simple bi-directional RoF systems. In RoF systems, radio signals are optically transmitted between central and base stations, resulting in low loss transmission of radio signals

through optical fibers. Therefore, for 60 GHz signals having high attenuation characteristics in free-space, RoF system technologies can extend transmission distance. In addition, direct transmission of radio signals can help reducing complex and expensive devices and equipment at many base stations, and controlling many base stations at one central station. In case of downlink data transmission, radio signals are generated by only photodetection process at the base station, and data signals are transmitted to mobile users after simple electrical amplification. Therefore, very simple base station architectures are expected. High speed operation of optical components is also very useful for 60 GHz systems. However, the single-mode fiber transmission of optically intensity-modulated millimeter-wave signals like 60 GHz can suffer severe signal fading due to fiber chromatic dispersion [14-15]. In case of optical intensity modulation, double-sideband signals are produced and each sideband experiences different phase shift during fiber transmission, so that destructive interference occurs between two beat signals at the receiver at certain transmission points, which causes degradation of generated signal power. Fig. 1-5 schematically shows this phenomenon and the calculated signal responses for 60 GHz and 1 GHz as a function of transmission distance are also shown below [15]. When modulation frequency is high, wavelength separation between two sidebands is wide, resulting in faster phase shift at short transmission distance. Therefore, the signal degradation of 60 GHz signals occurs at very short transmission point.

On the other hand, for 1 GHz signals, the wavelength difference between the sidebands is very small, so that dispersion effects are far less severe.

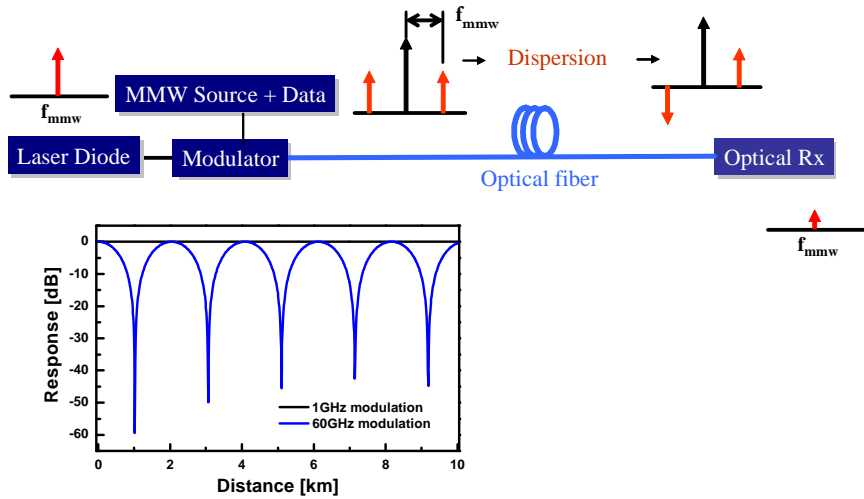


Figure 1-5. Schematic of dispersion-induced signal fading problems in intensity modulated millimeter-wave signal transmission.

Various techniques for dispersion-insensitive transmission of millimeter-wave signals have been proposed using dispersion compensation techniques [16-17] and remote frequency conversion techniques [18-19]. In optical communication systems for long-haul, gigabit data transmission, fiber chromatic dispersion was a limitation of error-free data transmission. Many kinds of dispersion compensators have been presented, and some techniques can be applied to RoF systems. Basic concept is that the unwanted phase difference between

two sidebands caused by fiber dispersion is controlled by dispersion compensators not to occur destructive interferences. Fig. 1-6 shows this principle. However, the problem is that the dispersion compensation techniques are sensitive to fiber transmission distances and optical signal wavelengths, and, as a result, RoF systems need many adaptable dispersion compensators, making system design difficult. In remote frequency conversion techniques, intermediate frequency (IF) signals are optically transmitted between central and base stations, and frequency up-conversion to and down-conversion from millimeter-wave-bands occur at each base station. Fig. 1-7 shows the simple remote frequency conversion systems in the bi-directional RoF link. Since fiber transmission of low frequency signals in the form of IF is hardly affected by dispersion as explained before, frequency conversion at the remote base stations can be a simple solution for the dispersion-induced signal fading problem. However, expensive millimeter-wave-band oscillators and mixers are needed for remote frequency conversion, which makes the base stations complex and expensive.

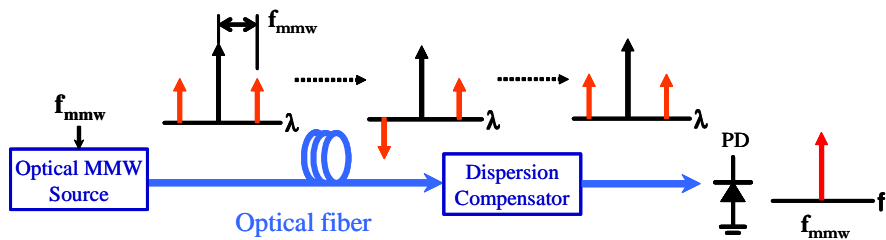


Figure 1-6. Dispersion compensators for optical millimeter-wave signal transmission without signal penalty.

To solve this problem, optical/optoelectronic frequency conversion techniques can be used [20-27], in which data carried in IF signals are frequency up- and down-converted at the base stations with the help of dispersion insensitive optical local oscillator (LO) signals generated at the central station by optical heterodyne techniques or optical single-sideband modulation techniques. Consequently, there is no need for expensive electrical oscillators and mixers at the base stations, allowing simple and cost-effective base station architecture. Fig. 1-8 shows a downlink RoF system example using remote frequency up-conversion scheme based on heterojunction phototransistors (HPTs) [21]. The optical heterodyne LO signals, which is two correlated optical modes separated by  $f_{LO}$ , are generated at the central station, and transmitted to the base station combined with optical IF signals having  $f_{IF}$  signals. When these two optical signals are injected into the HPT,  $f_{LO}$  and  $f_{IF}$  signals are generated by the HPT photodetection, and  $f_{IF}$  signals are frequency up-converted to the  $f_{LO}$  band by the optoelectronic mixing process of HPT. Therefore, no LO sources are required at the base station, and photodetection and frequency mixing functions can be obtained with only one device, HPT, leading to very simple base stations.

This dissertation focuses on optical/optoelectronic remote frequency conversion techniques for 60 GHz bi-directional RoF links. For downlink data transmission, remote optical frequency up-conversion technique is used, for which cross-gain modulation (XGM)

of semiconductor optical amplifier (SOA) is applied. For uplink data transmission, remote optoelectronic frequency down-conversion technique is used, for which nonlinearity of electroabsorption modulator (EAM) is applied. The LO signals are provided from the central station in the form of optical heterodyne signals.

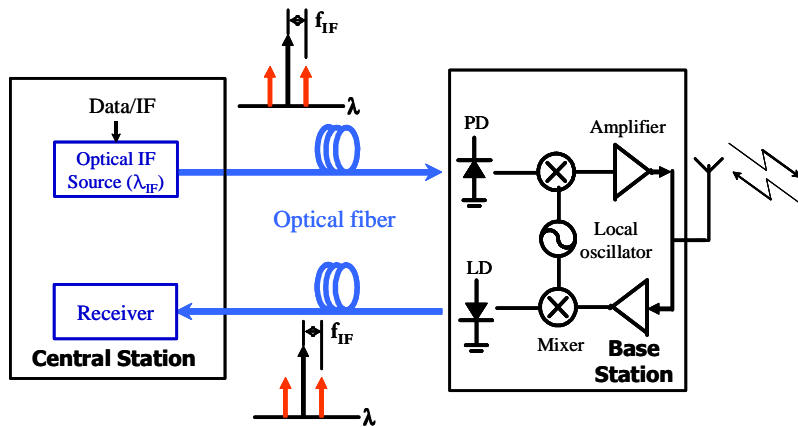


Figure 1-7. Simple bi-directional RoF link based on remote frequency conversion technique.

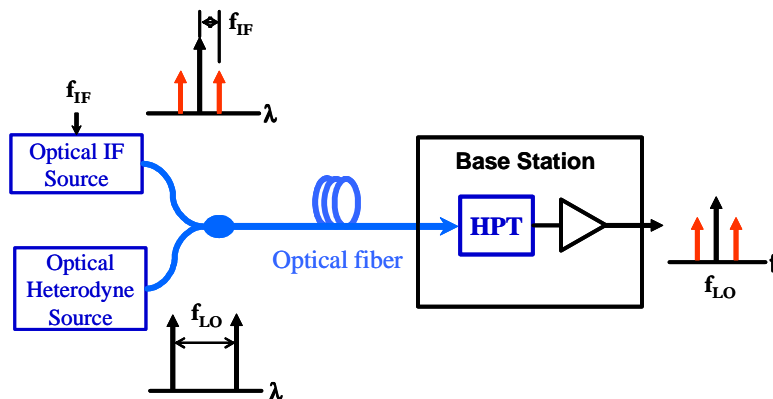


Figure 1-8. RoF downlink system configuration based on optoelectronic frequency up-conversion using HPT.

### **1-3. Bi-Directional RoF Link**

To communicate between wireless service providers and mobile users, bi-directional links are indispensable. Except broadcasting networks, most wireless systems are established bi-directionally, and RoF links are not exceptions for full network services. The problem is that additional high speed optical devices are required at each base station to send uplink radio signals to central station, which makes base stations complex and expensive. In case of optical millimeter-wave transmission, expensive optical components operating millimeter-wave-bands should be equipped at the base station. EAM transceivers allow the simple antenna base station architecture for bi-directional RoF links because EAM can perform the dual functions of photodetection and optical modulation [28-32]. The EAM is a reverse biased p-i-n diode with bulk active region [33] or multiple quantum-wells [34] as the absorption layer. Bias conditions determine the amount of light absorption, such that modulation of bias voltage changes the transmitted optical signal power of EAM, making optically modulated data signals. In addition, from the absorption layer, photocurrent is generated like conventional PDs. Fig. 1-9 shows a bi-directional millimeter-wave link using EAM. The optical millimeter-wave signals from the central station are photodetected in EAM, and generated downlink data signals are transmitted to mobile users. Conversely, uplink millimeter-wave signals from mobile users modulate EAM using the same optical source provided for downlink,

and optically transmitted uplink signals are photodetected at the central station. Therefore, a simple bi-directional RoF link can be realized with only one EAM.

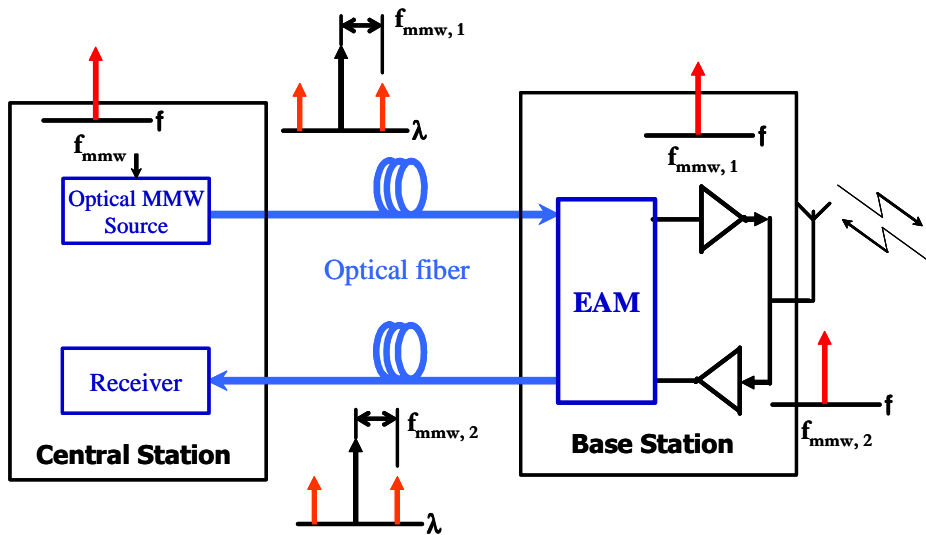


Figure 1-9. Bi-directional millimeter-wave RoF link using EAM.

However, as explained in chapter 1-2, direct fiber transmission of double sideband millimeter-wave signals causes dispersion-induced signal fading problems, so that by combining optical/optoelectronic mixing techniques, signal penalty from the fading can be overcome. In this dissertation, we investigate a 60 GHz photonic frequency converter, which performs frequency up-conversion and frequency down-conversion at the remote base station based on a cascaded SOA-EAM configuration. SOA cross-gain modulation and photodetection in EAM are used for frequency up-conversion, and EAM nonlinearity is used

for frequency down-conversion. Both LO and IF signals for frequency conversion are optically provided by the central station. Therefore, a simple base station having only one cascaded SOA-EAM configuration can be realized. Moreover, since optical LO signals are separated from optical IF signals, optical LO signals can be shared among several base stations and wavelength division multiplexing (WDM) techniques can be applied for accessing different base stations with different IF wavelengths. Fig. 1-10 shows a bi-directional RoF system architecture where proposed SOA-EAM frequency converters are to be used.

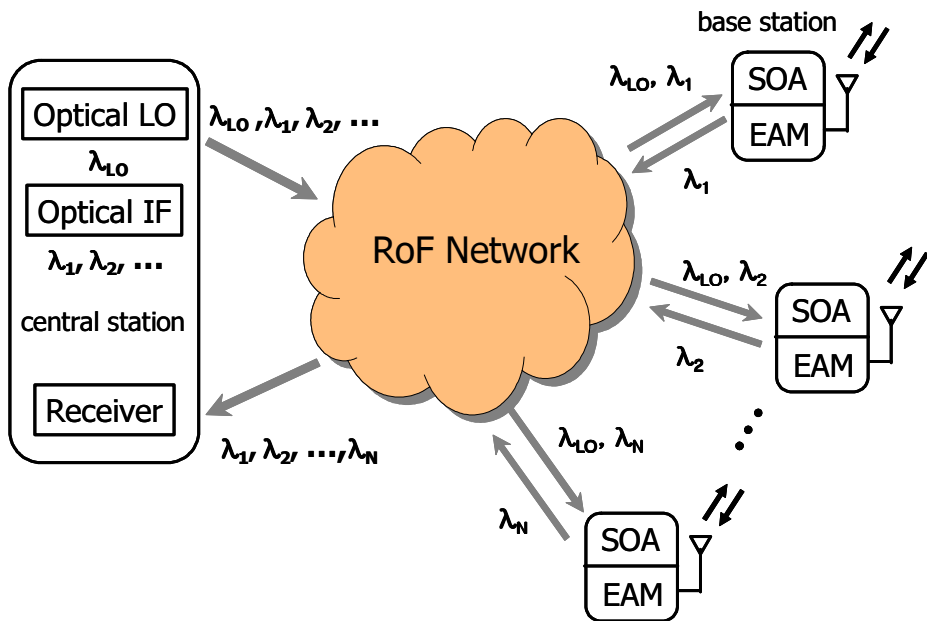


Figure 1-10. Bi-directional RoF systems using remote frequency conversion based on a cascaded SOA-EAM configuration proposed in this dissertation.

## **1-4. Outline**

This dissertation will focus on photonic frequency converters based on SOA and EAM, and their applications to 60 GHz RoF systems. Each frequency up- and down-conversion scheme will be explained at first, and then the frequency converter combining two schemes is proposed. The 60 GHz RoF systems will be also demonstrated for every frequency conversion technique. Details of dissertation outline are as follows.

In chapter 2, the optical frequency up-conversion method based on SOA is introduced at first. Section 2-1 explains the operation principles of frequency up-conversion, for which basic SOA characteristics are shown through the simulation model of SOA using a transfer matrix method, and up-conversion processes are clarified through this SOA model. The simulation results of the frequency up-converter are shown in section 2-2. To show the broadband operation properties of the frequency up-converter, 1.244 Gbit/s downlink RoF data transmission consequences at 60 GHz band are placed at the end of this chapter.

Next, the optoelectronic frequency down-conversion scheme based on EAM nonlinearity is described in chapter 3. After explaining the useful characteristics of EAM for RoF uplink data transmission in section 3-1, the operation principles of frequency down-conversion are accounted for in section 3-2. Section 3-3 presents the operation characteristics of the EAM frequency down-converter based on measurement results of internal conversion efficiency at 30 GHz band.

QPSK uplink RoF data transmission results at 60 GHz band are followed in section 3-4.

Chapter 4 introduces the frequency up- and down-conversion technique employing only one cascaded SOA and EAM configuration. Section 4-1 suggests a bi-directional link architecture using this frequency converter, and then the operation principles of proposed frequency up/down-converter are explained in section 4-2. The conversion efficiency is also defined for this frequency converter in section 4-3, and then the measurement results of frequency conversion efficiencies and their characteristics at 60 GHz band are discussed in detail. The last section shows the bi-directional RoF data transmission results at 60 GHz band. QPSK and 16QAM data transmission are demonstrated, and its system performances are analyzed through the error vector magnitudes.

Finally, chapter 5 summarizes the proposed photonic frequency conversion techniques, and 60 GHz RoF system demonstration results using these converters. A brief comment about the practicability of this frequency converter closes this dissertation.

## 2. Remote Frequency Up-Conversion Using SOA-PD Configuration

### 2-1. Operation Principle of Frequency Up-Conversion

Conventional downlink RoF systems based on remote frequency up-conversion use mixers and oscillators for low frequency IF signals to be frequency up-converted to application bands as shown in Fig. 2-1, making the base station design complex. To alleviate this problem, photonic frequency up-converter can be used, and as depicted in Fig. 2-1, electrical mixers and oscillators can be eliminated at the base station, for which optical LO signals are supplied from the central station, and optically delivered IF data signals are frequency up-converted by the photonic frequency up-converter. In this dissertation, this photonic frequency up-converter is realized by using SOA and PD configuration. However, this frequency conversion concept is originated from the following references [35-36], and this dissertation shows the analysis results and broadband data transmission results using this idea.

Fig. 2-2 schematically shows the operation of SOA-PD frequency up-conversion for downlink IF data transmission. The basic constitution of this frequency up-converter includes optical LO sources, optical IF sources, SOA, and PD. Optical LO signals at  $\lambda_{LO}$  are generated by the optical heterodyne method, resulting in two optical sidebands separated by  $f_{LO}$ . When optical LO signals along with optical

signals at  $\lambda_{IF}$  carrying IF signals are injected into SOA, two sidebands of optical heterodyne LO signals are cross-gain modulated by the IF data signals at  $\lambda_{IF}$ , and frequency up-converted data signals at  $f_{LO}$  are created by the signal beating process in a photodiode. More detailed explanation will be followed in next sections.

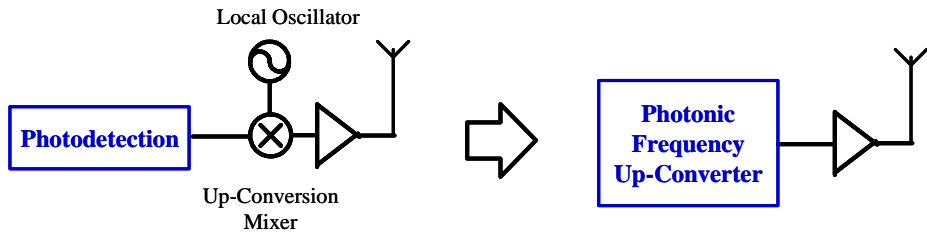


Figure 2-1. Base station of downlink RoF systems based on remote frequency up-conversion and photonic frequency up-converter.

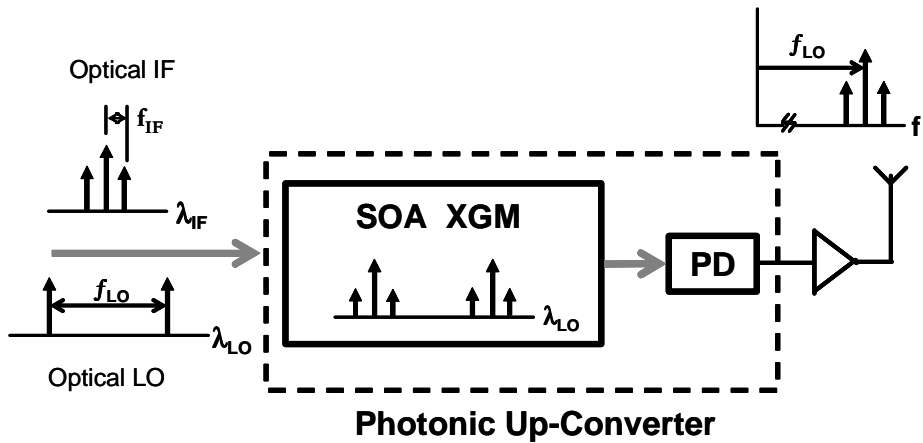


Figure 2-2. Schematic of photonic frequency up-conversion based on SOA-PD configuration.

### 2-1-1. Optical LO and IF signal generation

At first, it is explained how to generate optical LO and IF signals for this frequency up-conversion as shown in Fig. 2-3. Basically, the optical LO is generated by the optical heterodyne method [9]. Two optical modes separated by  $f_{RF}$  are given by

$$E_1 = A \cos((\omega_o + \omega_{RF}/2)t + \phi_1(t)) \quad 2-(1)$$

$$E_2 = A \cos((\omega_o - \omega_{RF}/2)t + \phi_2(t)) \quad 2-(2)$$

where  $\omega_o$  is optical center frequency, and  $\phi_{1, 2}(t)$  is optical phase. When these two modes are injected into PD, generated current due to the square-law beating inside PD are the following:

$$I \propto E_1 \times E_2^* = I_{DC} + A^2 \cos(\omega_{RF}t + \phi_1(t) - \phi_2(t)) \quad 2-(3)$$

where the signal having frequency sum results is not expressed, because its frequency is too high to be considered at RF range. As shown in equation 2-(3), the RF signal having  $\omega_{RF}$  frequency is generated, and theoretically, any frequency components can be produced by this optical heterodyne technique. In addition, this beat frequency signal power is not changed by the chromatic dispersion effect, which is a very useful characteristic for 60 GHz RoF data transmission. However, the phase components written as  $\phi_1(t) - \phi_2(t)$  are randomly changed, which causes severe phase noise in generated RF signals [37]. Therefore, phase-correlated two optical modes are required to eliminate randomly changed phase components, and optical

heterodyne signals mean two dominant phase-correlated optical modes for low-phase noise RF signal generation.

Many researchers have been developed two phase-correlated optical signal generation techniques [38-41], and one of the easy and popular methods is a double-sideband with suppressed carrier (DSB-SC) method using a Mach-Zehnder modulator (MZM) [42-43]. This was also selected as an optical millimeter-wave generation method at the RACE project R-2005-MODAL (Microwave Optical Duplex Antenna Link) [44]. Following is the brief analytical model of DSB-SC method based on reference [42] and [43]. The output electric field of an MZM can be described by

$$E_{out}(t) = E_{in}(t) \cos\left(\frac{\pi}{2} \cdot \frac{V_m(t)}{V_\pi}\right) \quad 2-(4)$$

where  $V_m(t)$  is modulating voltage applied to the modulator and  $E_{in}(t)$  is the incident optical field. When the frequency of modulating voltage is  $w_{RF}$ , this voltage signal summed with a bias voltage can be written as

$$V_m(t) = V_\pi(1 + \varepsilon) + \alpha V_\pi \cos(w_{RF}t) \quad 2-(5)$$

The terms  $\varepsilon$  and  $\alpha$  are the bias and modulation levels applied to the modulator normalized to  $V_\pi$ . The output field from the modulator for  $V_m(t)$  is given by

$$E_{out}(t) = \cos\left(\frac{\pi}{2} [(1 + \varepsilon) + \alpha \cos(w_{RF}t)] \cos(w_0t)\right) \quad 2-(6)$$

where the optical frequency is  $w_0$ . Equation 2-(6) can be expanded with Bessel functions, and the resulting spectral components can be written as

$$\begin{aligned}
E_{out}(t) = & \frac{1}{2} J_0\left(\alpha \frac{\pi}{2}\right) \cos\left[\frac{\pi}{2}(1+\varepsilon)\right] \cos(w_0 t) \\
& - J_1\left(\alpha \frac{\pi}{2}\right) \sin\left[\frac{\pi}{2}(1+\varepsilon)\right] \cos(w_0 t \pm w_{RF} t) \\
& - J_2\left(\alpha \frac{\pi}{2}\right) \cos\left[\frac{\pi}{2}(1+\varepsilon)\right] \cos(w_0 t \pm 2w_{RF} t) \\
& + J_3\left(\alpha \frac{\pi}{2}\right) \sin\left[\frac{\pi}{2}(1+\varepsilon)\right] \cos(w_0 t \pm 3w_{RF} t) + \dots
\end{aligned} \tag{2-7}$$

where  $J_i$  is the  $i$ th Bessel function of the first kind. If the modulator is biased at  $V_\pi$  ( $\varepsilon=0$ ), then the component at  $w_0$  will be suppressed as are all even terms. Two dominant components separated by  $2w_{RF}$  are produced, and these are completely phase-correlated, so that very low phase noise signals can be generated after square-law beating process of photodetection. Although, other spectral components are also generated by signal beating, they can be eliminated by electrical filtering after photodetection. As a result, Fig. 2-3 shows that if an MZM is modulated by half of target LO frequency ( $f_{LO}/2$ ) signals,  $f_{LO}$  separated two optical modes can be obtained, and these are the optical heterodyne LO signals for photonic frequency converters. Although the DSB-SC technique has stability problems due to the voltage drift in MZM, the control circuits to adjust MZM bias voltages in voltage supply units can solve this problem, and commercial products are

already released for this purpose. In this dissertation, all the optical heterodyne signals are generated by the DSB-SC technique.

For optical IF signals, all kinds of optical modulation techniques can be used, however, the bandwidth of optical components should be large enough not to distort IF data signals. Fig. 2-3 shows direct laser modulation of IF data signals for optical IF.

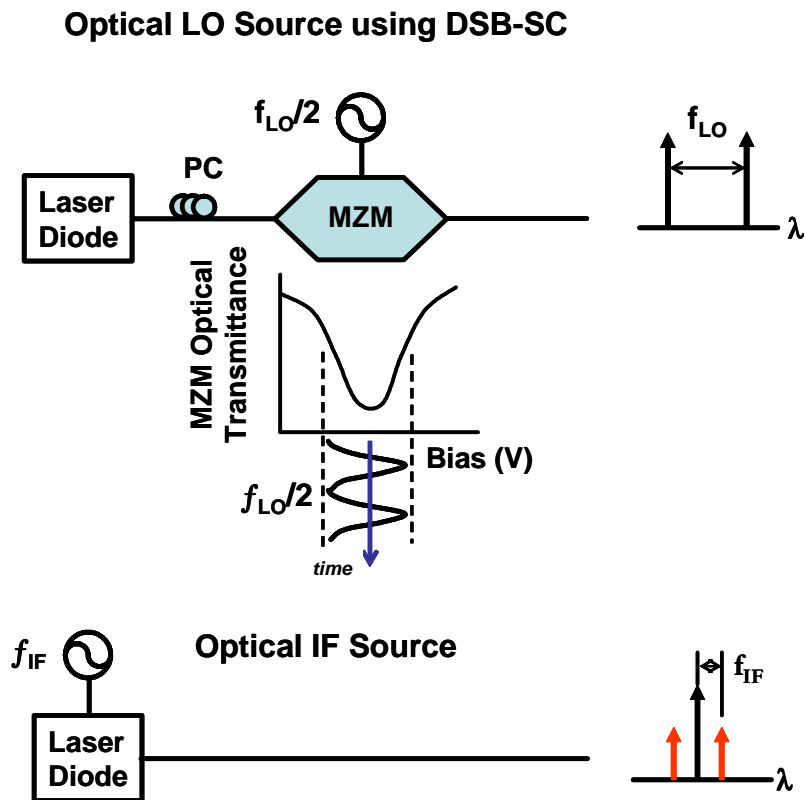


Figure 2-3. Optical LO generation using DSB-SC method, and optical IF generation using direct laser diode modulation.

### **2-1-2. Cross-gain modulation (XGM) of SOA**

Next, SOA XGM for IF signal modulation to optical LO signals is explained. In this frequency up-converter, SOA is operating as a remote signal modulator using XGM. However, SOA in itself is an optical signal amplifier, and to explain XGM process, the simple principle of optical amplification is necessary [45-46]. Fig. 2-4 shows the stimulated processes in a two level system. In an SOA, electrons are injected from an external current source into the active region of semiconductors. These make carriers occupy energy states in the conduction band of the active region material, leaving holes in the valence band. When a photon having energy larger than energy gap, its energy stimulates electrons to be moved to conduction band and photon energy disappears, which is called stimulated absorption. However, a photon having suitable energy is incident on the semiconductor, it can cause stimulated recombination of a conduction band carrier with a valence band hole. The recombining carrier loses its energy in the form of a photon. This new stimulated photon is perfectly coherent with the inducing photon, which means identical phase and frequency with the incident photon. This process is called stimulated emission, and while these photons are inside semiconductor materials, they can give rise to more stimulated emission, which is an optical gain process. However, these two processes occur statistically, so that external management to increase the probability of stimulated emission is needed to obtain optical gain. If the injected current is sufficiently high then a population

inversion is created when the carrier population in the conduction band exceeds that in the valence band. In this case the stimulated emission becomes statistically dominant process, so that optical gain appears in the semiconductors.

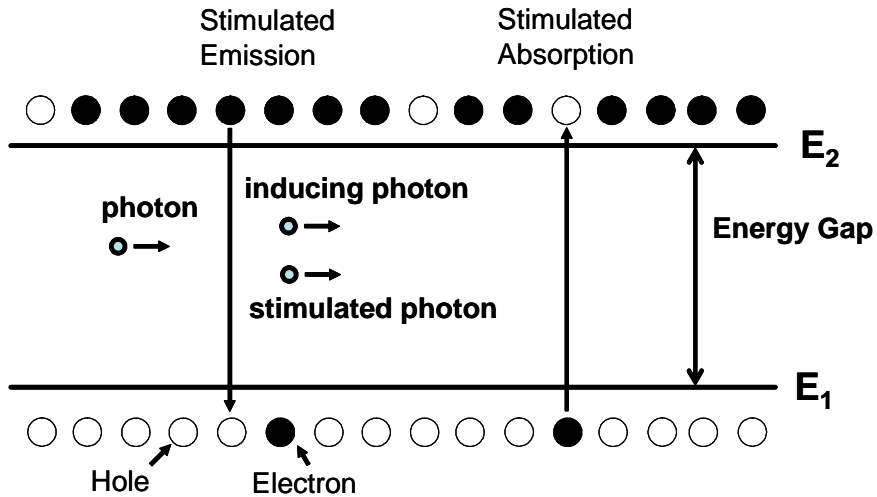


Figure 2-4. Stimulated processes in a two level system.

In SOA, optical gain and saturation input optical power are basic performance parameters. When an optical signal is injected into SOA, its amplitude is amplified as much as SOA gain, however, if the input signal power is beyond saturation power condition, the signal gain is reduced due to limited carriers inside SOA, which is called gain saturation, and the input power condition occurring gain saturation is called saturation input optical power. The XGM process uses this gain saturation phenomenon [47-48]. In principle, when two different

optical signals, one of which has higher optical power than saturation input optical power, are injected into SOA, a higher power optical signal acquires more optical gain than a lower power optical signal. Therefore, output signal power of one optical signal can be controlled by another wavelength optical signal. Fig. 2-5 shows the XGM principle schematically. When an optical signal having data ( $P_1$ ) and a CW optical signal ( $P_2$ ) are incident on SOA, the gain of the  $P_2$  signal is changed by the  $P_1$  signal power, such that the  $P_2$  signal is optically modulated by the  $P_1$  signal. In this case, modulated data in the  $P_2$  signal has inverted form of original data signals.

Therefore, as shown in Fig. 2-5, when optical LO at  $\lambda_{LO}$  and optical IF at  $\lambda_{IF}$  are injected into SOA, two modes of optical heterodyne LO signals are cross-gain modulated by optical IF, and each mode has double-sideband IF signals.

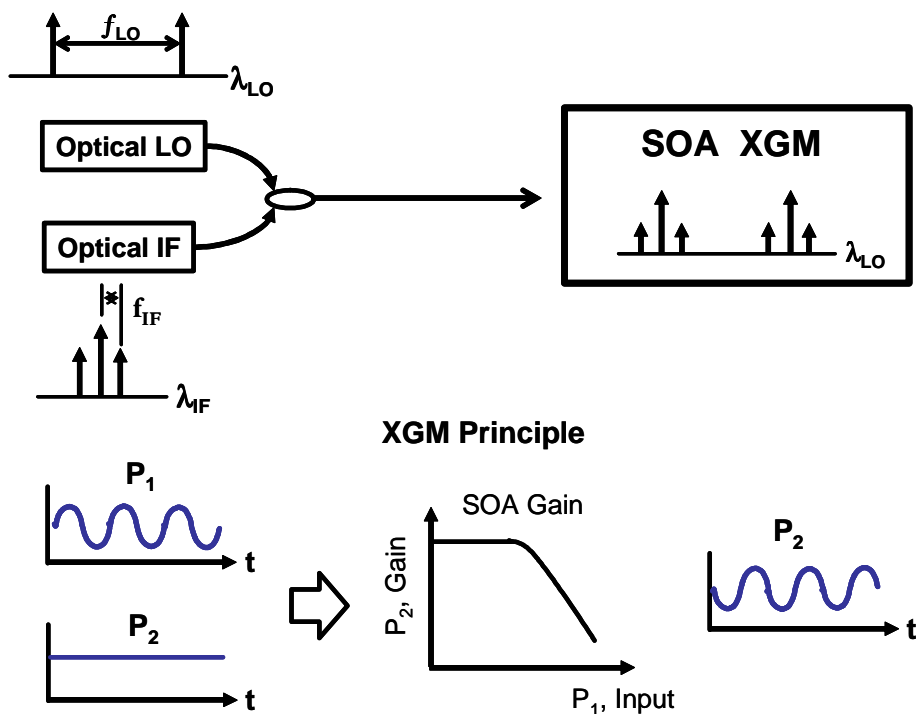


Figure 2-5. Process of optical IF signal modulation in optical LO signals by SOA XGM. Below is a simple operation principle of XGM.

### 2-1-3. Frequency up-conversion at a PD

In chapter 2-1-1, it is explained how to generate optical heterodyne LO and optical IF signals, and in chapter 2-1-2, it is described what is XGM and how the optical IF signals modulate optical LO signals by SOA XGM. Finally, a brief signal beating process in a PD will be shown, which is a final process to accomplish frequency up-conversion.

A PD is a device to convert optical signals into electrical current signals, which is modeled with following equation:

$$I_{PD} = R \cdot P_{optical} = R \cdot E \times E^* \quad 2-(8)$$

where R is responsivity of PD that explains signal loss due to optical signal scattering, reflection, and so on,  $P_{optical}$  is incident optical power, and E is the electrical field of optical signals. Therefore, it means that produced current is a result of square-law beating with incident electric fields. RF signal generation using optical heterodyne methods also uses this characteristic as explained in section 2-1-1. Frequency up-converted signals can be obtained by this signal beating process in PD as shown in Fig. 2-6. After SOA XGM, ideally, six optical modes are created, and they can be briefly written as

$$\begin{aligned} E = & \cos(\omega_0 t - \omega_{IF} t) + \cos(\omega_0 t) + \cos(\omega_0 t + \omega_{IF} t) \\ & + \cos((\omega_0 + \omega_{LO})t - \omega_{IF} t) + \cos((\omega_0 + \omega_{LO})_0 t) \\ & + \cos((\omega_0 + \omega_{LO})t + \omega_{IF} t) \end{aligned} \quad 2-(9)$$

where optical phases and signal amplitudes are omitted for simplification. If these six optical modes are incident on PD, resulting electrical signals after beating processes are the following:

$$I = \cos((w_{LO} - w_{IF})t) + \cos(w_{LO}t) + \cos((w_{LO} + w_{IF})t) \quad 2-(10)$$

where other signal products are eliminated, because they are far from the LO frequency band. Therefore it shows that low frequency IF signals are frequency up-converted to LO frequency band. In this frequency up-conversion process, XGM can cause phase modulation in SOA. However, this phase modulation does not affect the system performance, and also the short optical transmission length between SOA and PD can not change optical phases of LO signals enough to affect frequency up-conversion. If SOA and PD are monolithically integrated, the phase variation of optical LO is completely disappeared.

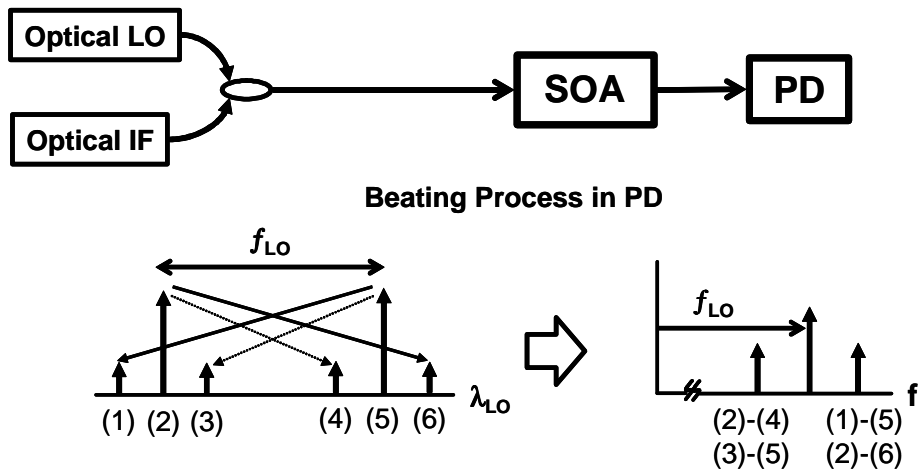


Figure 2-6. Frequency up-conversion by the signal beating process in PD.

This frequency up-converter is at first designed to make base stations simple and cost-effective, however there are many other advantages. Because this frequency up-converter uses optical

amplifiers, conversion efficiency is very high. In addition, SOA offers optical gain in wide wavelength range, where XGM can occur, so that the operation wavelength range is wide. This characteristic is very useful to adopt wavelength division multiplexing (WDM) technologies in this remote up-conversion system. Another advantage is that optical heterodyne LO signals having any frequency separation can be used, which makes frequency up-converters insensitive to LO frequency. Therefore, it can operate at any millimeter-wave and sub-millimeter-wave bands. However, for IF bandwidth, because the speed of SOA XGM is limited by carrier recombination time, IF signal frequency is restricted within several GHz, which is nonetheless enough to transmit broadband data signals [45-48]. The details of these frequency up-converter characteristics are well explained in reference [35] and [36]. The nonlinearity of SOA-PD frequency up-converter is also investigated in reference [49], where spurious-free dynamic range of around  $77 \text{ dB/Hz}^{2/3}$  is obtained experimentally. Therefore, in this dissertation brief characteristics of the SOA-PD frequency up-converter will be shown in next chapters.

#### 2-1-4. Frequency up-conversion experiment

In this chapter, this frequency up-conversion is experimentally verified at 25 GHz band. Fig. 2-7 shows the experimental setup for this measurement. For 25 GHz optical LO signals, 12.5 GHz RF signals modulate an MZM biased at minimum transmission conditions for DSB-SC method. An erbium-doped fiber amplifier (EDFA) was used to boost optical LO power. The optical LO wavelength was 1535.4 nm, and the optical power before SOA was -13 dBm. For optical IF signals, 1 GHz signals modulated another MZM biased at voltage conditions for maximum modulation efficiency. The optical IF wavelength and power before SOA was 1546.18 nm, and -11 dBm, respectively.

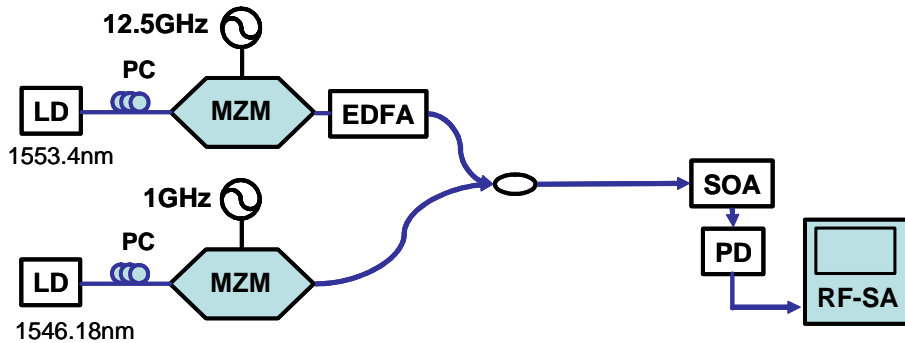
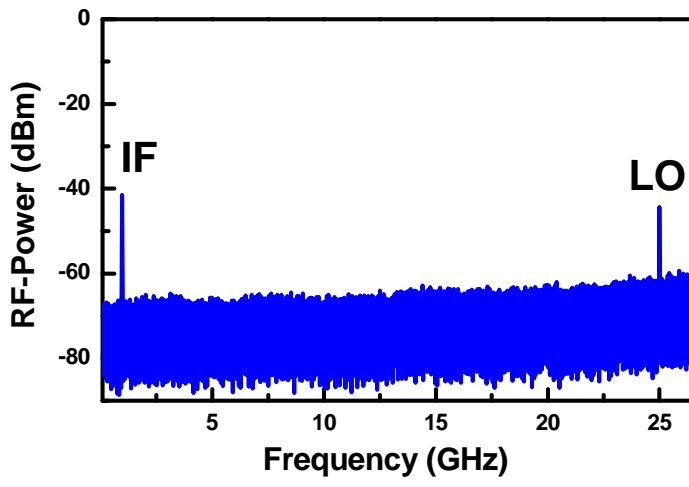
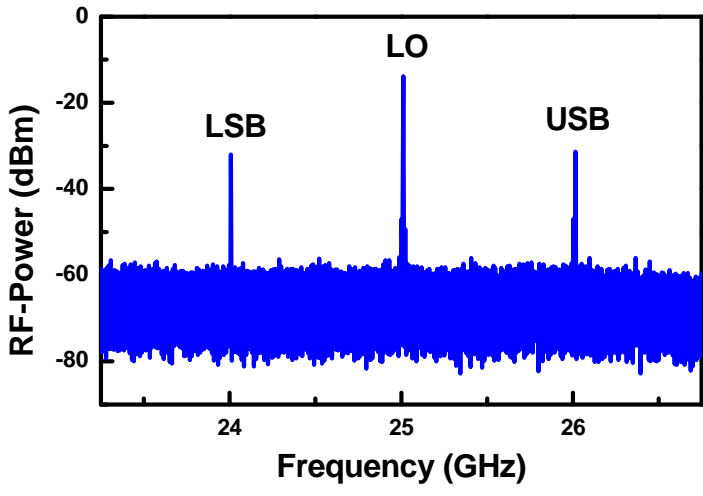


Figure 2-7. Experimental setup to verify optical frequency up-conversion at 25 GHz band. LD : Laser Diode, RF-SA : RF-Spectrum Analyzer, PC : Polarization Controller

When these optical signals were combined and injected into SOA, two modes of optical LO signals were cross-gain modulated by 1 GHz IF signals. After photodetection of optical LO signals, 1 GHz IF signals were frequency up-converted to 25 GHz band. Fig. 2-8(a) shows the RF spectrum measured before SOA, which means no frequency up-conversion occurs, and Fig. 2-8(b) shows the RF spectrum measured after SOA. For these measurement, the same broadband 25 GHz PD was used. As shown in Fig. 2-8(b), 1 GHz IF signals are successfully frequency up-converted to upper sideband (26 GHz), and lower sideband (24 GHz). Moreover, frequency up-converted signals have larger RF power by about 10 dB compared to 1 GHz IF signal power measured before SOA. This implies that the up-converted IF signal in SOA can have conversion gain because the SOA gain directly contributes to up-conversion process. It should be noted, however, that the noise level increases due to SOA amplified spontaneous emission noise. Therefore, for better system performance, SOA noise should be reduced or filtered out.



(a)



(b)

Figure 2-8. RF Spectrum measured before SOA (a), and after SOA (b).

## **2-2. Simulation of Frequency Up-Conversion Using a Transfer Matrix Method**

In chapter 2-1, the operation principles of SOA-PD frequency up-converter are introduced, and its operation is verified with simple frequency up-conversion experiment. In this chapter, the basic operation characteristics will be explained through frequency up-conversion simulation. This frequency up-converter uses SOA XGM and square-law beating in PD, however, the important process is SOA XGM. Therefore, to make a simulation model of SOA-PD frequency up-converter, SOA XGM modeling places at the most important part. In order to have high optical gain of SOA, the length of SOA is generally designed long, so that the gain dynamics inside SOA becomes very complex [45-46]. When optical field propagates inside SOA, carrier distribution change occurs at different location of SOA, resulting in optical gain variation inside SOA. To model this phenomenon, time-dependent transfer matrix method (TMM) can be used [46, 50-52]. The SOA is divided into many small SOA units having no longitudinal carrier change, and the amplitude and phase variation of optical fields at each SOA unit are calculated until the input optical fields arrive at final SOA unit. The amplitude and phase variation are determined by a signal propagation equation and a rate equation at each SOA section. Based on this method, the basic SOA characteristics will be shown at first, and then the frequency up-conversion process will be simulated and analyzed at 60 GHz band.

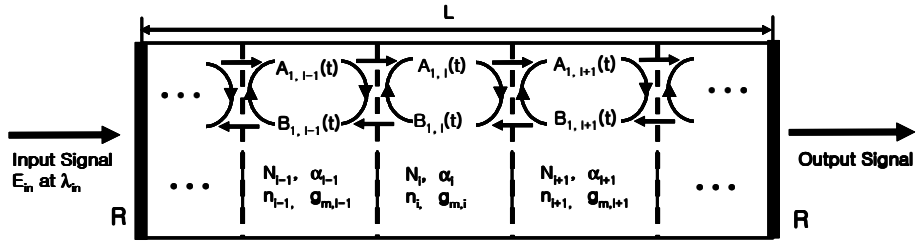


Figure 2-9. Schematic of SOA model based on time-dependent TMM.

### 2-2-1. SOA Modeling using TMM

Fig. 2-9 shows the schematic of SOA simulation model presented in reference [50]. The SOA has length  $L$  and reflectivity  $R$  at each end side, and is divided into  $N$  small SOAs. Input optical field,  $E_{in}$  at  $\lambda_{in}$  is incident on one facet of SOA, and its field variation at each SOA section is calculated using a signal propagation equation and a rate equation. Because the longitudinal variation of carriers causes the change of refractive index, reflected field appears in SOA, and its effects should be considered. Therefore, the optical field is divided into propagating one ( $A_i$ ) and reflecting one ( $B_i$ ) at each SOA section. For this calculation, number of carrier  $N$ , refractive index  $n$ , gain  $g$ , chirp parameter  $\alpha$  should be determined in every small SOA unit. They are the basic parameters of the SOA model. For simplicity of explanation, the calculation process at one small SOA unit is shown at first [46]. Fig. 2-10(a) shows the field model of unit SOA, where field propagation constant is  $\gamma$ , and Fig. 2-10(b) shows the field propagation and

reflection model according to refractive index variation ( $n_1$  and  $n_2$ ) at unit SOA facet. Fig. 2-10(a) is modeled as following matrix form:

$$\begin{bmatrix} E_{A,L} \\ E_{B,L} \end{bmatrix} = \begin{bmatrix} e^{\gamma L} & 0 \\ 0 & e^{-\gamma L} \end{bmatrix} \begin{bmatrix} E_{A,0} \\ E_{B,0} \end{bmatrix} \quad 2-(11)$$

where output fields at  $Z=L$  can be obtained by multiplying the propagation matrix by input field matrix at  $Z=0$ . The matrix model of Fig 2-10(b) is the following:

$$\begin{bmatrix} E_{A,n_2} \\ E_{B,n_2} \end{bmatrix} = \begin{bmatrix} \frac{n_2 + n_1}{2n_2} & \frac{n_2 - n_1}{2n_2} \\ \frac{n_2 - n_1}{2n_2} & \frac{n_2 + n_1}{2n_2} \end{bmatrix} \begin{bmatrix} E_{A,n_1} \\ E_{B,n_1} \end{bmatrix} \quad 2-(12)$$

The propagation index and reflective index of the optical field is determined by the refractive index change, and the resulting field variation is calculated. As a result, when optical field propagates from  $i_{\text{th}}$  SOA unit to  $(i+1)_{\text{th}}$  SOA unit as shown in Fig. 2-9, resulting matrix equation can be written as

$$\begin{bmatrix} A_{i+1}(t + \Delta t) \\ B_{i+1}(t) \end{bmatrix} = \begin{bmatrix} a_{11}(t) & a_{12}(t) \\ a_{21}(t) & a_{22}(t) \end{bmatrix} \begin{bmatrix} A_i(t) \\ B_i(t + \Delta t) \end{bmatrix} \quad 2-(13)$$

where matrix elements  $a_{ij}(t)$  are the multiplication results of 2-(11) and 2-(12). The problem is that the initial condition of reflecting field components ( $B_i$ ) is determined by the input optical field from opposite side of propagation field ( $A_i$ ). Therefore the equation 2-(13) should be modified into the following matrix:

$$\begin{bmatrix} A_{w,i+1}(t + \Delta t) \\ B_{w,i}(t + \Delta t) \end{bmatrix} = \begin{bmatrix} a_{11}(t) - \frac{a_{12}(t)a_{21}(t)}{a_{22}(t)} & \frac{a_{12}(t)}{a_{22}(t)} \\ -\frac{a_{21}(t)}{a_{22}(t)} & \frac{1}{a_{22}(t)} \end{bmatrix} \begin{bmatrix} A_{w,i}(t) \\ B_{w,i+1}(t) \end{bmatrix} \quad 2-(14)$$

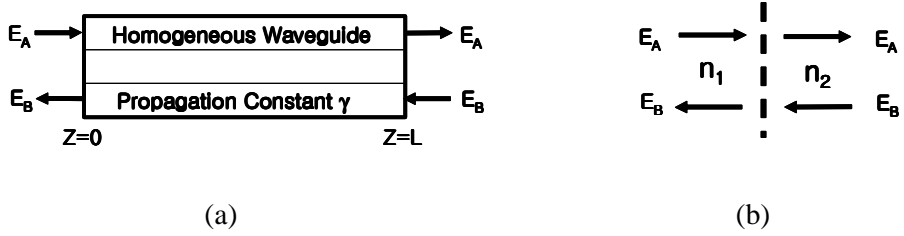


Figure 2-10. (a) Field model in unit SOA, (b) Field propagation and reflection model in different refractive index layers.

To obtain matrix elements in 2-(14), propagation constant  $\gamma$  should be calculated at first from the following signal propagation equation:

$$\frac{\partial A(z,t)}{\partial z} + \frac{1}{v_g} \frac{\partial A(z,t)}{\partial t} = -\frac{i}{2} \alpha \Gamma g_m A(z,t) + \frac{1}{2} g A(z,t) + \mu(z,t) \quad 2-(15)$$

$A(z, t)$  is the normalized signal envelope such that  $|A(z, t)|^2$  represents the optical power, and  $\alpha$  is chirp parameter which accounts for carrier-induced index changes.  $v_g$  is group velocity,  $\Gamma$  is confinement factor of SOA,  $g_m$  is material gain, and  $g$  is net gain [53-54]. The amplified spontaneous emission noise is represented by two statistically independent Gaussian distributed random processes for  $\mu(z, t)$  that satisfy the following correlation:

$$\langle \mu(z,t) \cdot \mu(z',t')^* \rangle = \beta \Gamma R_{sp} \delta(t-t') \delta(z-z') \times (v_g EA_{cross}) \quad 2-(16)$$

where  $\beta$  is a spontaneous emission coupling factor,  $R_{SP}$  is a spontaneous emission rate assuming bimolecular recombination,  $\delta(x)$  is defined as  $\delta$  function,  $E$  is photon energy, and  $A_{cross}$  is cross-sectional area of the active layer. This noise is treated as an additive noise, and the carrier distribution change determines noise amount. However, for simplicity only average noise is added in this dissertation. Equation 2-(17) shows the derived  $\gamma$  expression from equation 2-(15).

$$\gamma = \frac{1}{2}g - \frac{i}{2}\alpha\Gamma g_m + i\frac{nw}{c} \quad 2-(17)$$

The parameter values in 2-(17) are mainly determined by the carrier density in each SOA unit, which is calculated by the carrier rate equation in SOA written as

$$\frac{\partial N_i}{\partial t} = \frac{I}{qV} - (A_{nr}N_i + BN_i^2 + CN_i^3) - v_g\Gamma g_{m,i}S_i \quad 2-(18)$$

where  $N$  represents carrier density,  $S$  is photon density, the index  $i$  corresponds to different sections of SOA,  $I$  is injection current,  $V$  is active volume,  $q$  is electronic charge, and  $A_{nr}$ ,  $B$ ,  $C$  are related to recombination constants. The average photon density is represented as following equation:

$$S_i = \frac{|A_i|^2 + |A_{i+1}|^2 + |B_i|^2 + |B_{i+1}|^2}{2v_g hf A_{cross}} \quad 2-(19)$$

where  $h$  is plank constant,  $f$  is optical frequency,  $A_i$  is propagation wave amplitude, and  $B_i$  is reflected wave amplitude.

In order to model the asymmetric gain profile in wavelength domain, the gain spectrum is assumed to be cubic and the material gain is approximated by [55]

$$g_m(N_i, \lambda) = \frac{a_0(N_i - N_0) - a_1(\lambda - \lambda_p)^2 + a_3(\lambda - \lambda_p)^3}{1 + \varepsilon S_i} \quad 2-(20)$$

where  $a_0$ ,  $a_1$ , and  $a_3$  represent gain constant,  $\varepsilon$  is gain compression factor, and  $\lambda_p$  is gain peak wavelength, which is given as

$$\lambda_p = \lambda_0 - a_2(N - N_0) \quad 2-(21)$$

where  $\lambda_0$  represents wavelength at transparency,  $a_2$  is gain constant, and  $N_0$  is carrier density at transparency. The net gain is given by [56] as

$$g_i = \Gamma(g_{mi} - \alpha_a) - (1 - \Gamma)\alpha_c - \alpha_{scat} \quad 2-(22)$$

where  $\alpha_a$ ,  $\alpha_c$  and  $\alpha_c$  are active layer loss, cladding layer loss, and scattering loss, respectively. The  $\alpha$  parameter can be obtained by differentiating equation 2-(20) and refractive index with carrier density, resulting in the following equation:

$$\alpha_i(N_i, \lambda_w) = \frac{-4\pi}{\lambda} \frac{dn/dN}{dg/dN} \quad 2-(23)$$

All the parameters depending on carrier density are calculated at every SOA section, and the parameter  $\gamma$  is determined by the obtained parameters.

Finally, the refractive index changes should be calculated to complete matrix elements. The refractive index at each SOA unit has dependence on carrier density, which can be written as

$$n_i = n_g - \alpha \Gamma g_m \frac{c}{2\omega} \quad 2-(24)$$

where  $n_g$  is group refractive index,  $\omega$  is angular frequency of optical signals.

To simulate SOA with these equations, the simulation time step should be considered carefully not to make the same time-varying optical signals to be calculated twice at the same SOA section. This time step is calculated based on the length of unit SOA and the group velocity of input optical signals.

### **2-2-2. Simulation results of SOA gain characteristics**

In this chapter, the SOA gain characteristics are simulated by SOA model explained in section 2-2-1. In fact, the simulation model described in section 2-2-1 is suitable for large signal analysis, and other simple SOA models can be used for static characteristics, however, this model is also good enough to show SOA gain characteristics. The simulation parameters of SOA are selected from reference [50], and shown in table 2-1. The input optical signal is assumed to be a CW, and the wavelength is 1530 nm.

Firstly, SOA gain was simulated as a function of output optical powers with different SOA injection currents from 50 mA to 200 mA. Because the optical amplification occurs due to stimulated emission, limited carriers inside SOA cause SOA gain saturation. As shown in Fig. 2-11, gain starts to saturate rapidly after saturation point. SOA output power at the 3 dB gain saturation condition is an important parameter of SOA to represent its output limit not having signal distortion. As SOA injection current increases, SOA gain increases due to the increase of carriers inside SOA [45-46]. However, it should be noted that SOA gain does not increase linearly with SOA injection current because of carrier saturation to lasing condition.

Next, the dependence of SOA gain on bias current in SOA was simulated. For this, SOA input optical power was assumed to be -40 dBm, at which condition input optical power does not affect gain saturation. Fig. 2-12 shows the SOA gain as a function of SOA current.

As explained above, the SOA gain does not increase linearly with high SOA injection current, and saturates to about 32 dB. When the injection current approaches to the threshold current condition, where SOA can operate as a laser, the carrier density in SOA converges to a certain level. Therefore SOA gain saturates to certain level [45].

Finally, SOA gain characteristics according to input optical signal wavelengths were simulated. The input optical power was also selected to -40 dBm not to affect optical gain. The SOA bias current was varied from 50 mA to 200 mA. Fig. 2-13(a) shows the calculated material gain, which is expressed in equation 2-(20). The material gain increases with SOA injection current, which also shifts peak value to shorter wavelength [50]. The peak gain wavelength condition has a dependence on carrier density, so that injection current shifts gain peak. As injection current increases, the carrier density in SOA increases, which makes gain peak shifted to shorter wavelength conditions. The SOA gain spectrum in wavelength domain is similar to the shape of material gain as shown in Fig. 2-13(b), because material gain parameters are the dominant factor of SOA gain. Therefore, SOA gain shows similar characteristics of material gain, and the SOA gain peak is shifted to shorter wavelengths with the increase of SOA bias current [45-46].

**Table 2-1. SOA simulation parameters**

Symbol	Description	Value	Unit
$\Gamma$	Confinement factor	0.3	
L	SOA length	$1000 \times 10^{-6}$	m
V	Active layer volume	$1.5 \times 10^{-16}$	$m^3$
$\beta$	Spontaneous coupling factor	$2 \times 10^{-5}$	
$A_{nr}$	Recombination rate	$1 \times 10^{-8}$	$s^{-1}$
B		$2.5 \times 10^{-17}$	$m^3/s$
C		$9.4 \times 10^{-41}$	$m^6/s$
$a_0$	Material gain constant	$2.5 \times 10^{-20}$	$m^2$
$a_1$		$0.074 \times 10^{20}$	$m^{-3}$
$a_2$		$3.0 \times 10^{-32}$	$m^4$
$a_3$		$3.155 \times 10^{25}$	$m^{-4}$
$N_0$	Carrier density at transparency	$1.1 \times 10^{24}$	$m^{-3}$
$\lambda_0$	Wavelength at transparency	$1.605 \times 10^{-6}$	m
$v_g$	Group velocity	$7.5 \times 10^7$	m/s
$\varepsilon$	Nonlinear gain compression	$1.3 \times 10^{-23}$	$m^3$
dn/dN	Differential refractive index	$-1.2 \times 10^{-26}$	$m^3$
$\alpha_a$	Loss in active layer	$140 \times 10^2$	$m^{-1}$
$\alpha_c$	Loss in claddings	$20 \times 10^2$	$m^{-1}$
$\alpha_{scat}$	Scattering loss	$1.0 \times 10^2$	$m^{-1}$

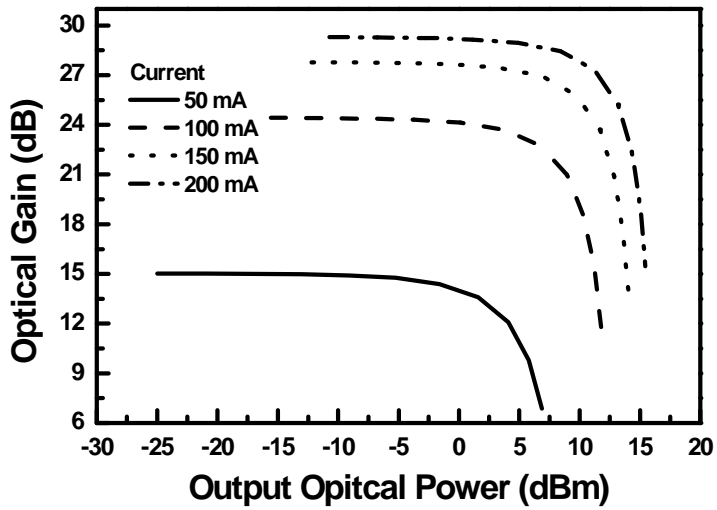


Figure 2-11. Optical gain of SOA as a function of output optical power with different SOA injection currents.

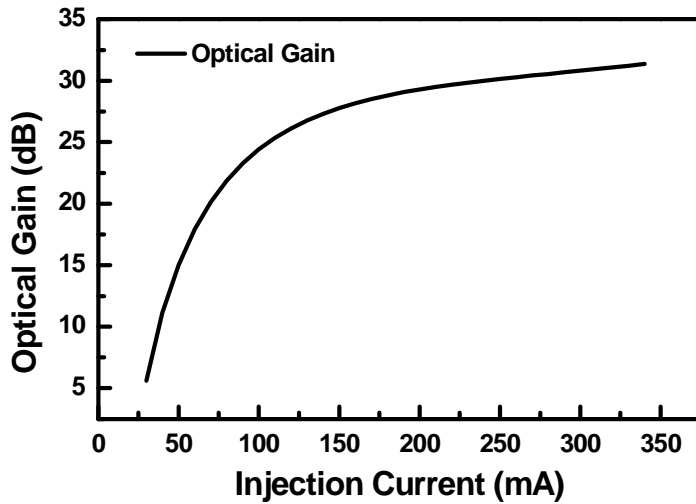
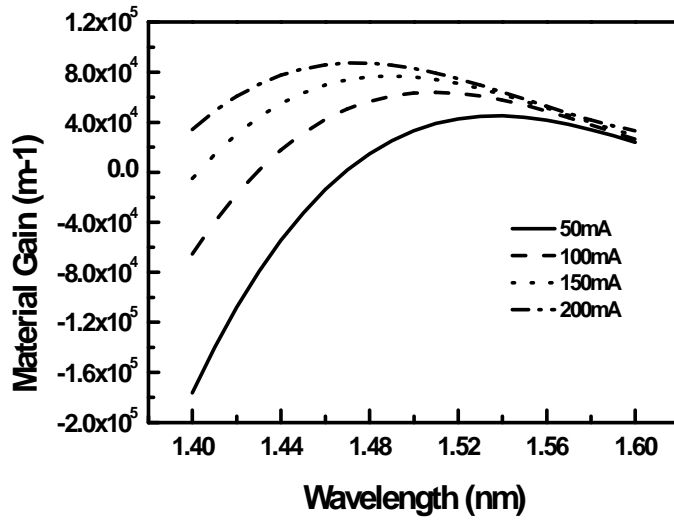
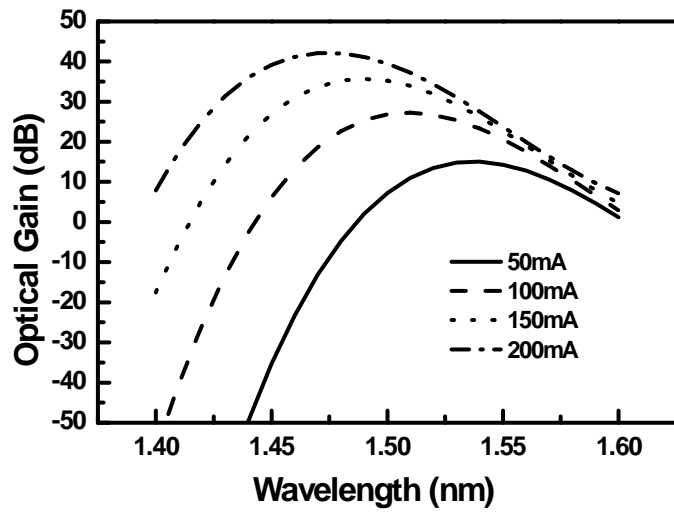


Figure 2-12. Optical gain of SOA as a function of SOA injection current.



(a)



(b)

Figure 2-13. Material gain of SOA (a) and optical gain of SOA (b) as a function of input signal wavelength with different SOA injection currents.

### 2-2-3. Simulation results of frequency up-conversion

In this chapter, frequency up-conversion simulation is performed based on the TMM. Because the TMM is suitable for dynamic large signal modeling of SOA, it can well explain the frequency up-conversion process, which uses SOA gain dynamics inside SOA. The characteristics of the SOA-PD frequency up-converter will be presented with frequency up-conversion efficiency calculation. Fig. 2-14 shows the schematic of frequency up-conversion efficiency, which is the electrical power ratio of frequency up-converted USB signals to IF signals calculated before SOA. Equation 2-(25) represents the efficiency definition:

$$Efficiency = 10\log\left(\frac{USB\ signal\ power\ after\ SOA}{IF\ signal\ power\ before\ SOA}\right) \quad 2-(25)$$

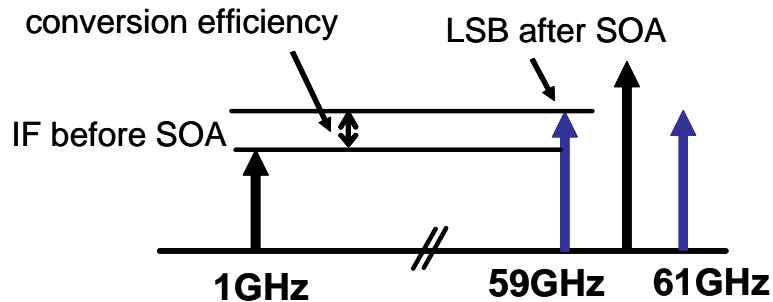


Figure 2-14. Schematic of frequency up-conversion efficiency.

For simulation conditions, the wavelength of optical heterodyne LO signals was assumed to be 1550 nm, and the mode separation was 60

GHz. For optical IF, 1535 nm wavelength, and 1 GHz IF was selected. These input optical signals can be given as

$$E_{LO}(t, z = 0) = \sqrt{p_{LO}/2}(e^{-j\Omega_{LO}t/2} + e^{j\Omega_{LO}t/2})e^{-jw_{LO}t} \quad 2-(26)$$

$$E_{IF}(t, z = 0) = \sqrt{p_{IF}(1 + m \sin \Omega_{IF}t)} \cdot e^{-jw_{IF}t} \quad 2-(27)$$

where  $P_{LO}$  and  $P_{IF}$  are the average optical power of optical LO and optical IF, respectively,  $w_{LO, IF}$  represents optical angular frequency,  $m$  is modulation index. In addition,  $\Omega_{LO, IF}$  means angular frequency of modulating LO and IF signals. For this simulation,  $\Omega_{LO}$  was  $2\pi*30$  GHz, and  $\Omega_{IF}$  was  $2\pi*1$  GHz.

These two signals were input signals to SOA, and IF modulated optical LO signals were obtained after the TMM simulation. After square-law beating calculation of PD, resulting signals were converted to frequency domain by fast Fourier transform. For photodetection simulation, it was assumed that PD has responsivity 1, and the output impedance was  $50 \Omega$ . No speed limit of PD was also assumed for this simulation. From this process, the power of IF signals before SOA and frequency up-converted signals can be obtained, and the conversion efficiency is calculated through equation 2-(25).

At first, the dependence of conversion efficiency on input optical LO signal power was calculated at different SOA bias currents of 100 mA and 150 mA. As shown in Fig. 2-15, the conversion efficiency increases with input optical LO power. Because frequency up-

conversion occurs due to signal beating between optical LO modes and cross-gain modulated IF signals, the increase of optical LO power can increase beating power, resulting in the increase of conversion efficiency. However, conversion efficiency is saturated at high LO power conditions [36]. As explained in section 2-2-2, high input optical power saturates SOA gain, so that optical gain saturation caused by high LO power decreases conversion efficiency. In this condition, XGM efficiency is also reduced, which can decrease conversion efficiency, too.

Because, XGM efficiency has dependence on input optical signal wavelengths, frequency conversion efficiency varies with different input optical IF wavelengths. To analyze this, conversion efficiency change at different optical IF wavelength conditions is calculated. SOA bias current was fixed at 200 mA, and the wavelength and the power of optical LO were 1550 nm and -5 dBm, respectively. The power of optical IF was -17 dBm. Fig. 2-16 shows calculated results. The conversion efficiency is higher at around SOA gain peak wavelength condition. Because optical gain affects conversion efficiency, high conversion efficiency can be obtained around optical gain peak. However, when the SOA is saturated by high power optical input, the gain peak is shifted to longer wavelength due to carrier depletion in SOA [36]. Therefore, the wavelength condition of maximum frequency up-conversion efficiency is a little longer than peak gain wavelength. All these simulation results show the same characteristics presented in

reference [35] and [36], where the conversion efficiency was measured experimentally.

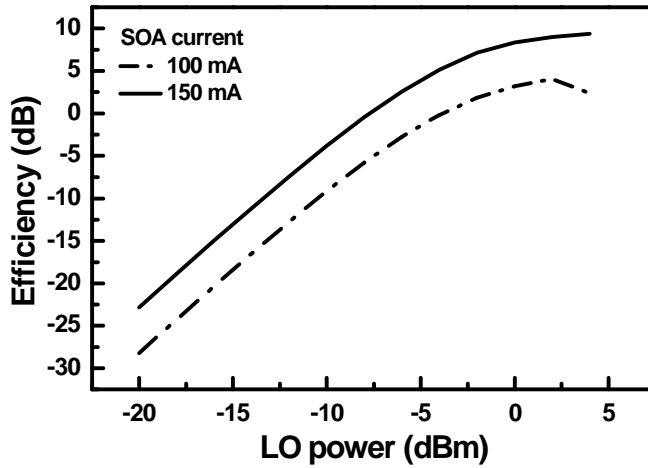


Figure 2-15. Frequency up-conversion efficiency as a function of SOA input optical LO powers.

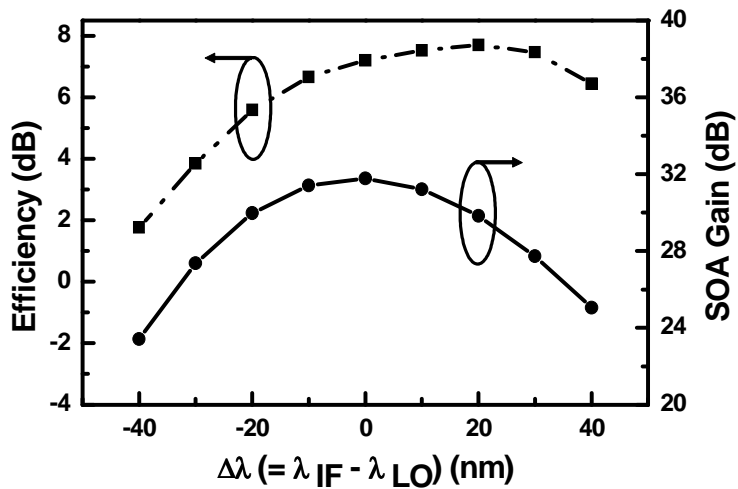


Figure 2-16. Frequency up-conversion efficiency and SOA gain as a function of input optical IF wavelengths.

## **2-3. Gigabit Data Transmission using SOA-PD Frequency Up-Converter at 60 GHz band**

60 GHz wireless systems are attracting research interests for future broadband multimedia services, wireless interconnection of backbone networks, and wireless LAN and personal area network services [1-6]. The reason is that high directivity and high oxygen absorption loss of 60 GHz signals are useful for these system applications. In addition, the license-free, wide bandwidth covering several GHz in 60 GHz band is very attractive. Therefore, bandwidth efficiency technologies in 60 GHz are not as important as several GHz-band wireless systems. In case of WPAN being discussed in IEEE 802.15.3c working group, more than 2 Gbit/s data transmission is considered. However, the implementation cost of 60 GHz systems is still very high, and RoF technology can alleviate this problem as explained before. There are many techniques to realize low cost RoF systems, and recently, transmission of gigabit data using RoF systems have been reported [57-58]. Optical remote up-conversion method using SOA-PD configuration is also very attractive for its simplicity, high conversion efficiency, LO frequency insensitivity, and so on, and its operation has enough bandwidth for gigabit data transmission [35-36].

In this chapter, measurement results of the SOA cross-gain modulation bandwidth are presented to validate the wide-bandwidth mixing operation and 1.244 Gbit/s ASK data transmission at 63 GHz is demonstrated experimentally. For frequency up-conversion experiment,

63 GHz optical heterodyne LO signals and 1.244 Gbit/s optical baseband signals are used. The dependence of bit-error rates (BERs) on optical baseband signal power in a wide wavelength range is investigated. The influence of optical LO power is also analyzed.

### **2-3-1. Measurement of SOA XGM frequency response**

In this frequency up-conversion scheme, the SOA cross-gain modulation (XGM) bandwidth is an important parameter. Since LO frequency is usually beyond the SOA XGM bandwidth, optical LO signals themselves do not cause any significant XGM. However, when data and/or IF signals are within the XGM bandwidth, they can cross-gain modulate each of optical heterodyne LO modes, resulting in frequency up-conversion after beating in a PD. Consequently, the XGM bandwidth limits data and/or IF frequencies that can be frequency up-converted. Previously, it was reported that the theoretical bandwidth of SOA-PD frequency up-conversion method can be several GHz [59-60], which is verified with the frequency response measurement of SOA XGM.

Fig. 2-17 shows the experimental setup to measure SOA XGM frequency response. For a pump signal, a 1548.5 nm DFB laser and an MZM having 3 dB bandwidth of 8 GHz were used, and for a probe signal, a 1545 nm CW light source was used. An optical bandpass filter was placed before a PD having 15 GHz bandwidth to block the pump source. The SOA was biased at 200 mA, at which condition the optical

gain and saturation output power at 1550 nm was 29 dB and 9 dBm, respectively. Before XGM frequency response measurement, the frequency response of the pump signal was measured for calibration. The frequency responses were measured with a 13.5 GHz network analyzer. The SOA input power of the probe signal was fixed at -30 dBm, and the power of pump signals was varied from -30 dBm to -12 dBm. Fig. 2-18 shows the normalized frequency response for -12 dBm pump signal and the fitted results with the double-pole system response as reported in [36]. Discrepancies between measured and fitted data at high frequencies are believed due to the incomplete SOA model. 3 dB bandwidth was extracted from the fitted results. For -30 dBm pump signals, 3 dB bandwidth is 4.2 GHz, and for -20 dBm and -12 dBm signals, 3 dB bandwidth is 4.5 GHz and 5.8 GHz, respectively, which are sufficient for gigabit data transmission using our frequency up-conversion scheme. The reason for 3 dB bandwidth increase with the pump signal power is that XGM speed is limited by the effective carrier recombination rate,  $\gamma_{\text{eff}}$ , in SOA as shown below [36, 60]:

$$f_{3dB} \propto \gamma_{\text{eff}} = \frac{1}{\tau_s} + \frac{1}{\tau_{\text{pump}}} + \frac{1}{\tau_{\text{probe}}} \quad 2-(28)$$

where  $\tau_s$  is spontaneous carrier lifetime in SOA,  $\tau_{\text{pump,probe}}$  is stimulated recombination lifetime for optical pump or probe signals. Since  $\tau_{\text{pump}}$  is inversely proportional to the SOA input pump signal power, the increase in pump signal power increases  $\gamma_{\text{eff}}$ , resulting in XGM bandwidth increase.

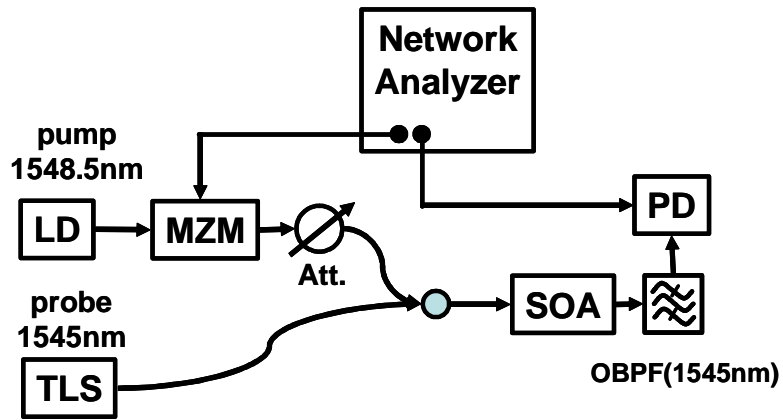


Figure 2-17. Measurement setup for SOA XGM frequency response. OBPF: Optical Band Pass Filter, TLS: Tunable Laser Source.

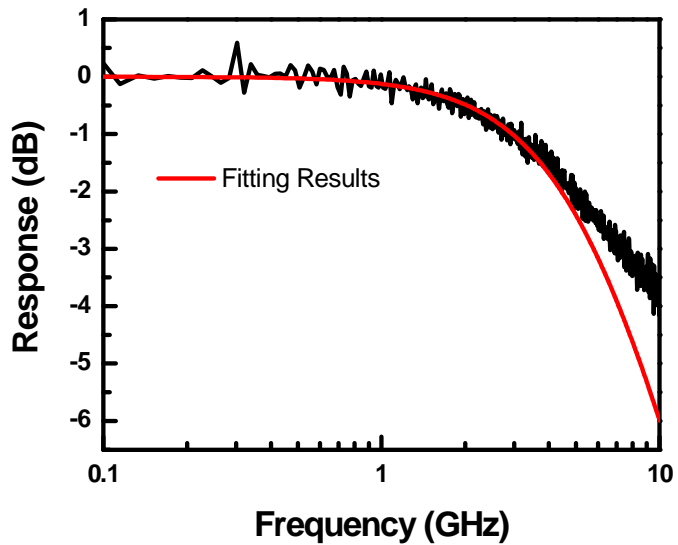


Figure 2-18. Frequency response for SOA XGM for a -12 dBm SOA input pump signal power.

### 2-3-2. Data transmission experiments and results

Fig. 2-19 shows the experimental setup for 60 GHz band RoF systems using SOA-PD frequency up-converter. The 63 GHz optical heterodyne LO signals at 1553.3 nm were generated using a DSB-SC method, for which a 40 GHz MZM was biased at the minimum transmission condition, and modulated by a 31.5 GHz RF signals. An EDFA was used to increase heterodyne optical LO power along with an optical bandpass filter having about 0.4 nm passband for amplifier noise reduction. For data signals, another wavelength optical signal was externally modulated by 2 V peak-to-peak, 1.244 Gbit/s non-return-to-zero pseudo-random bit sequences having pattern length of  $2^{15}-1$ . These two optical signals were combined, and then transmitted to the base station via 10 km optical fiber. Fig. 2-20(a) shows the spectrum of optical heterodyne LO signals at 1553.3 nm and baseband data signals at 1550 nm before SOA. The peak at 1553.3 nm marked with 'o' is due to incomplete carrier suppression with DSB-SC generation and peaks marked with 'x' are harmonics of 31.5 GHz modulation.

At the base station, two optical signals were injected into SOA, and optical heterodyne signals were cross-gain modulated by optical baseband signals. The SOA was biased at 150 mA, which gave 25 dB optical gain and 8 dBm output saturation power. Fig. 2-20(b) shows the optical spectrum after SOA, and these signals were photodetected by a 60 GHz broadband PD. In Fig. 2-20(b), spurious peaks marked with asterisks around 1550 nm are the result of optical heterodyne signals

cross-gain modulating the optical baseband signal. However, their effects are negligible to the link performance, because 31.5 GHz signals resulting from the photodetection of spurious peaks are far off from 63 GHz data signals, and their harmonics are very low as shown in the figure 2-20(b). Fig. 2-21(a) shows the frequency up-converted RF spectrum of 1.244 Gbit/s data at 63 GHz. In this measurement, the optical LO power before SOA was -13 dBm, and the optical baseband signal power and wavelength was -13 dBm and 1550 nm, respectively. As shown in the figure, baseband data signals are successfully up-converted to 63 GHz. The peaks marked with asterisks having 1.244 GHz separation appear because baseband data are ASK modulated. The center peak at 63 GHz due to optical LO signals can saturate amplifiers and limit output data signal power at the base station. Other modulation techniques using antipodal signals and LO rejection filtering at 60 GHz band can avoid this problem.

To demodulate 63 GHz ASK data signals, a commercially-available direct conversion demodulator based on a Schottky diode was used. In this demodulator, input 63 GHz data signals are recovered at baseband due to square-law detection characteristics of the Schottky diode. The data signal was attenuated by 25 dB since the demodulator that we used has a maximum power limit of -30 dBm. Fig. 2-21(b) shows the RF spectrum of 1.244 Gbit/s baseband data. After baseband amplification and additional low pass filtering of data signals, demodulated data

signals were analyzed by a sampling oscilloscope for eye diagram measurement, and an error detector for BER measurement.

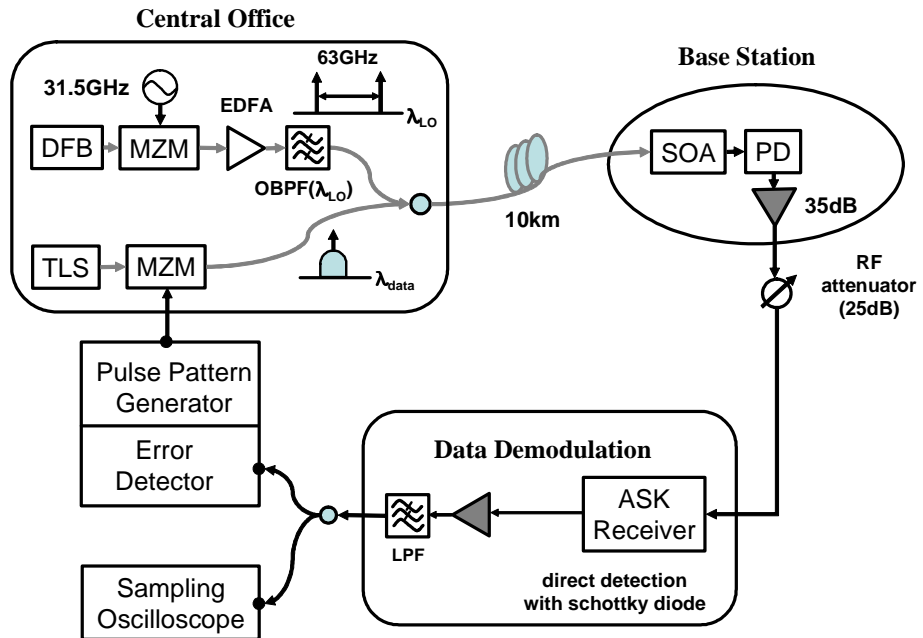
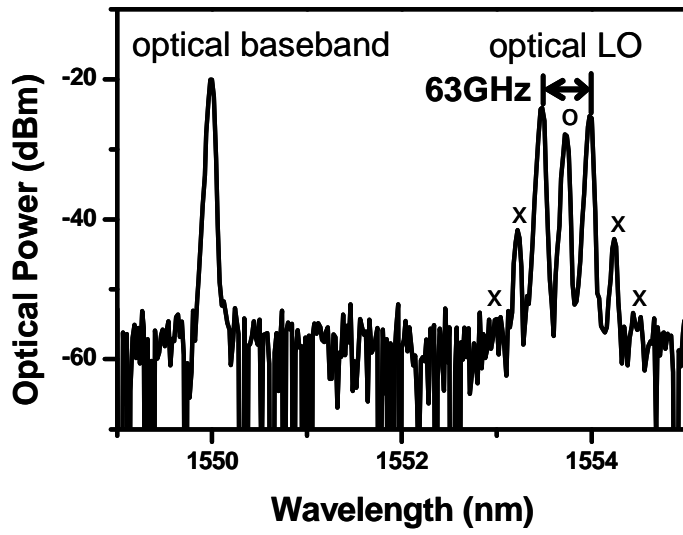
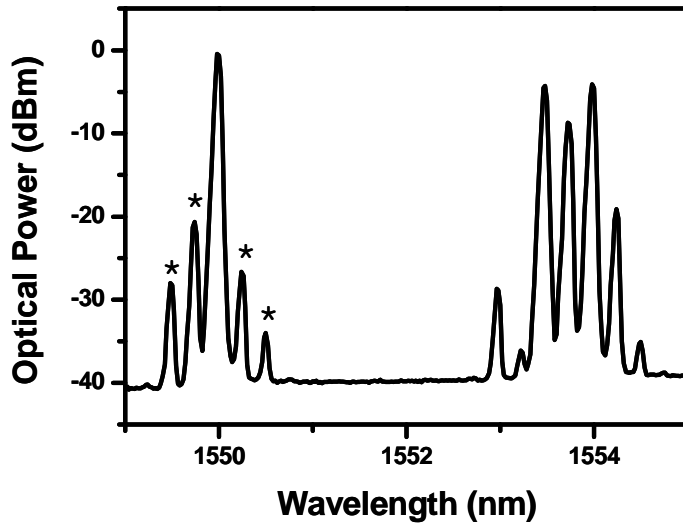


Figure 2-19. Experimental setup for 1.244 Gbit/s 63 GHz RoF downlink data transmission. LPF: LowPass Filter.

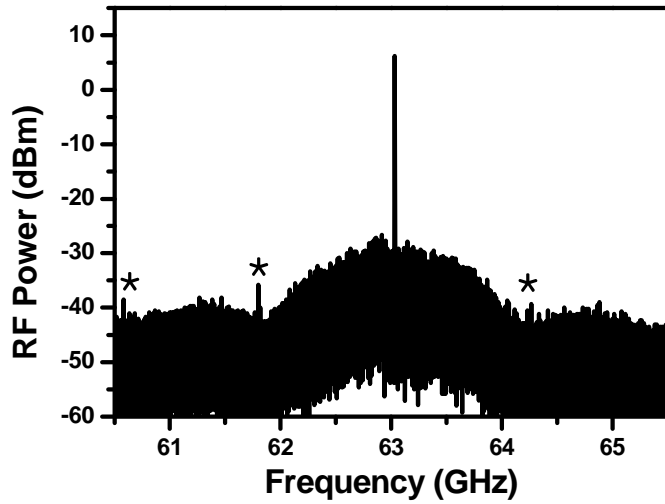


(a)

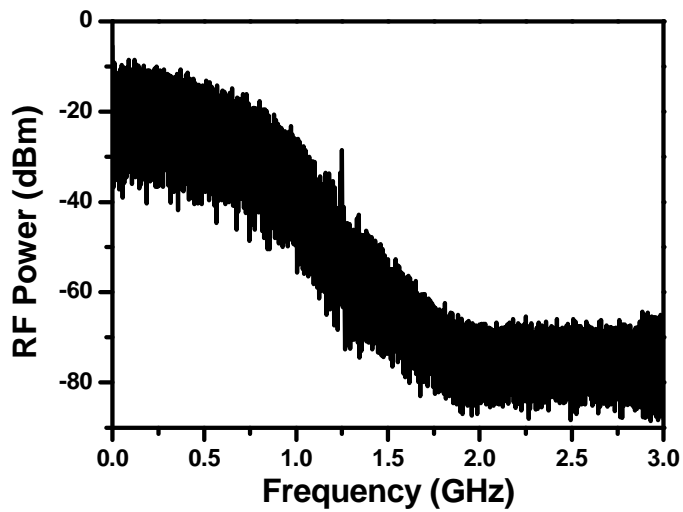


(b)

Figure 2-20. Optical spectrum of downlink optical LO and data signals before SOA (a) and after SOA (b).



(a)



(b)

Figure 2-21. RF spectrum of frequency up-converted 63 GHz data signals (a) and demodulated baseband signals (b). Resolution bandwidth for both spectra is 1 MHz.

Fig. 2-22 shows the measured BER as a function of the optical baseband signal power before SOA at several different wavelengths varying from 1540 nm to 1570 nm. The optical baseband signal power before SOA influences frequency conversion efficiency affecting signal-to-noise ratios (SNRs), but the optical power after SOA does not change very much due to SOA gain saturation. For this measurement, optical LO signal power before SOA was fixed at -13 dBm. As can be seen in the figure, the BER decreases as optical baseband signal power increases. The increased optical data signal power before SOA can improve XGM efficiency in SOA, which results in SNR improvement. In the wavelength range from 1550 nm to 1570 nm, the power penalty for  $10^{-9}$  BER is less than 1 dB. The eye diagram for error free conditions at 1550 nm data signals is also shown in Fig. 2-22. However, the power penalty for the 1540 nm wavelength signal is about 2.5 dB. The unsaturated gain spectrum of the SOA used in this study has a peak at around 1550 nm. But the SOA gain peak shifts to longer wavelength due to the carrier depletion when the SOA gain is saturated, which is well explained in chapter 2-2. Therefore, frequency up-conversion efficiency is higher for wavelengths longer than 1550 nm. For shorter wavelength signals, large power penalties occur due to low frequency up-conversion efficiency. Nevertheless, error-free data transmission is accomplished for a wide range of data wavelengths proving that WDM data transmission is possible with this scheme.

The dependence of BER on optical LO power was also measured. The optical data signal power was fixed at -13 dBm, and the data wavelength was 1550 nm. Fig. 2-23 shows the results of optical LO power dependence. As the optical LO power increases, the BER is decreased. The reason for this improvement is that the high optical LO power results in high frequency up-conversion efficiency as explained in chapter 2-2.

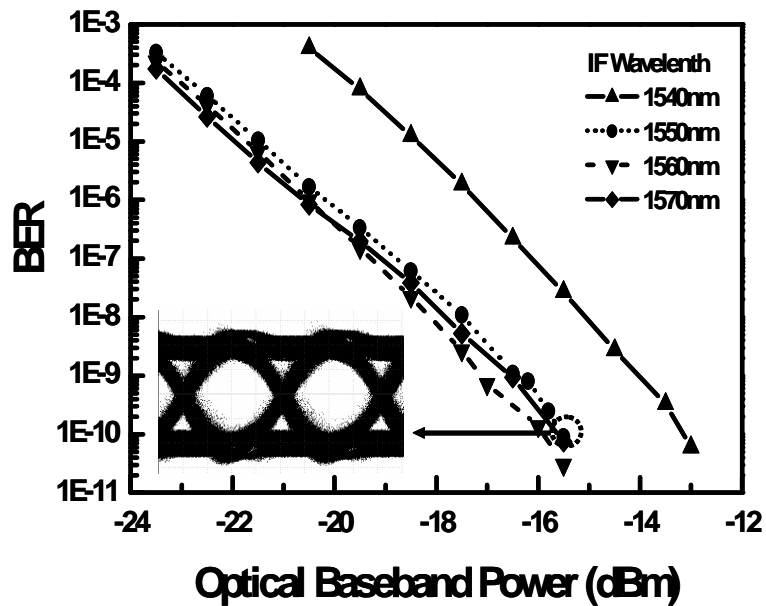


Figure 2-22. Dependence of BERs performance on SOA input optical baseband signal power.

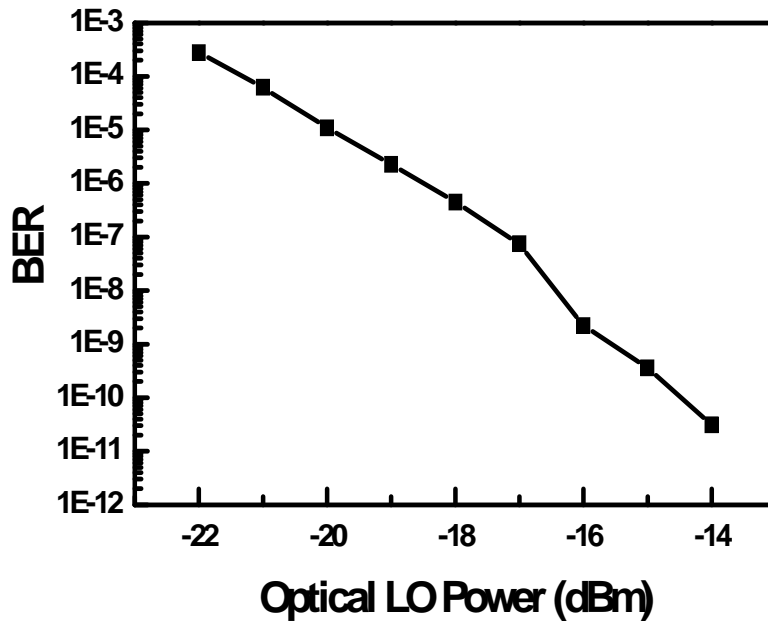


Figure 2-23. Dependence of BER performance on SOA input LO signal power.

As explained in this section, error-free broadband data transmission was performed successfully. However, this experimental setup for downlink data transmission and the SOA used for frequency up-conversion did not optimized for the best performance. In RoF link, link loss is a very important parameter, and especially, optical to electrical conversion loss and vice versa affect system performance very much. In this downlink setup, the optical components are not designed for low link loss in RoF systems, which should be improved for the best system performance. In addition, SOA is not also designed for this frequency up-conversion. As shown in previous chapters, high

SOA gain and XGM efficiency can increase frequency conversion efficiency, which surely results in system performance enhancement. Furthermore, the low noise SOA design can help increasing SNR after frequency up-conversion. The used RF components and the 60 GHz ASK receiver are not also designed for this experiment. Due to the input power limit of the ASK receiver, the input data signal power is reduced unnecessarily. In addition, other RF components for data demodulation have a room for better system performance in 60 GHz. Therefore, the system performance can be surely improved after these optimizations.

### **3. Remote Frequency Down-Conversion Using EAM**

#### **3-1. Uplink RoF Systems for Bi-Directional Data Transmission**

The conventional wireless networks consist of downlinks and uplinks to deliver data signals to and from mobile users. 60 GHz wireless systems also need bi-directional links to make full access between service providers and users, and the base station design for full links is another challenging problem. For simple base stations, RoF technologies can be used, however, it is also very difficult. Fig. 3-1 shows two RoF schemes for uplink data transmission. The direct transmission of RF signals as shown in Fig. 3-1(a) looks very simple. The received RF signals are converted to optical domain without any electrical processing. However, high speed optical components are needed at each base station, which is a burden contrary to downlink RoF systems having high speed components at the central station. Another system configuration is that high frequency data signals are frequency down-converted to IF/baseband, and then transmitted to the central station after electrical-to-optical conversion with low speed optical components. The problem is that high frequency electrical devices for frequency down-conversion and high speed signal processors should also be equipped at each base station.

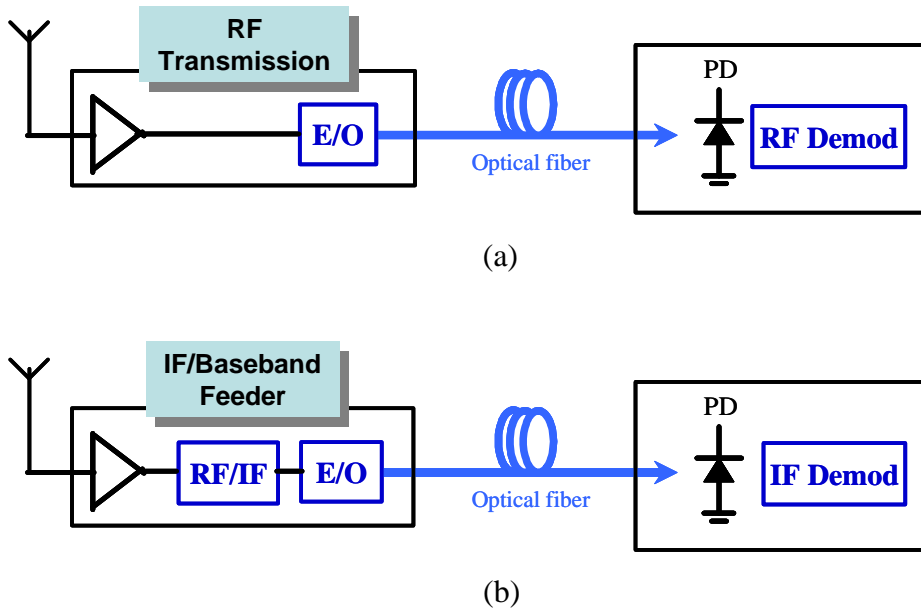


Figure 3-1. Uplink RoF system configurations. (a) direct RF transmission systems, (b) IF/Baseband Feeder systems.

EAM transceivers can allow the simple antenna base station architecture for bi-directional RoF links because EAM can perform the dual-functions of photodetection and optical modulation [28-32]. EAM is a reverse biased p-i-n diode with bulk active region [33] or multiple quantum-wells [34] as the absorption layer. Bias conditions determine the amount of light absorption, and optical modulation is possible by the modulation of bias voltages. In addition, photocurrent is generated at the absorption layer like conventional PDs. Fig. 3-2 shows uplink RoF systems using EAM. Uplink millimeter-wave signals modulate optical signals transmitted from the central station using EAM, which eliminates optical sources for uplink data transmission. As shown in

Fig. 1-9, very simple bi-directional RoF systems can be realized by combining with downlink RoF system configuration. However, as explained in chapter 1, direct transmission of double-sideband optical signals having uplink millimeter-wave data suffers dispersion-induced signal fading, and low frequency IF optical signal transmission insensitive to chromatic dispersion can be used for uplink, too. It also needs expensive electrical mixers and oscillators for frequency down-conversion from millimeter-wave frequency to IF. To eliminate this problem, various frequency down-conversion schemes using EAM have been introduced [61-64].

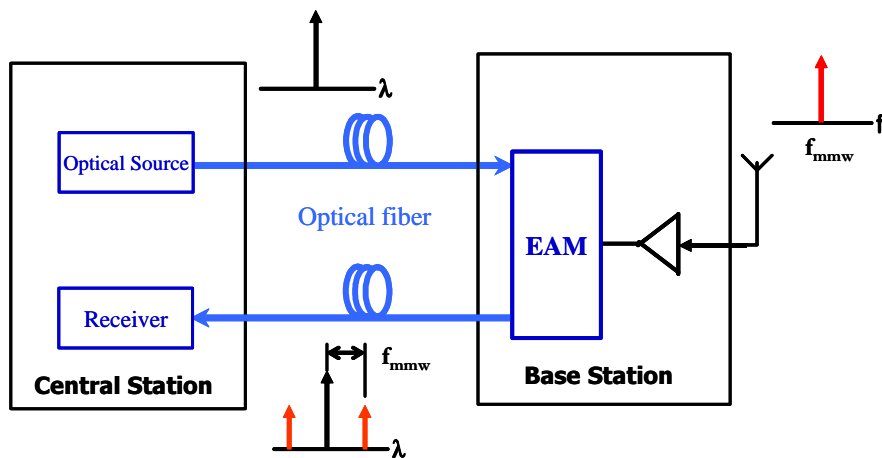


Figure 3-2. Uplink millimeter-wave RoF systems based on EAM.

In this dissertation, an EAM-based optoelectronic millimeter-wave frequency down-conversion method is proposed for IF-band optical uplink transmission. Using remotely-fed millimeter-wave optical

heterodyne LO signals, the uplink millimeter-wave signals are optoelectronically frequency down-converted to the IF-band optical signals by EAM, and then transmitted to central station. Therefore, for uplink data transmission, only EAM is needed in base stations. Fig. 3-3 shows the schematic of proposed frequency down-conversion uplink systems using EAM, which is compared with conventional remote frequency down-conversion RoF systems. The basic idea was proposed in paper [61] and [62], but this dissertation will expand this idea to 60 GHz uplink system applications, and analyze its characteristics in detail. In addition, a bi-directional RoF link using this idea will be presented in chapter 4.

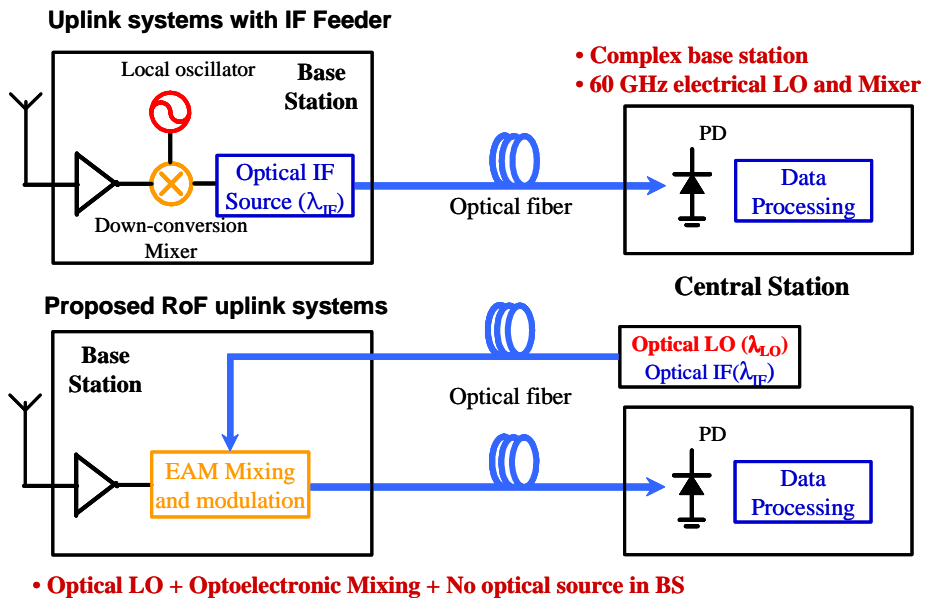


Figure 3-3. Remote frequency down-conversion RoF uplink systems using EAM.

## 3-2. Operation Principle of EAM Frequency Down-Conversion

### 3-2-1. Characteristics of EAM

EAM is the abbreviation of electroabsorption modulator, where ‘electroabsorption’ means that the amount of light absorption is changed by the electric field applied to semiconductors, and ‘modulator’ means that such characteristics are used for optical modulation. Although the insertion loss is a weakness of EAM, its other advantages such as low driving voltage, low or negative chirp, high speed operation, integration with DFB laser are very attractive to optical communications. Two types of EAM are well used, one of which is bulk type using a Franz-Keldysh effect [33], and another is multiple quantum-well type using a Quantum Confined Stark Effect (QCSE) [34]. Both are simply designed as a reverse biased p-i-n diode, and both effects are predominant at near the bandgap of semiconductors. In this dissertation, the used EAM had multiple quantum-well structures, so that the simple operation principle based on QCSE is discussed [34, 65]. Fig. 3-4 shows the change of single quantum-well layer explaining EAM operation. As the reverse bias applied to the p-i-n diode increases, the whole band edge absorption shifts to lower energies resulting from the distortion of single quantum-well potential. In Fig. 3-4, the energy  $E_{e1-h1}$  decreases as the applied field increases. Therefore, the increase of reverse bias can make the

semiconductor absorb optical signals having lower energy compared with bandgap energy ( $E_g$ ), and the transmitting optical power from the semiconductor is determined by the applied electrical field controlled by reverse bias conditions.

### Quantum-Well

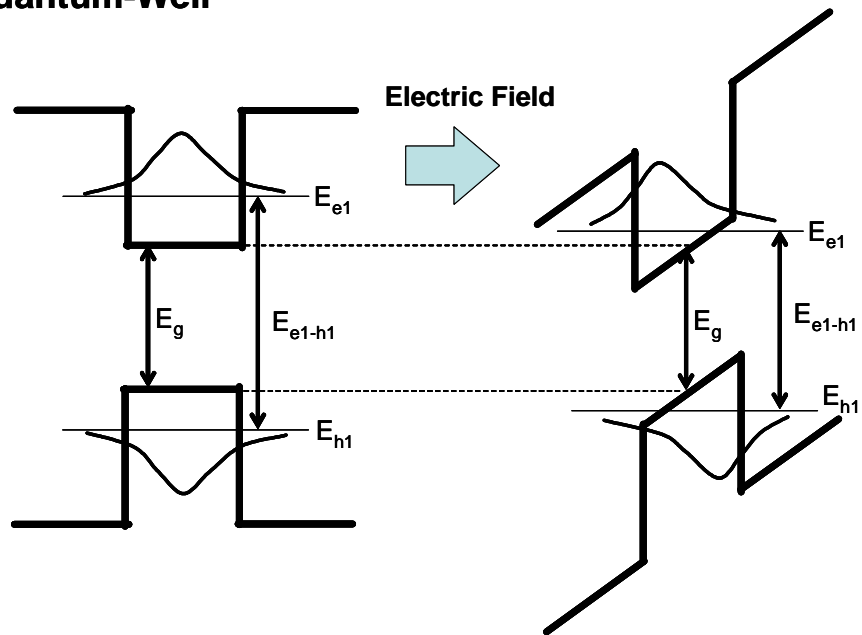


Figure 3-4. Operation principle schematic of multiple quantum-well EAM.

Such characteristics are used for optical modulation, and EAM transfer function can be expressed as the following [30]:

$$P_{out}(V) = P_{in} \exp(-\Gamma \alpha(V)L) \quad 3-(1)$$

where  $P_{in, out}$  is the input and output optical power of EAM,  $\Gamma$  is confinement factor,  $\alpha$  is absorption coefficient depending on applied bias voltage, and  $L$  is the length of EAM. The interesting thing is that

the reverse shape of EAM transfer function is the same as the absorption one of EAM, i.e. some of optical signals not transmitting EAM are absorbed in EAM [66].

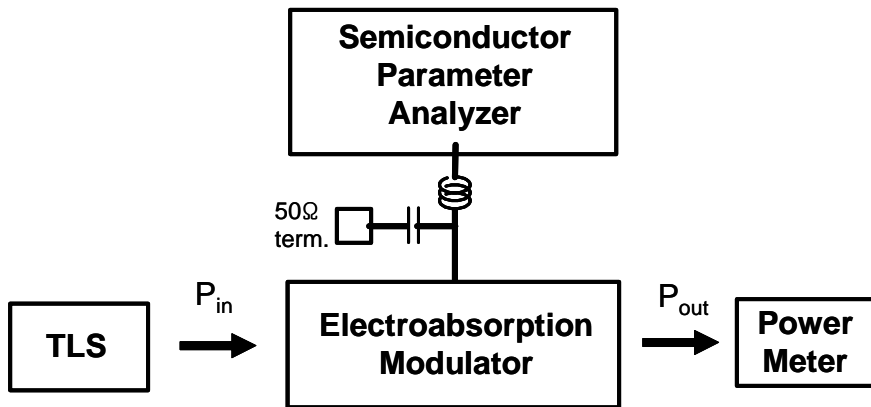
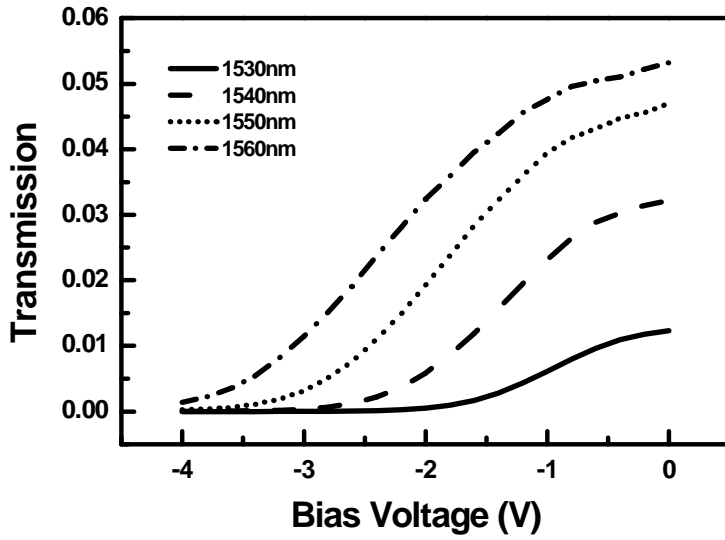


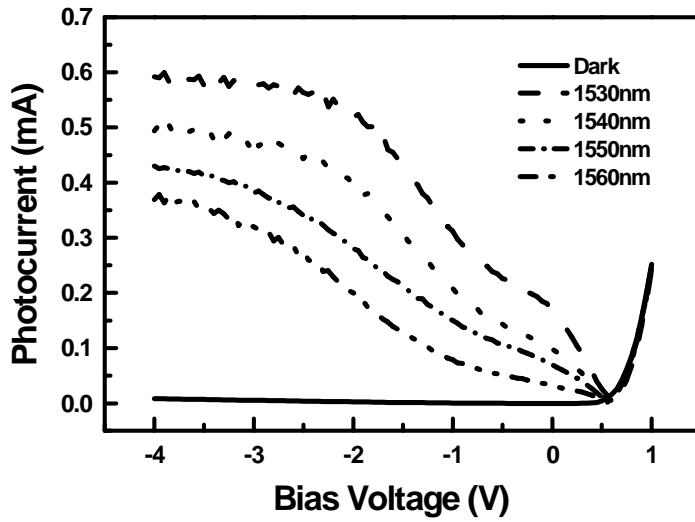
Figure 3-5. Experimental setup to measure optical transmission and absorption characteristics of EAM.

Fig. 3-5 shows the measurement setup of optical transmission and absorption characteristics of EAM. A tunable light source was used to change wavelength of input optical signals. Input optical power was fixed at 0 dBm, and output power was measured by an optical power meter. A semiconductor parameter analyzer was used to apply reverse biases to EAM, and to measure photocurrent generated from input optical signal absorption. The used EAM was designed and fabricated for 1550 nm optical signal modulation by Electronics and Telecommunications Institute (ETRI) of Korea, and details about EAM are well explained in [67-68].

Fig. 3-6(a) shows optical transmission curve of EAM at different wavelength conditions. Optical transmission means the optical power ratio of output signals to input signals. As the applied reverse bias increases, the transmitting signal power decreases due to electroabsorption phenomenon. For short wavelength optical signals, large signal absorption in EAM occurs. Since shorter wavelength optical signals have higher energy than longer wavelength optical signals, it is easily absorbed in EAM. For analog signal modulation, the EAM is usually biased at maximum slope efficiency point, where the highest link gain can be obtained. The photocurrent measurement shows the absorption characteristics of EAM. As shown in Fig. 3-6(b), large signal absorption occurs at high reverse bias conditions due to the same electroabsorption effects, and also short wavelength signals generate large photocurrent. These represent that high reverse bias and short wavelength signals are necessary for efficient signal detection using EAM. As explained above, EAM can perform both optical modulation and photodetection, which is useful for EAM to be adopted in base stations of bi-directional links. The problem is that the bias and wavelength conditions for optimum detection and modulation are different, so that system designs considering this trade-off are necessary.



(a)



(b)

Figure 3-6. Optical transmission (a) and photodetection characteristics (b) of EAM as a function of applied voltage at different input wavelength conditions.

### 3-2-2. Optoelectronic frequency down-conversion in EAM

The proposed frequency down-conversion technique uses three functions of EAM, photodetection, optoelectronic mixing, and optical modulation [61, 62, 69]. Fig. 3-7 schematically shows the operation principle of the optoelectronic frequency down-conversion scheme for uplink data transmission. To obtain LO signals, the optical heterodyne technique is used, and the generated heterodyne signals can be given by

$$E_{LO} = E_0(\cos[2\pi(f_0 + \frac{f_{LO}}{2})t] + \cos[2\pi(f_0 - \frac{f_{LO}}{2})t]) \quad 3-(2)$$

where  $E_{LO}$  represents electrical field of optical LO signals,  $E_0$  is electrical field amplitude,  $f_0$  is center frequency of optical LO,  $f_{LO}$  is LO frequency. The optical phase terms are neglected for simplicity. This optical LO at  $\lambda_{LO}$  are transmitted from the central station, and  $f_{LO}$  signals are generated at the base station by EAM photo-detection. This process can be written as

$$I_{LO} = RE \cdot E^* = RI_0 \cos(2\pi f_{LO} t) \quad 3-(3)$$

where  $R$  is responsivity of EAM photodetection, and  $I_0$  is generated signal amplitude coming from optical signals. At the same time, the EAM is modulated by  $f_{RF}$  uplink signals given by

$$V_{RF} = V_0 \cos(2\pi f_{RF} t) \quad 3-(4)$$

where  $V_{RF}$  represents uplink RF voltage signals, and  $V_0$  is the amplitude of modulating signals. The responsivity,  $R$  of EAM is dependent on applied voltage, which is well shown in Fig. 3-6(b).

Therefore, nonlinear mixing terms are generated by uplink RF signal modulation, which can be given by [61]

$$I_{mix} = \left. \frac{dR}{dV} \right|_{V=V_b} I_0 V_0 \cos(2\pi(f_{RF} \pm f_{LO})t) \quad 3-(5)$$

where  $dR/dV$  is first-order derivative of responsivity evaluated at DC bias voltage,  $V_b$ . As given in equation 3-(5), frequency down-converted IF signals ( $f_{IF}=f_{RF}-f_{LO}$ ) are produced. This nonlinear optoelectronic mixing process is well explained in [61-62]. Next, to deliver these uplink signals to central station, the  $\lambda_{IF}$  uplink optical carrier is modulated by frequency down-converted IF signals as given by

$$P_{out} = P_{in} \exp[-\Gamma\alpha(I_{mix})L] \quad 3-(6)$$

, and is transmitted to the central station with negligible dispersion-induced signal fading problems. The equation 3-(6) is also shown in chapter 3-2-1. After filtering of optical LO signals, optical IF signals are photodetected at the central station, and frequency down-converted IF signals are generated. Because uplink RF signals also modulate optical LO signals, they should be filtered out not to generate unwanted IF signals coming from optical LO [62]. Effectively, a single EAM device is acting as a four-terminal device which simultaneously performs photo-detection, frequency down-conversion, and uplink optical IF signal modulation.

Fig. 3-8 shows the experimental verification results using 25 GHz optical heterodyne LO signals and 25.2 GHz uplink RF signals. When 25 GHz optical heterodyne signals are photodetected in EAM along

with electrical modulation of 25.2 GHz, 200 MHz IF signals are generated and modulate another optical source provided from the central station. After photodetection of optical IF, 200 MHz IF signals are generated at the central station as shown in Fig. 3-8(a). In this photodetection, EAM modulating 25.2 GHz uplink signals and photodetected 25 GHz LO signals can be also obtained as shown in Fig. 3-8(b), which indirectly shows the frequency down-conversion processes. Although 25.2 GHz RF signals are generated at the central station, this RF signal power is dependent on chromatic dispersion of optical fibers.

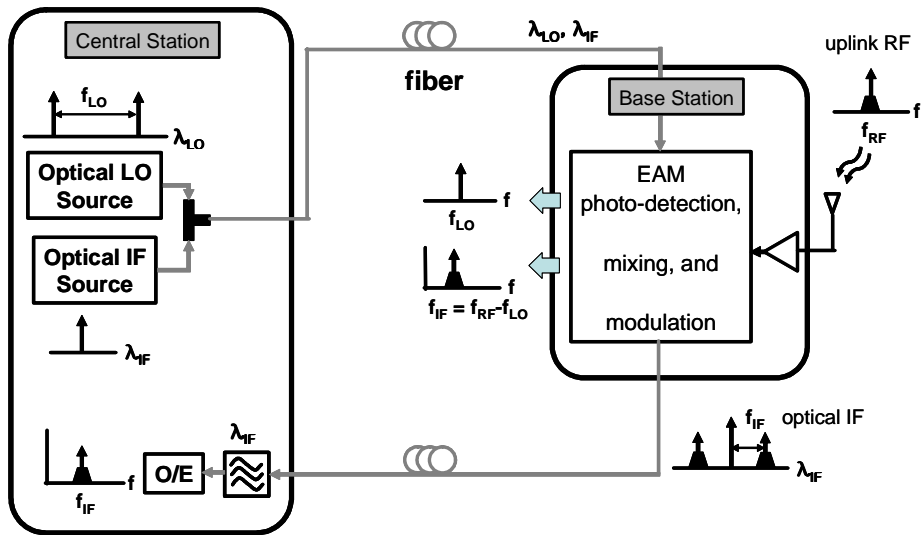
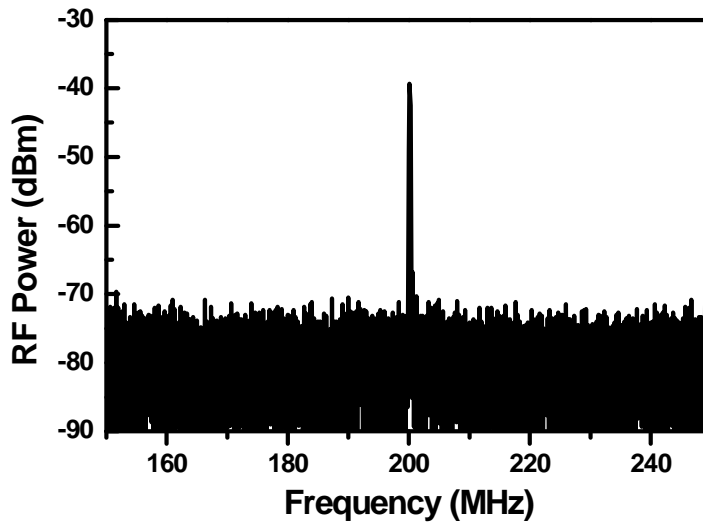
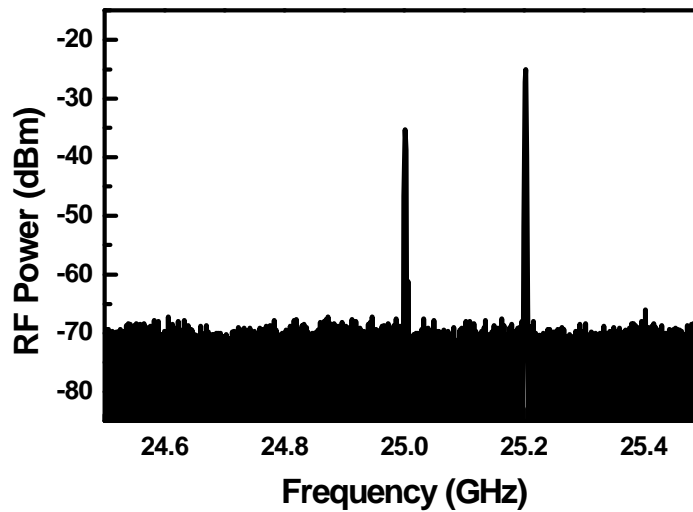


Figure 3-7. Schematic of optoelectronic frequency down-conversion for uplink RoF systems.



(a)



(b)

Figure 3-8. RF spectrum of frequency down-converted signals (a) and RF and LO signals after photodetection of optical IF signals.

### **3-3. Conversion Efficiency of EAM Frequency Down-Conversion**

For frequency converters, the conversion efficiency is an essential parameter to design RF systems of base stations [70]. Therefore, in this chapter, the frequency down-conversion efficiencies of proposed EAM frequency down-converter are investigated at 30 GHz band. To measure it, internal conversion efficiency is defined to exclude link loss effects that do not influence down-conversion process [10]. In down-conversion systems, signal loss caused by electrical to optical conversion and optical to electrical conversion, and fiber and waveguide transmission loss affect frequency converted signal power, which is not related to the real frequency conversion processes. Therefore, internal conversion efficiency should be defined for this frequency down-converter. Using this definition, down-conversion efficiency is investigated as functions of EAM biases, optical local oscillator (LO) signal powers, and optical IF signal powers and wavelengths, all of which are important system parameters in RoF links.

#### **3-3-1. Experimental setup and conversion efficiency definition**

Fig. 3-9 schematically shows the experimental setup to measure frequency down-conversion efficiency. For 29.6 GHz optical LO signals, 8 dBm, 29.6 GHz RF signals modulated a 40 GHz Mach-Zehnder modulator biased at the quadrature point. In real systems, optical heterodyne LO signals should be used to avoid dispersion

problems, however, in this experiment double-sideband optical LO signals are used for simplicity, and it does not affect frequency down-conversion characteristics because the same electrical LO signals are generated. The wavelength of optical LO was 1553.3 nm. For the optical IF signals, a tunable laser source was used. Fig. 3-10(a) shows the optical spectrum of optical LO and IF signals measured before EAM. These two optical signals were combined and injected into EAM, and 29.6 GHz signals were generated by EAM photodetection. The used EAM was designed and packaged for 40 GHz broadband applications in ETRI. When 30 GHz RF signals for frequency down-conversion modulated EAM, optoelectronic mixing with photodetected 29.6 GHz signals produced frequency down-converted signals at 400 MHz by EAM nonlinearity, which were then modulated optical IF signals. After the optical amplification and filtering of optical IF signals, they are photodetected using a 32 GHz broadband photodetector, and 400 MHz frequency down-converted IF signals were generated. Fig. 3-10(b) shows the optical spectrum measured after optical filtering of optical LO signals not to affect conversion efficiency calculation. As shown in Fig. 3-10(b), optical LO signals are suppressed enough. During the photodetection process, 30 GHz RF signals were also generated, because 30 GHz signals modulated optical IF signals, too. The small peaks marked with 'x' are the result of 30 GHz signal modulation.

Fig. 3-11(a) and (b) show the RF spectra of frequency down-converted signals at 400 MHz and photodetected 30 GHz signals, respectively. Input optical LO power was 3 dBm and optical IF power was 0 dBm. The wavelength of optical IF was 1550 nm. With these results, the frequency down-conversion efficiency can be defined as the photodetected signal power ratio of frequency down-converted signals at 400 MHz (A in Fig. 3-11(a)) to 30 GHz RF signals (B in Fig. 3-11(b)), by which link loss effects on frequency down-converted signals are removed and internal conversion efficiency can be calculated.

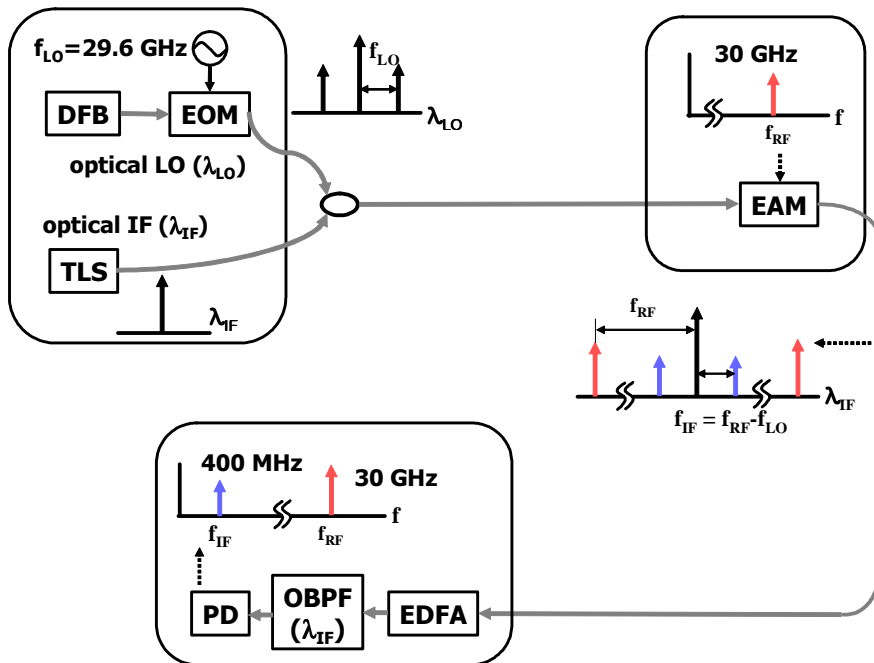
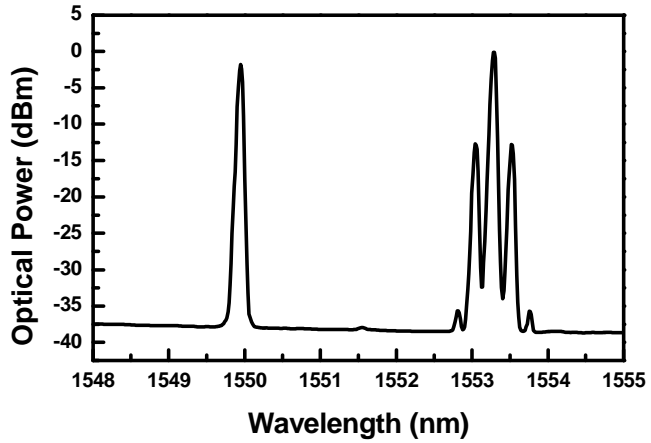
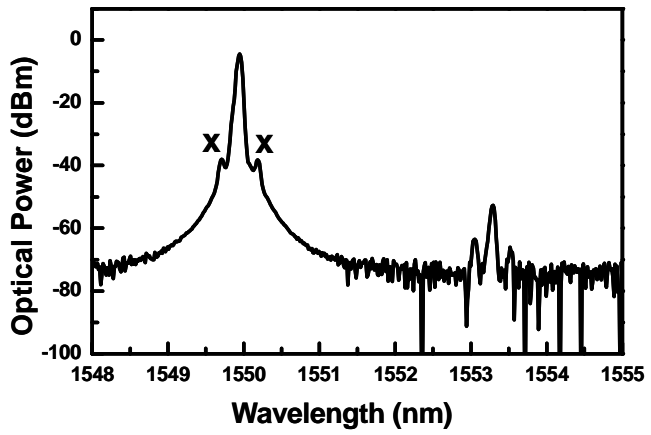


Figure 3-9. Experimental setup to measure frequency down-conversion efficiency. EOM : Electrooptic Modulator.

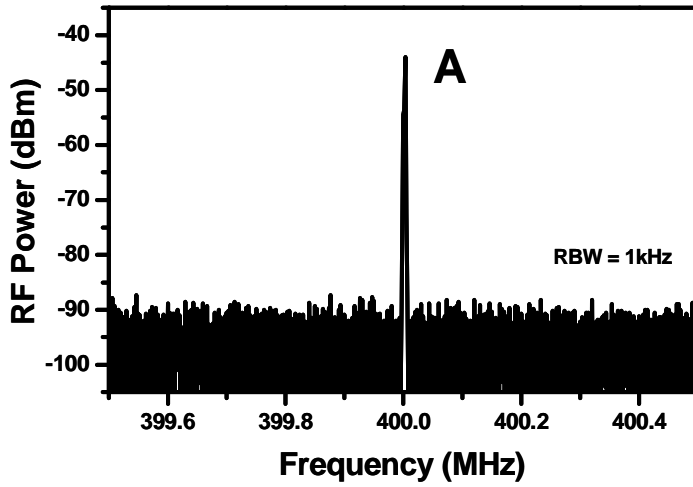


(a)

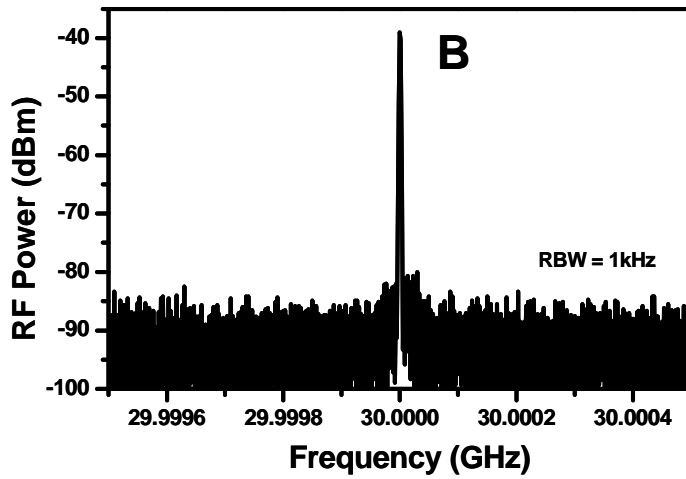


(b)

Figure 3-10. Optical spectrum measured before EAM (a) and after optical filtering of optical LO signals (b).



(a)



(b)

Figure 3-11. RF spectrum of uplink IF signals (a) and RF signals (b) after photodetection of optical IF signals.

### 3-3-2. Down-conversion efficiency results

Fig. 3-12 shows the dependence of frequency down-conversion efficiency on EAM bias. The power of optical LO was 3 dBm, and optical IF at 1550 nm was 0 dBm. After the RF power measurement of each signal, the gain of an electrical amplifier for 400 MHz signals and the different frequency response of the 32 GHz PD were corrected for the efficiency calculation. These corrections were applied to every down-conversion efficiency measurement. As shown in the figure, the conversion efficiency is the highest at around -1.4 V, and the dependence of bias voltage is similar to the EAM modulation efficiency characteristics, i.e. high conversion efficiency is obtained at around bias conditions for highest slope efficiency. Because the frequency down-converted IF signals should modulate optical IF signals, EAM modulation efficiency affects down-conversion efficiency very much in this frequency converter.

Next, down-conversion efficiency as a function of EAM input optical LO power was measured. The power of optical IF at 1550 nm was 0 dBm, and the EAM was biased at -1.4 V. The LO signal power is an important parameter for electrical frequency converters, because it determines the performance of frequency converters very much. For this frequency down-converter, optical LO power affects the conversion efficiency greatly. Fig. 3.13 shows the measured results of frequency down-conversion efficiency. When optical power increases 1 dB, photodetected LO power inside EAM increases 2 dB, which results

in the about 2 dB increase of frequency down-converted signal power. However, the change of optical LO power hardly affects 30 GHz signals. Therefore, the slope of frequency down-conversion efficiency according to optical LO power is about two. The conversion efficiency saturation is also observed when optical LO power is larger than -2 dBm, which is due to the saturation of EAM photodetection.

The dependence of frequency down-conversion efficiency on EAM input optical IF signals was also evaluated. Fig. 3.14(a) shows the effects of optical IF power on down-conversion efficiency. For this measurement, the optical LO power was 3 dBm, and optical IF wavelength was 1550 nm. EAM was biased at -1.4 V. The frequency down-conversion efficiency was decreased about 5 dB with the increase of optical IF power from -15 dBm to 0 dBm. In fact, the down-conversion efficiency should remain constant because the optical IF power equally affects both frequency down-converted signals and photodetected 30 GHz signals. However, when the optical IF power increased 1 dB, the frequency down-converted signals increased at the rate of about 1.7 dB contrary to the 2 dB increase of 30 GHz RF signals, which makes about 5 dB efficiency change. This is believed due to EAM saturation caused by high optical LO power of 3 dBm.

Fig. 3.14(b) shows the measurement results of down-conversion efficiency as a function of optical IF wavelength. The optical LO and IF power was 3 dBm and 0 dBm, respectively. EAM was biased at -1.4 V. The wavelength of optical IF was changed from 1535 nm to 1565

nm. As shown in the figure, the down-conversion efficiency is changed about 2.5 dB within this optical IF wavelength range. This range is wide enough to adopt this frequency down-converter for the WDM RoF systems.

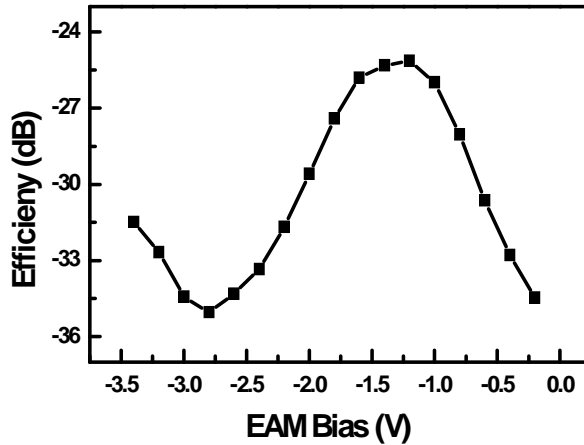


Figure 3-12. Frequency down-conversion efficiency as a function of EAM bias condition.

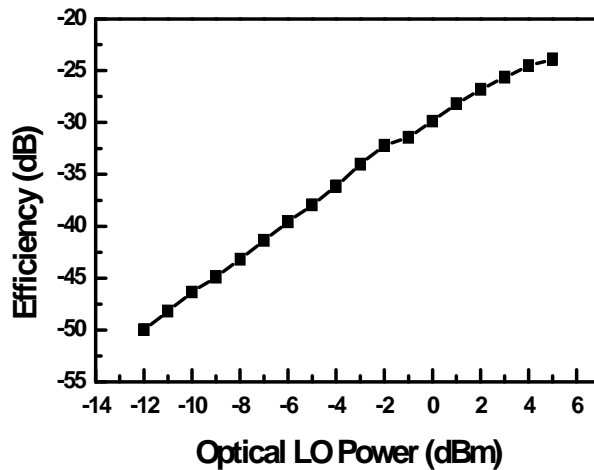
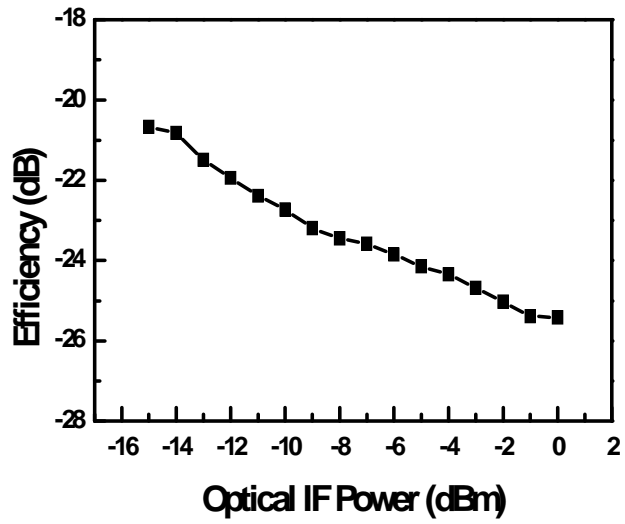
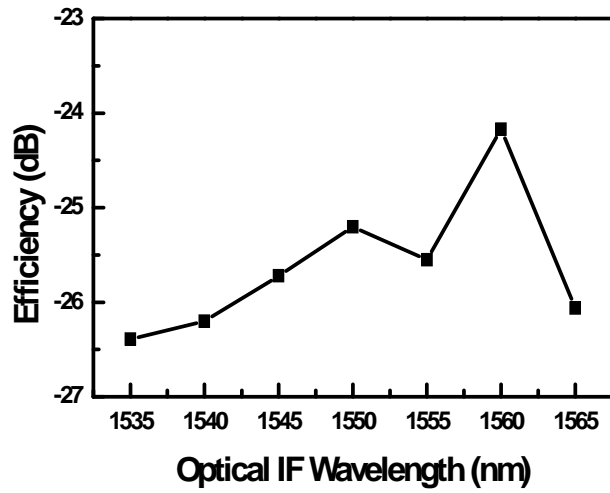


Figure 3-13. Frequency down-conversion efficiency as a function of EAM input optical LO power.



(a)



(b)

Figure 3-14. Frequency down-conversion efficiency as a function of EAM input optical IF power (a) and wavelength (b).

### **3-4. 60 GHz Uplink RoF Systems using Frequency Down-Conversion**

In previous chapters, the operation principle of EAM optoelectronic frequency down-conversion and the conversion efficiency characteristics are investigated. Finally, 60 GHz band uplink RoF systems are experimentally demonstrated based on remote frequency down-conversion using EAM. For this, 59.5 GHz optical LO was delivered from the central station, and 60 GHz QPSK data signals modulated EAM. After frequency down-conversion processes, 500 MHz IF data signals were produced at the central station and system performance was analyzed.

#### **3-4-1. Experimental setup and results for 60-GHz data transmission**

The EAM used in this experiment has a multiple-quantum well structure and is packaged for 60 GHz narrow-band application. Details of EAM characteristics can be found in [67-68]. Although a different kind of EAM device from the one in previous chapters was used for this experiment, the optical transmission and photodetection characteristics as a function of bias voltages are similar to the results shown in Fig. 3-6(a) and (b). Fig. 3-15 shows measured  $S_{11}$  parameter characteristics at the input RF port. As can be seen in the figure,  $S_{11}$  parameter values near 60 GHz are small enough to transmit about 2 GHz bandwidth data signals.

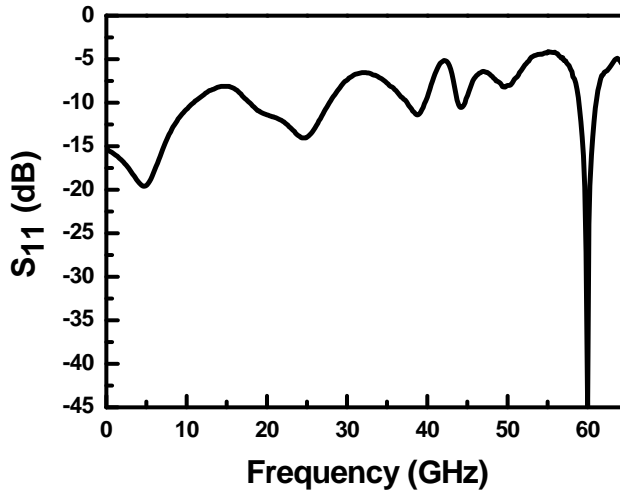


Figure 3-15.  $S_{11}$  parameter characteristics at the input port of 60 GHz narrow-band packaged EAM.

Fig. 3-16 shows the experimental setup for the 60 GHz optoelectronic frequency down-conversion experiment. 59.5 GHz optical heterodyne LO signals were generated by an MZM biased at the minimum transmission point with 29.75 GHz signal for DSB-SC method. An EDFA was used after the MZM to increase optical LO power. For the uplink optical carrier, a DFB laser at  $\lambda_{IF} = 1552.5$  nm was used. These two signals were combined by a 3-dB optical coupler and injected into EAM. For generating 60 GHz uplink RF signals, a subharmonic RF mixer was used. For IF signal source, either CW signals at 500 MHz or 10 Mbps QPSK data signals at 500 MHz were used. After the RF mixer, an RF bandpass filter was placed for reducing image signals from the mixer. The resulting 60 GHz signals

were applied to EAM after passing an amplifier and a bias-T. At the central station, a 20 dB gain EDFA was used to compensate the insertion loss of EAM, and an optical attenuator was placed not to exceed the PD saturation optical power. An optical bandpass filter was also used to suppress unwanted optical heterodyne LO signals. In the present investigation, all the measurements were done in back-to-back conditions.

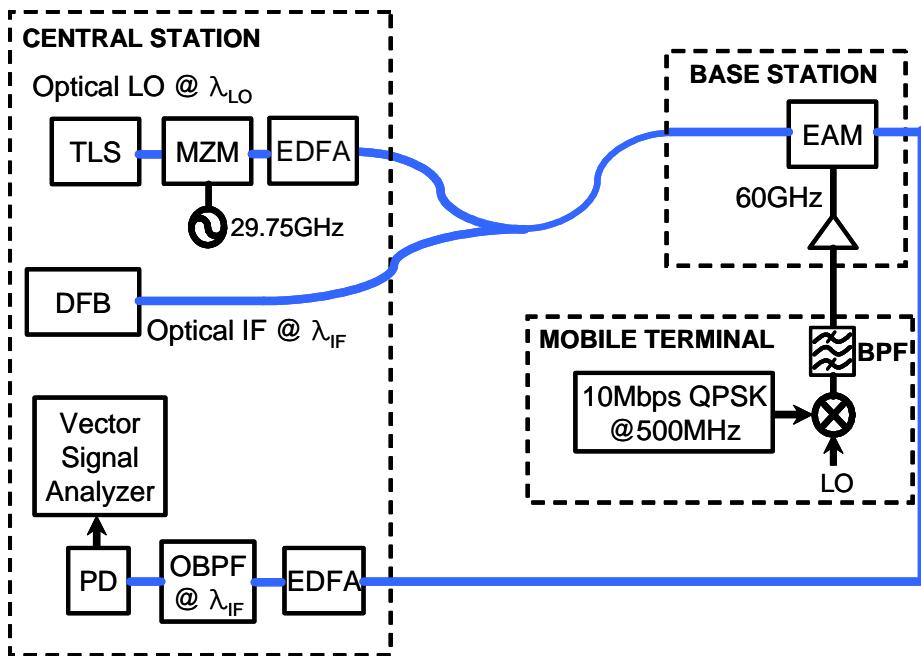


Figure 3-16. Experimental setup for 60 GHz frequency down-conversion and uplink data transmission. BPF : Bandpass Filter.

Fig. 3-17 shows an example of the RF spectrum for frequency down-converted 500 MHz IF signals at the central station. For this

measurement, 5 dBm optical LO signals at 1550 nm and 0 dBm optical IF carriers at 1552.5 nm were applied to the EAM biased at -1.8 V. The input RF power of the uplink signal was 5 dBm.

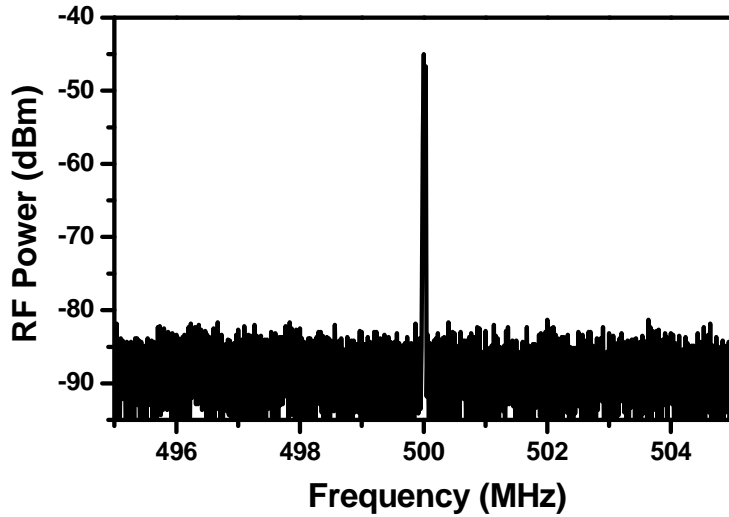


Figure 3-17. Frequency down-converted 500 MHz IF signal spectrum. Resolution bandwidth is 10 kHz

Next, 60 GHz band uplink data transmission was demonstrated. For the IF data transmission, 10 Mbps QPSK data at 500 MHz were generated from a QPSK signal generator and frequency up-converted to 60 GHz by a subharmonic mixer. Fig. 3-18(a) shows the QPSK data spectrum at the 60 GHz band before applied to EAM. This signal was frequency down-converted by EAM and transmitted to the central station on 1552.5 nm optical IF carrier. Optical heterodyne LO signals at 1560 nm were used and the EAM was biased at -2 V. Fig. 3-18(b)

shows the spectrum of 500 MHz QPSK data transmitted to the central station. The received QPSK data were analyzed with a vector signal analyzer (VSA). The incoming digital data signals have their original vector positions in complex domain, and the VSA can provide the discrepancy information between the original vector positions and the demodulated signal vector positions in the form of error vector magnitude (EVM). The EVM is used as a figure-of-merit of most wireless system performance, and it can be converted to SNR easily. The measured EVM in this experiment was about 14.7 %, which corresponds to the SNR of 16.6 dB evaluated from the following relation [71]:

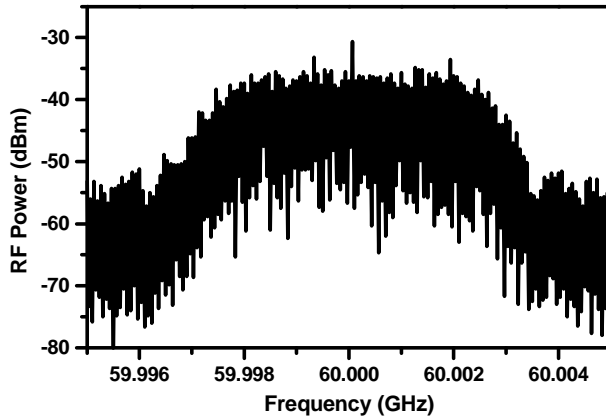
$$SNR = -20\log_{10}\left(\frac{EVM}{100}\right) \quad 3-(7)$$

When the wireless channel is assumed to be additive white Gaussian noise (AWGN), the BER for MPSK digital modulation can be analytically extracted from the following equation [74]:

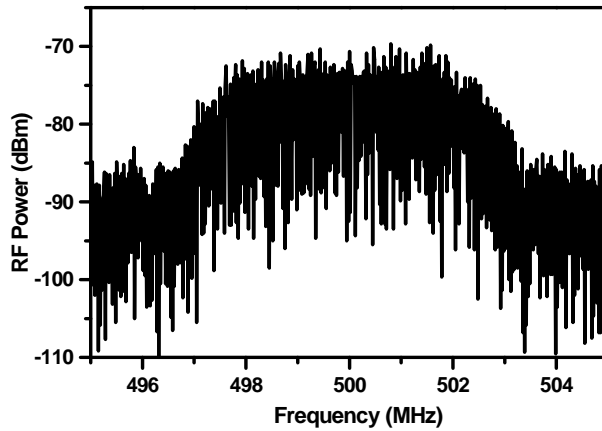
$$BER = \frac{2}{\log_2 M} \times Q(\sqrt{2SNR} \sin \frac{\pi}{M}) \quad 3-(8)$$

The calculated BER from the SNR in this equation was low enough to transmit error-free QPSK data in this uplink system. The eye diagram of demodulated signals is shown in Fig. 3-19. It should be noted that much higher data rate transmission as well as other data modulation methods should be possible with this scheme, but in this feasibility experiment, only 10 Mbps QPSK data transmission was possible due to

limited equipment available. Moreover, the system performance can be enhanced after the optimization of RoF link and EAM design. As explained in chapter 2, the RoF link loss and the most 60 GHz RF components are not designed for this purpose. This system optimization can improve data transmission quality. At least, high SNR uplink data signals at 60 GHz should have been generated for better performance in this system experiment. As explained before, the SNR of frequency down-converted signals is not degraded very much compared with original 60 GHz signals. EAM is not also designed as a frequency down-converter. In this scheme, the nonlinearity of EAM is the origin of frequency down-conversion, so that nonlinear EAM design is necessary. In addition, the better modulation and photodetection efficiency of EAM can also increase the power of detected frequency down-converted signals at the central station. I believe that such system and device optimization surely enhance RoF uplink system performance.



(a)



(b)

Figure 3-18. (a) 10 Mbps QPSK modulated signal spectrum at 60 GHz, (b) frequency down-converted QPSK modulated signal spectrum at 500 MHz. Resolution bandwidth is 100 kHz.

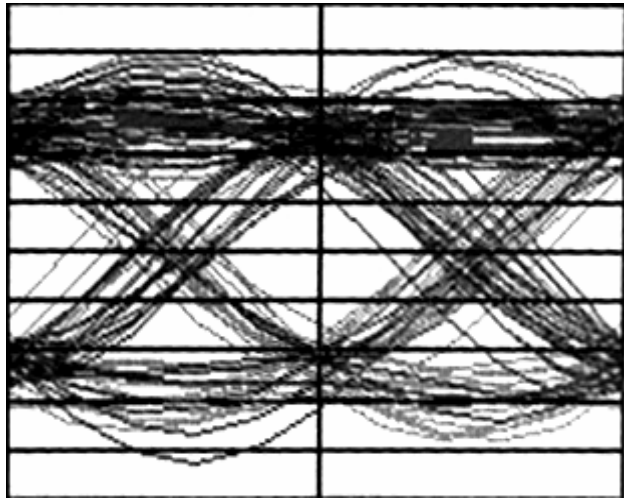


Figure 3-19. Eye diagram of demodulated 10 Mbps QPSK signals at 500 MHz.

## **4. Remote Frequency Up/Down-Conversion using Cascade SOA-EAM Configuration**

### **4-1. Bi-directional RoF systems**

In chapter 2 and 3, downlink RoF systems using remote frequency up-conversion based on SOA-PD configuration, and uplink RoF systems using remote frequency down-conversion based on EAM are investigated, respectively. Each system provides compact base station architectures, and uses low frequency optical IF signal transmission to avoid dispersion-induced signal fading problems for 60 GHz RoF systems. However, the final goal is to realize bi-directional 60 GHz RoF systems, and the basic system configuration to be proposed in this chapter is shown in Fig. 4-1. At the central station, optical heterodyne LO signals and optical IF signals having downlink IF data are generated and transmitted to the base station. In the base station, only a photonic mixer is installed, and frequency up-converted data signals are produced by detecting these two optical signals. For uplink, uplink RF data signals are inputted to the photonic mixer and frequency down-converted IF signals are generated with the help of detected optical LO signals. This uplink IF signals modulates optical IF signals used for downlink, which go back to the central station. After photodetection of optical IF, uplink IF data signals are created. Therefore, full link operation is achieved with only a single photonic frequency converter at the base station. For this, the photonic mixer is realized by

combining photonic frequency up- and down-conversion schemes, especially by the cascaded SOA EAM configuration [72]. Because EAM can be used for photodetection, the function of PD at SOA-PD frequency up-conversion can be replaced by EAM. In addition, EAM in itself can be used for the optoelectronic frequency down-converter. As a result, SOA-EAM configuration gives very compact base station architecture for bi-directional RoF systems.

In chapter 4, the simple operation principles of frequency up- and down-conversion using SOA-EAM configuration will be introduced, and then measured mixing characteristics will be shown. Finally, bi-directional RoF links will be demonstrated at 60 GHz band.

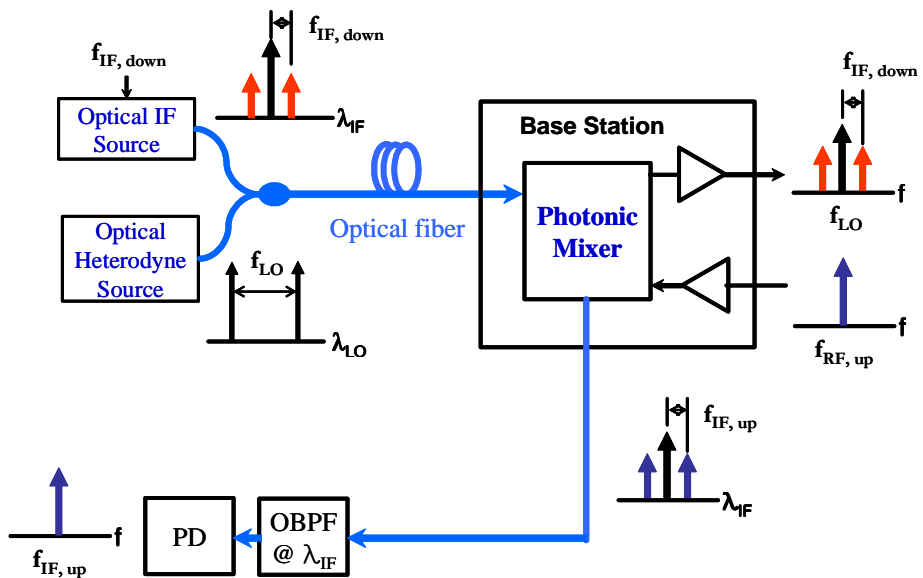


Figure 4-1. Proposed bi-directional RoF system configuration adopting a photonic mixer at a base station.

## 4-2. Operation Principles of Frequency Converters

Fig. 4.2 and 4.5 schematically show operation principles of frequency up- and down-conversion using the SOA-EAM configuration, respectively.

### 4-2-1. Frequency up-conversion for downlink transmission

For frequency up-conversion, optical LO at  $\lambda_{LO}$  having two optical modes separated by  $f_{LO}$ , and optical IF at  $\lambda_{IF}$  having two sidebands separated from the carrier by  $f_{IF, down}$  are transmitted from the central station and injected into SOA in the base station. Inside SOA, two modes of optical LO are cross-gain modulated by optical IF signals. After photodetection of optical LO signals in EAM, frequency up-converted signals at  $f_{LO} \pm f_{IF, down}$  are obtained as square-law beating products. This frequency up-conversion process is similar to that in SOA-PD configuration explained in chapter 2. In order to verify frequency up-conversion at 60 GHz band, the experimental setup shown in Fig. 4-2 was used. 60 GHz optical heterodyne LO signals were generated by modulation of an MZM biased at the minimum transmission point with 30 GHz RF signals for DSB-SC method. The wavelength of optical LO was 1553.3 nm and its power measured before SOA was -15 dBm. Optical IF signals were generated by modulation of another MZM biased at the quadrature point with 100 MHz, 10 dBm RF signals. The wavelength of optical IF can be any wavelength within SOA gain bandwidth. For the experiment, optical IF

wavelength was 1550 nm and its power measured before SOA was -8 dBm. The SOA bias current was 150 mA, which provided the SOA gain of 25 dB and saturation output power of 7 dBm. The EAM used in the experiment was designed and packaged for 60 GHz narrow-band operation [67-68], and biased at -2.5 V. Fig. 4-3(a) and (b) show the resulting RF spectra of downlink IF signals at 100 MHz without SOA (measured at Point A in Fig. 4.2) and frequency up-converted 60 GHz band signals (measured at Point B in Fig. 4.2), respectively. They clearly show frequency up-converted signals at 59.9 GHz ( $f_{LO}-f_{IF, down}$ ) and 60.1 GHz ( $f_{LO}+f_{IF, down}$ ).

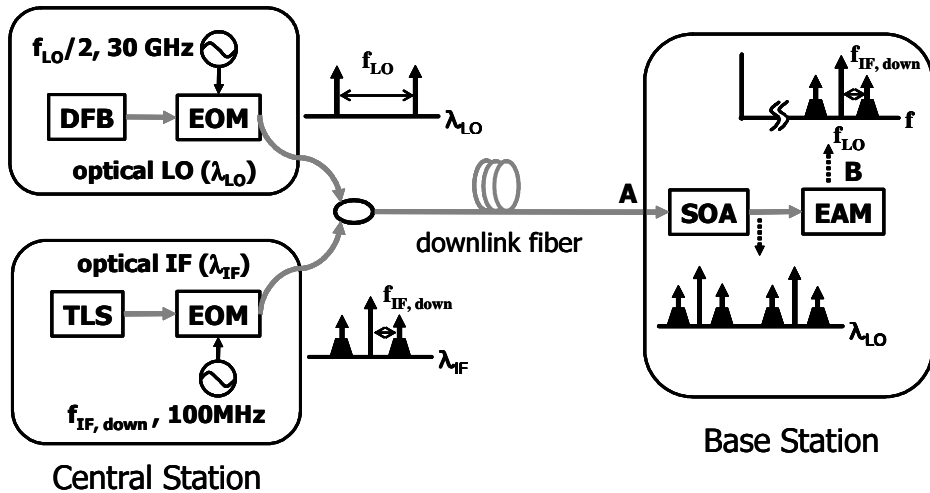
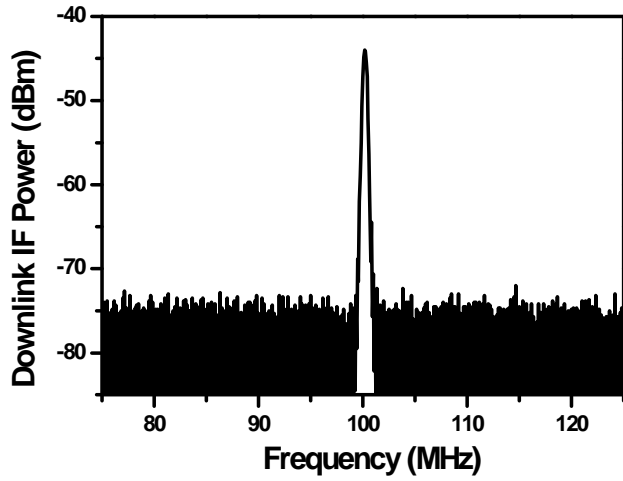
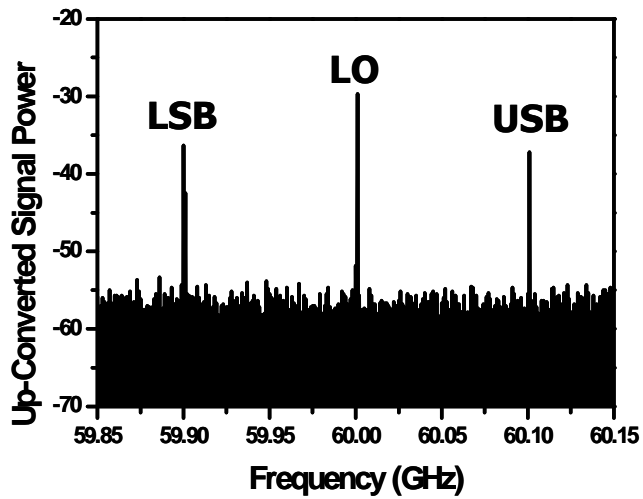


Figure 4-2. Schematic for frequency up-conversion processes and experimental setup used for verification.

The dispersion effects on remote frequency up-conversion scheme are also examined. The frequency up-converted 59.5 GHz signals are measured at different transmission distances up to 10 km, and the results are normalized to the power measured at back-to-back conditions. As shown in Fig. 4-4, signal degradation does not occur compared with double-sideband transmission of 60 GHz signals, which was calculated with analytical expression in [15]. For this calculation, it was assumed that the wavelength of 60 GHz signals is 1550 nm, and fiber loss is 0.2 dB/km. Many null points due to the signal fading appear in analytical results shown in Fig. 4-4. As a result, it is verified that remote frequency up-conversion method does not degrade system performance for long fiber transmission.



(a)



(b)

Figure 4-3. RF spectra for downlink frequency up-conversion: (a) IF signals without SOA, (b) frequency up-converted signals. The resolution bandwidth was 300 kHz for (a) and 100 kHz for (b). A 17 dB gain electrical amplifier was used for (b).

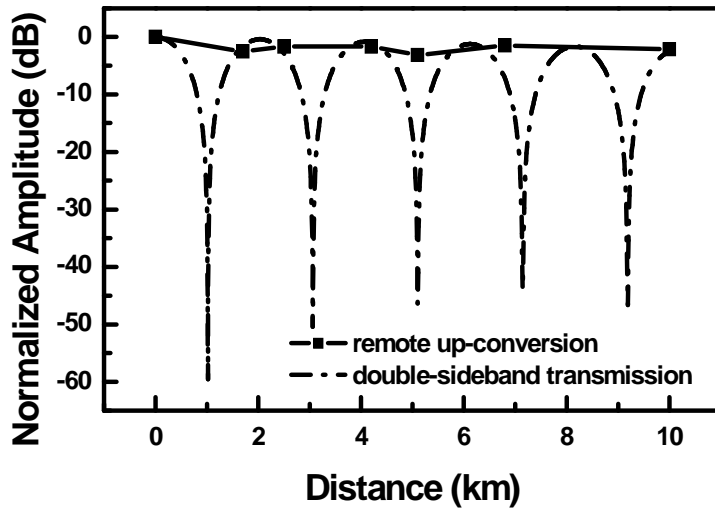


Figure 4-4. Normalized signal amplitude of frequency up-converted signals and calculated results of double-sideband signal transmission at 60 GHz band. The measured up-converted signal power is normalized to the power at back-to-back conditions.

#### 4-2-2. Frequency down-conversion for uplink transmission

For frequency down-conversion, optical LO and optical IF are injected into the SOA-EAM configuration. During the photodetection process in EAM, signals having  $f_{LO}$  component are generated inside EAM. These signals are frequency mixed with RF signals ( $f_{RF, up}$ ) externally applied to EAM due to EAM nonlinearity, causing frequency down-conversion to  $f_{IF, up} = f_{LO} - f_{RF, up}$ . The resulting  $f_{IF, up}$  signals then modulate optical IF signals at  $\lambda_{IF}$  in the same EAM, which are then sent back to the central station. This frequency down-conversion method was explained in chapter 3. However, with addition of SOA as in our scheme, both frequency up-conversion and down-conversion are possible and optical amplification by SOA results in better uplink performance. Moreover, EAM and SOA can be monolithically integrated [73], making the frequency converter more compact. Although the same optical IF are used for both downlink and uplink, this is not a problem since  $f_{IF, down}$  and  $f_{IF, up}$  are not the same and can be easily separated electronically. In this frequency converter, EAM is acting as a multi-functional device which simultaneously performs photo-detection, frequency down-conversion, and uplink optical IF signal modulation. Consequently, the antenna base station can be greatly simplified.

The setup shown in Fig. 4-5 was used for frequency down-conversion experiment. Optical LO was generated with the same method used for frequency up-conversion, and optical IF was supplied

from a tunable light source. In this experiment, optical IF did not include  $f_{\text{IF, down}}$  so that only frequency down-conversion characteristics for uplink can be investigated. 10 dBm 59.85 GHz signals were used as uplink RF signals, which were applied to EAM biased at -2.5 V. Inside EAM, 59.85 GHz signals were mixed with 60 GHz signals produced by photodetection of optical LO and produced  $f_{\text{IF, up}} = 150$  MHz signals, which then modulated optical IF. The uplink optical IF signals were transmitted to the central station, and photodetected after optical amplification. An optical bandpass filter having  $\lambda_{\text{IF}}$  passband was inserted before PD in order to block optical LO signals at  $\lambda_{\text{LO}}$  delivered to the central station. This filtering is necessary because optical LO signals modulated by uplink RF signals can produce interfering frequency down-converted signals at the central station [62]. Fig. 4-6(a) and (b) respectively show the RF spectra of uplink RF signals at 59.85 GHz and frequency down-converted IF signals at 150 MHz measured simultaneously at the central station (measured at Point C in Fig. 4.5). Uplink RF signals is delivered to the central station at  $\lambda_{\text{IF}}$  because EAM is modulated with both uplink RF signals and frequency down-converted IF signals.

Next, the dispersion effects on remote frequency down-conversion method are investigated using the same methods applied to remote frequency up-conversion case. The frequency down-converted 150 MHz signals are measured according to different transmission distance, and the results are normalized to the signal power at back-to-back

conditions. Fig. 4-7 shows that dispersion-induced signal fading problems do not occur to the detected signals through the remote frequency down-conversion. The measurement results are also compared with the calculated signal power transmitted by double-sideband 60 GHz signals. The same assumption was used for this calculation, and several signal fading phenomena appear within 10 km transmission as shown in Fig. 4-7. From these results, it is proved that the remote frequency down-conversion technique can also provide dispersion insensitive uplink data transmission.

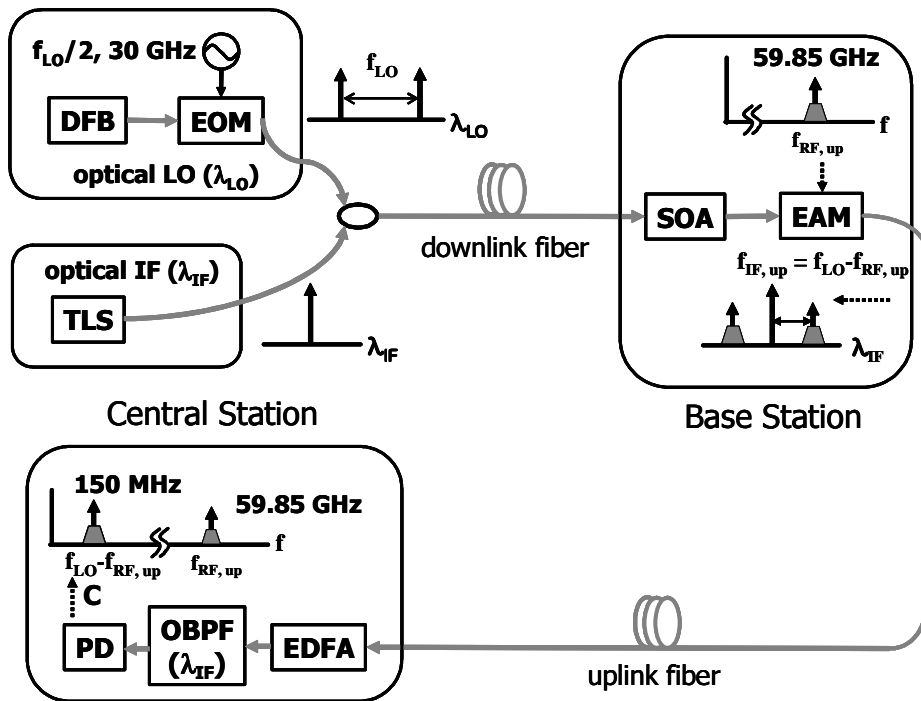
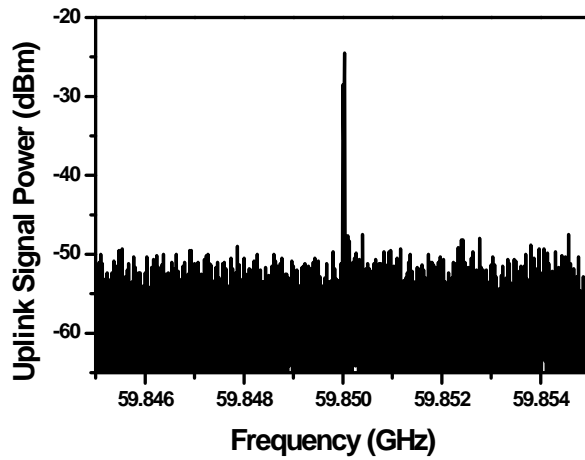
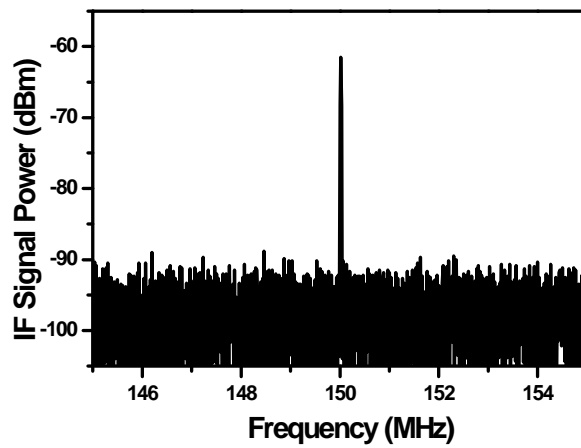


Figure 4-5. Schematics for frequency down-conversion processes and experimental setup used for verification.



(a)



(b)

Figure 4-6. RF spectra for uplink frequency down-conversion: (a) RF signals measured at the central station, (b) frequency down-converted signals measured at the central station. The resolution bandwidth was 1 kHz for both. A 17 dB gain electrical amplifier was used for (a), and a 20 dB gain electrical amplifier was used for (b).

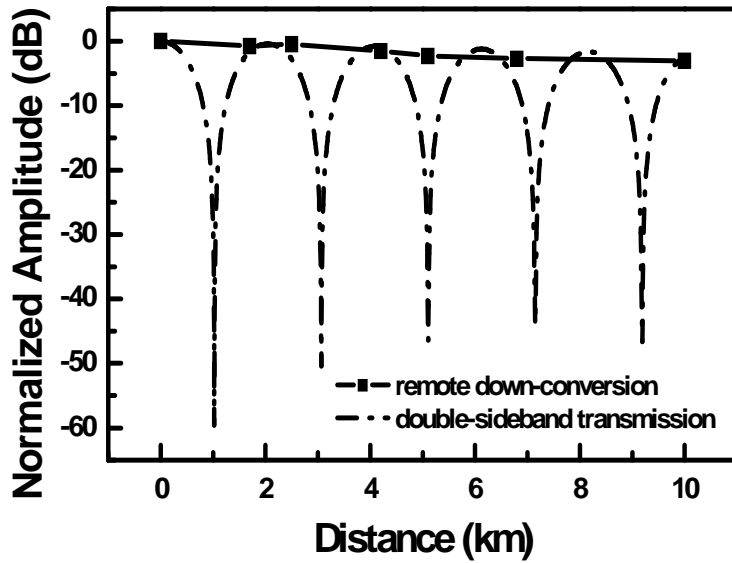


Figure 4-7. Normalized signal amplitude of frequency down-converted signals and calculated results of double-sideband signal transmission at 60 GHz band. The measured down-converted signal power is normalized to the power at back-to-back conditions.

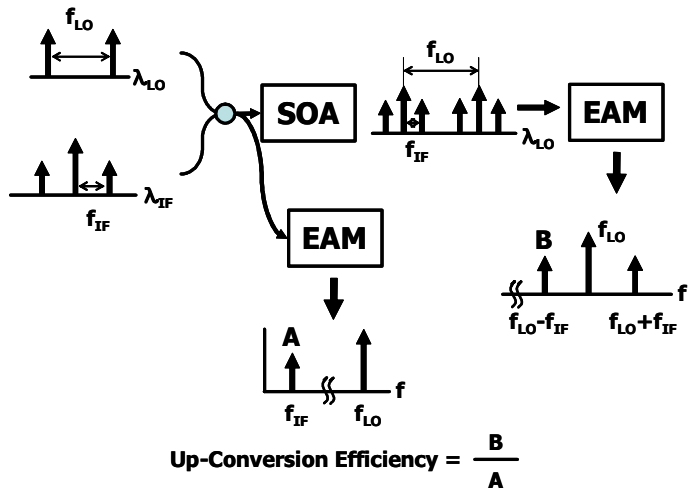
## 4-3. Conversion Efficiency Characteristics of SOA-EAM Frequency Converters

### 4-3-1. Conversion efficiency definition

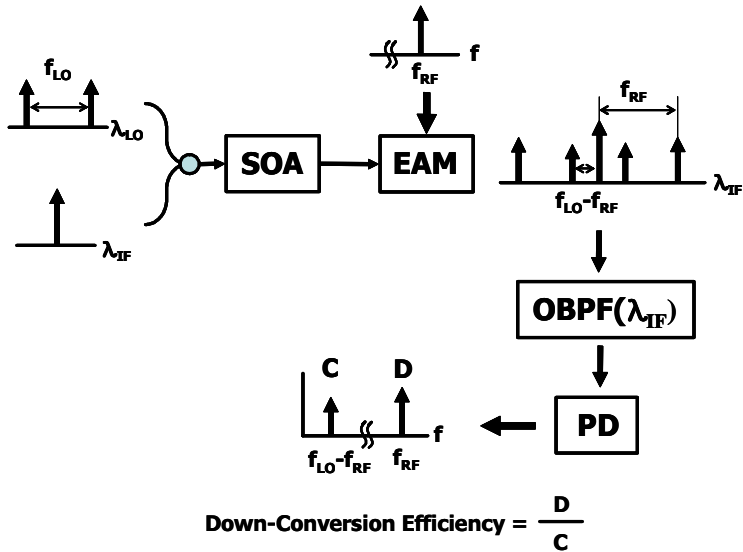
For electrical frequency converters, important specifications are frequency conversion efficiency, isolation between RF and LO ports, and intermodulation distortions caused by nonlinearity of frequency converters [70]. Among them, frequency conversion efficiency is essential for RF design of base stations. The conventional definition of conversion efficiency is the RF power ratio between input signals and frequency converted output signals. However, it is very difficult to directly apply this definition to this frequency converter because it is difficult to measure exact signal powers related to frequency up- and down-conversion due to many optical components used in the scheme. Therefore, a method to estimate frequency up- and down-conversion efficiencies is devised.

At first, up-conversion efficiency ( $\eta_{\text{up}}$ ) is defined as the ratio of EAM photodetected frequency up-converted signal power to EAM photodetected IF signal power. For example, the ratio of lower sideband power in Fig. 4-3(b) to peak power in Fig. 4-3(a) is  $\eta_{\text{up}}$ . The frequency down-conversion efficiency ( $\eta_{\text{down}}$ ) is defined as the ratio of frequency down-converted signal power to uplink RF signal power measured at the central station simultaneously. For example, the ratio of peak power in Fig. 4-6(b) to peak power in Fig. 4-6(a) is  $\eta_{\text{down}}$ . As

explained in chapter 4-2, the frequency down-conversion process is a complex one involving photodetection, mixing and modulation. By comparing  $f_{\text{IF, up}}$  and  $f_{\text{RF, up}}$  delivered at  $\lambda_{\text{IF}}$  to the central station, the influence of EAM modulation efficiency can be eliminated, and internal mixing efficiency of EAM can be estimated. Fig. 4-8 shows the schematic of frequency conversion efficiencies for both up- and down-conversion.



(a)



(b)

Figure 4-8. Schematic of frequency up-conversion efficiency (a) and frequency down-conversion efficiency.

#### 4-3-2. Measurement results of conversion efficiency

The same experimental setup shown in Fig. 4-2 and Fig. 4-5 was used for conversion efficiency measurement. The 16 dB difference in EAM photodetection response between 100 MHz and 60 GHz was corrected for  $\eta_{\text{up}}$  calculation. The 5 dB difference in photodiode response between 150 MHz and 60 GHz was also corrected for  $\eta_{\text{down}}$  calculation. In addition, different electrical gains were corrected for both  $\eta_{\text{up}}$  and  $\eta_{\text{down}}$ . The measurement was performed in back-to-back condition.

At first, the dependence of frequency conversion efficiencies on EAM bias condition was measured. The power of optical IF signals at 1550 nm and optical LO signals at 1553.3 nm before SOA were -8 dBm and -15 dBm, respectively. As shown in the Fig. 4-9,  $\eta_{\text{up}}$  increases with increasing EAM reverse bias voltages, because photocurrent in EAM increases at high reverse voltages. The dependence of photocurrent in EAM on bias conditions is the contrary of modulation characteristics, so that photocurrent in EAM within this bias range increases with reverse bias voltages. However,  $\eta_{\text{down}}$  decreases with increasing EAM reverse bias voltages, because EAM nonlinearity is more pronounced at low reverse voltages.

LO power influences the efficiency of frequency converters very much, so that the dependence of frequency conversion efficiencies on SOA input optical LO power is investigated. For this measurement, the optical IF power at 1550 nm was set at -8 dBm, and EAM was biased at

-2.5 V. The wavelength of optical LO signals was 1553.3 nm. The results were obtained at two different SOA current levels in order to see the influence of SOA gain on conversion efficiencies. As can be seen in Fig. 4-10(a) and (b), both  $\eta_{\text{up}}$  and  $\eta_{\text{down}}$  increase with optical LO power. For  $\eta_{\text{up}}$ , the increase is due to square-law beating power increase with optical LO signals in EAM.  $\eta_{\text{down}}$  increases because the photogenerated LO signal power in EAM increases with optical LO power. In both cases, the slight saturation of conversion efficiencies appears at high optical LO power conditions due to the SOA gain saturation. When the SOA bias increases from 100 mA to 150 mA, both frequency conversion efficiencies improve about 10 dB, which corresponds to about 5 dB increase in SOA optical gain.

Finally, conversion efficiencies were measured as functions of optical IF signal power and wavelength. Fig. 4-11 shows the conversion efficiency dependence on optical IF signal power. The optical LO signal power at 1553.3 nm was -15 dBm, and the wavelength of IF signals was 1550 nm. For frequency up-conversion, the conversion efficiency decreases with increase of optical IF power. This is due to SOA gain saturation, which causes decrease of both cross-gain modulation efficiency and gain that optical LO signals experience. As shown in Fig. 4-11, the conversion efficiency dependence is very similar to SOA gain saturation characteristics. For frequency down-conversion, the increase of optical IF power leads to the increase of photodetected power of both frequency down-converted

signals and RF signals. Therefore, constant conversion efficiency should be maintained. However, at high optical IF power conditions, the frequency down-conversion efficiency is slightly decreased, because the optoelectronic mixing at the EAM starts to saturate faster than RF modulation in EAM.

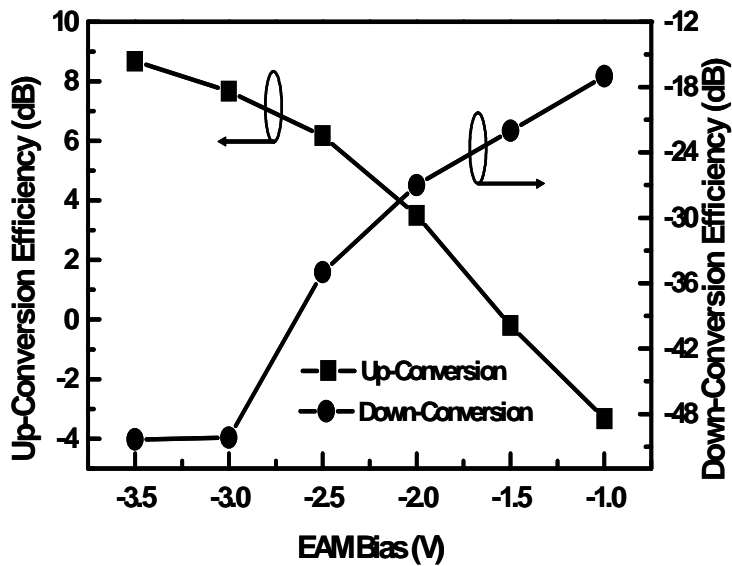
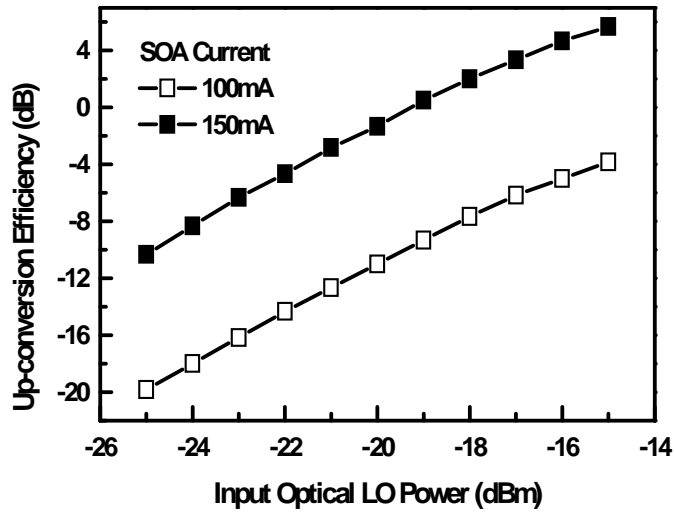


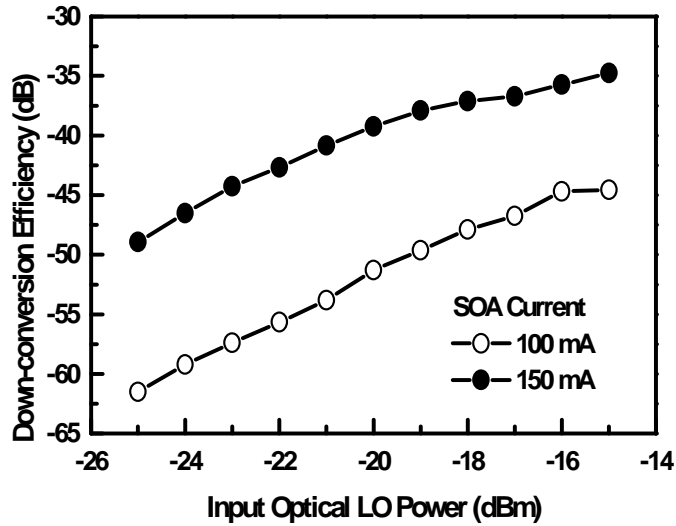
Figure 4-9. Dependence of frequency conversion efficiency ( $\eta_{up}$  and  $\eta_{down}$ ) on EAM bias conditions.

Fig. 4-12 shows the effects of optical IF wavelength on frequency conversion efficiencies. The wavelength of -8 dBm optical IF was changed from 1540 nm to 1560 nm. As shown in the figure, the frequency up-conversion efficiency is nearly constant over wide optical IF wavelength range. The reason is that the SOA gain bandwidth near

1550 nm is wide and cross-gain modulation efficiency is saturated with this high optical IF power. On the other hand, the frequency down-conversion efficiency varies about 4 dB. This is because the modulation efficiency and frequency mixing in EAM are changed at different wavelength conditions. These frequency conversion efficiency results show that this SOA-EAM frequency converter has wide operation wavelength range.



(a)



(b)

Figure 4-10. Frequency up-conversion efficiency ( $\eta_{up}$ ) (a), and frequency down-conversion efficiency ( $\eta_{down}$ ) (b) as a function of optical LO signal power. Optical LO power was measured in front of SOA.

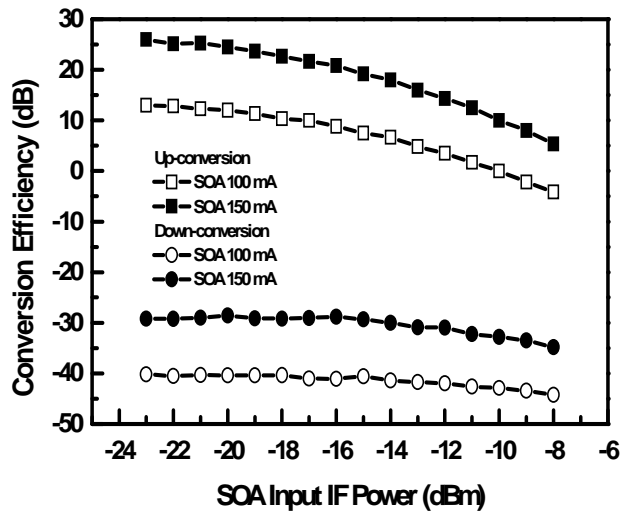


Figure 4-11. Frequency conversion efficiencies as a function of SOA input optical IF signal power.

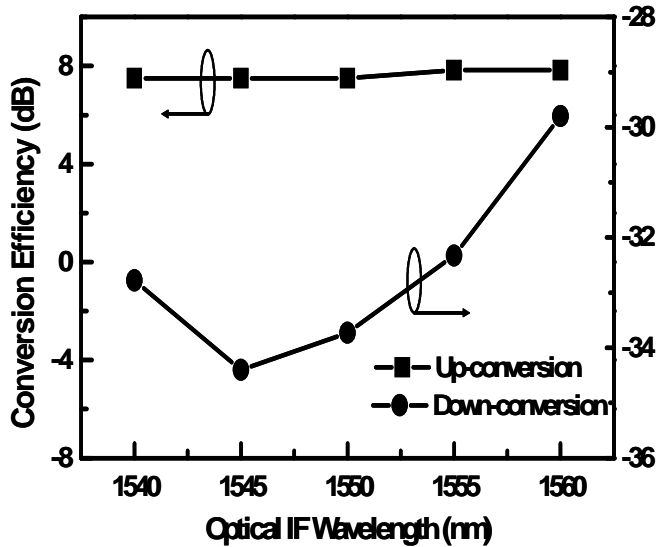


Figure 4-12. Frequency conversion efficiencies as a function of SOA input optical IF wavelength.

## **4-4. 60 GHz Bi-Directional RoF Systems using SOA-EAM Configuration**

In previous chapters, the operation principles and conversion efficiency characteristics of the SOA-EAM frequency converter are investigated. Now, 60 GHz bi-directional data transmission using this frequency converter is demonstrated. 60 GHz optical LO are transmitted from central station, and 5 Msymbol/s data signals using QPSK, and 16QAM digital modulation are bi-directionally transmitted. By measuring EVMs, error-free data transmission in both directions is verified, and the dependence of system performance on powers and wavelengths of optical IF signals is investigated.

### **4-4-1. Experimental setup and data transmission results**

Fig. 4-13 shows the experimental setup for 60 GHz band RoF systems using the SOA-EAM frequency converter. 60 GHz optical heterodyne LO signals at 1553.3 nm were generated by modulation of an MZM biased at the minimum transmission point with 30 GHz signals for DSB-SC method. For downlink, optical IF signals at 1550-nm were produced by modulation of another MZM with 5 Msymbol/s QPSK or 16QAM data at 100 MHz IF. Both optical signals were combined and injected into the cascaded SOA-EAM, producing frequency up-converted signals in 60 GHz band. These two sidebands of frequency up-converted signals were frequency down-converted to 100 MHz by a subharmonic mixer with a 30 GHz electrical LO signal.

The EVMs of recovered IF signals were analyzed by a VSA. The SOA was biased at 150 mA, and the EAM was biased at -2.5 V. For the uplink data transmission, the same 5 Msymbol/s QPSK or 16QAM data signals at 59.85 GHz were generated by up-converting 150-MHz IF data to 59.85 GHz. The RF bandpass filter was used to suppress both LO carrier and image signals. When the EAM was modulated by uplink RF signals, frequency down-converted signals at 150 MHz were produced by the SOA-EAM frequency converter, which then modulated optical IF signals returning to the central station. In the central station, optical IF signals were photodetected after optical amplification and filtering, and the resulting QPSK or 16QAM data at 150 MHz were analyzed for transmission quality by VSA. All the experiments were done in back-to-back condition with separate uplink and downlink data transmission. It should be noted that 60 GHz band should provide much higher bandwidth than the data bandwidth used in this demonstration. The bandwidth in this experiment was limited by data generation and analysis instruments available, not by the SOA-EAM frequency converter. The proposed frequency converter should have as wide conversion bandwidth as its optical modulation and photodetection bandwidth. The EAM used in the experiment has 2 GHz modulation bandwidth at 60 GHz, and SOA cross-gain modulation bandwidth should be in GHz range as explained in chapter 2.

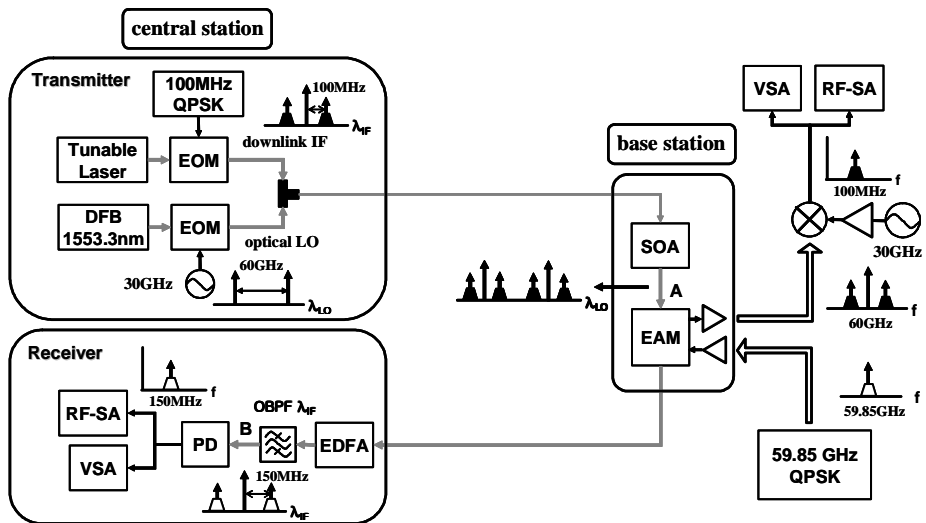
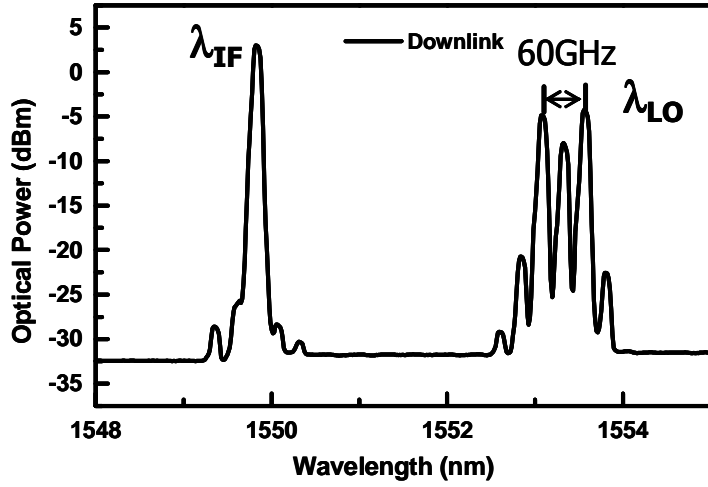
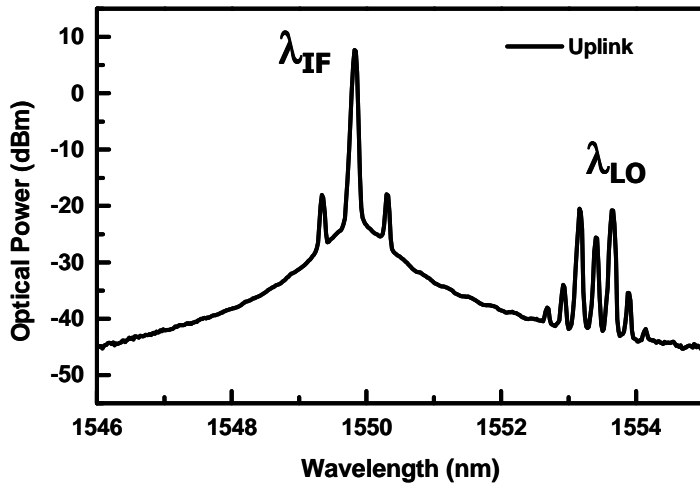


Figure 4-13. Experimental setup for 60 GHz bi-directional RoF systems.



(a)



(b)

Figure 4-14. Optical spectra of downlink signals (a) and uplink signals (b).

Fig. 4-14(a) and (b) show the optical spectra of downlink and uplink signals, respectively. The downlink optical spectrum shown in Fig. 4-14(a) was obtained from the optical signals coming out of SOA (measured at Point A in Fig. 4-13), and 1550 nm optical IF ( $\lambda_{\text{IF}}$ ), and 1553.3 nm optical LO ( $\lambda_{\text{LO}}$ ) signals can be seen. The additional peaks observed around  $\lambda_{\text{LO}}$  are due to modulation harmonics of the MZM caused by DSB-SC [42-43]. The small peaks around  $\lambda_{\text{IF}}$  are due to XGM between optical LO and IF signals. The uplink optical spectrum was measured after the optical bandpass filter ( $\lambda_{\text{pass}} = 1550$  nm) at the central station (measured at Point B in Fig. 4-13). As shown in Fig. 4-14(b), the optical LO signals are suppressed about 30 dB compared with optical IF signals. The side peaks around  $\lambda_{\text{IF}}$  are the results of  $f_{\text{RF}}$  modulation of EAM.

The RF spectra and EVMs of frequency converted data signals were measured. Fig. 4-15 shows the RF spectrum of frequency up-converted downlink signals, and Fig. 4-16(a) and (b) show the clear constellation and eye diagram of demodulated downlink QPSK and 16QAM data, respectively. For this measurement, -16.3 dBm optical LO and -10 dBm optical IF signals were injected into SOA, and the resulting EVM for QPSK was about 3.3 %, which corresponds to 29.6 dB SNR. The EVM for 16QAM was about 3.6 %, which corresponds to 29 dB SNR. When the wireless channel is also assumed to be AWGN same in chapter 3, the resulting performances of both directions are theoretically enough for error-free data transmission. The analytical

expressions for this calculation are well explained in [74]. Fig. 4-17 shows the 150 MHz RF spectrum of frequency down-converted uplink signals measured at the central station, and Fig. 4-18(a) and (b) show the clear constellation and eye diagram of demodulated uplink QPSK and 16QAM data, respectively. With -15 dBm optical LO and -8 dBm optical IF signals injected into SOA, the EVM for QPSK was about 7.4 %, which corresponds to 22.6 dB SNR. The EVM for 16QAM was about 8.6 %, which corresponds to 21.2 dB SNR. These results are also good enough for wireless systems. The reason for larger EVMs for uplink than downlink is that the frequency down-conversion efficiency is lower than up-conversion efficiency as explained in chapter 4-3. In addition, two optical amplifiers, which are SOA and EDFA, affect uplink optical IF signals, such that amplifier noise degrades system performance. Nevertheless such larger EVMs for uplink, the results are still good enough for real systems, and the system have rooms for better performance. Especially, less link loss and higher conversion efficiency design of SOA-EAM frequency converter surely lead to better system performance.

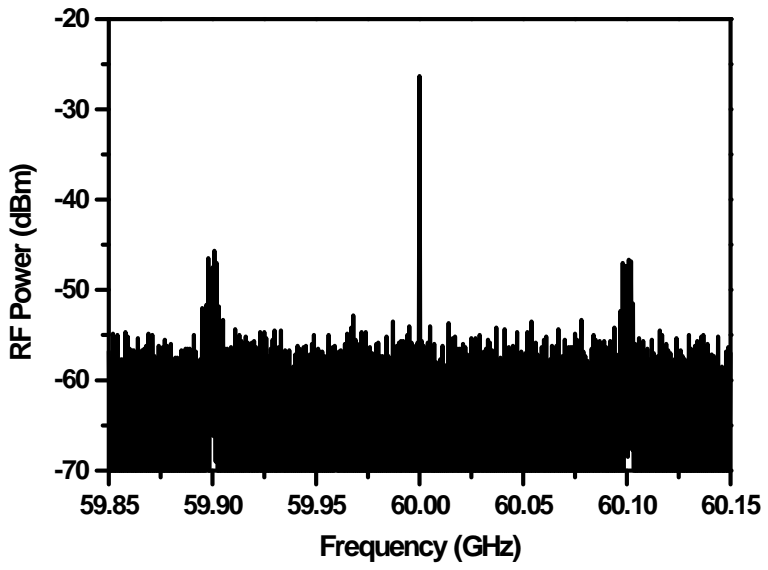
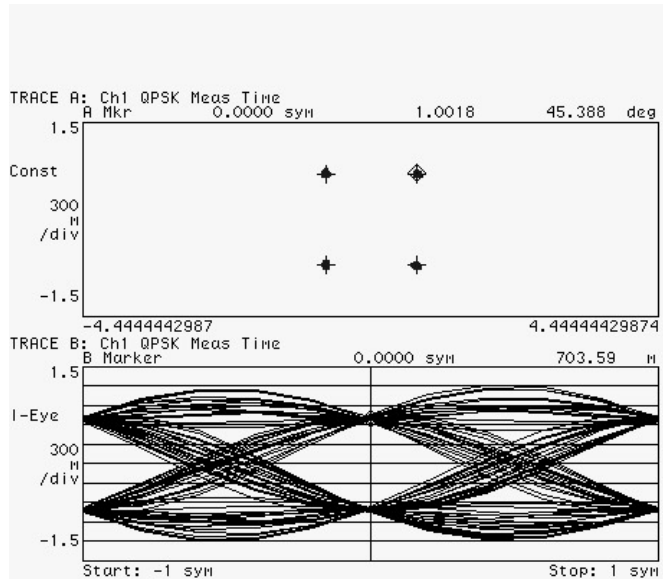
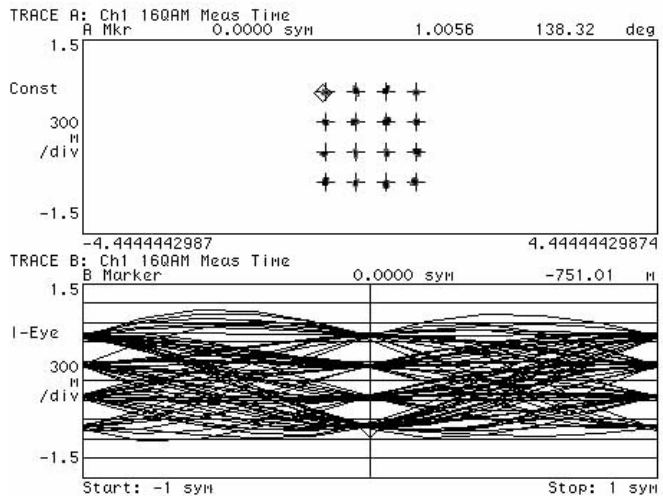


Figure 4-15. RF spectrum of frequency up-converted data signals.



(a)



(b)

Figure 4-16. Constellation and Eye diagram of demodulated downlink 5 Msymbol/s QPSK (a) and 16QAM data signals.

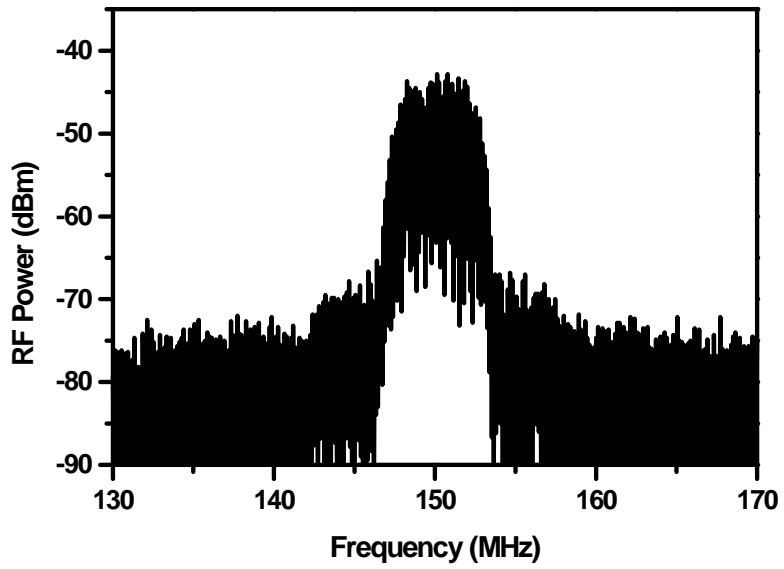
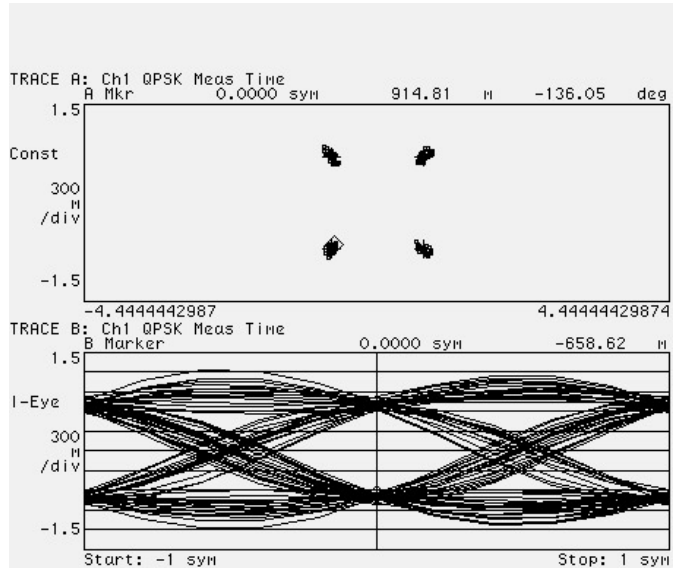
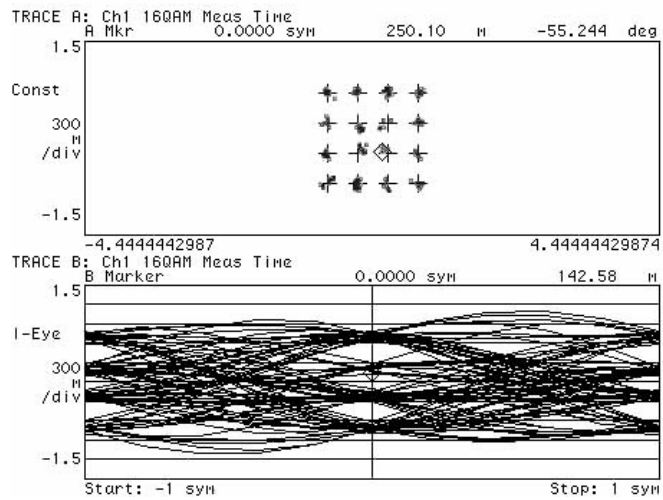


Figure 4-17. RF spectrum of the frequency down-converted uplink signals.



(a)



(b)

Figure 4-18. Constellation and Eye diagram of demodulated uplink 5 Msymbol/s QPSK (a) and 16QAM data signals.

EVMs for QPSK data as a function of optical IF powers before SOA were measured for both downlink and uplink. Fig. 4-19 shows the measurement results. The optical LO power was fixed at -16.3 dBm for downlink and -15 dBm for uplink. As shown in the figure, downlink EVM changes from 6 % to 3 % as optical IF power increases. This is simply because lower optical IF power reduces XGM efficiency and the frequency up-converted signal power. However, when optical IF power is high, both XGM efficiency and SOA gain of optical LO signals are saturated and, consequently, the EVM is also saturated at around 3 %. The EVM of the uplink data transmission also decreases from 13 % to 8 % as optical IF power increases. In uplink, the increase in optical IF power leads to increase in the detected uplink signal power, causing increase in SNR. Consequently, the EVM decreases until it is saturated due to SOA gain saturation. Although large EVMs were measured at low optical IF power conditions, their values are still good enough for QPSK data transmission.

The dependence of EVM for QPSK data on optical IF wavelengths was also investigated in order to identify the usable IF wavelength range. The optical LO power was -16.3 dBm for downlink and -15 dBm for uplink, and optical IF power was -10 dBm for downlink and -8 dBm for uplink. As shown in Fig. 4-20, EVMs for both downlink and uplink do not change very much with optical IF wavelength. This verifies that optical IF signals having different wavelengths can be used for accessing different base stations.

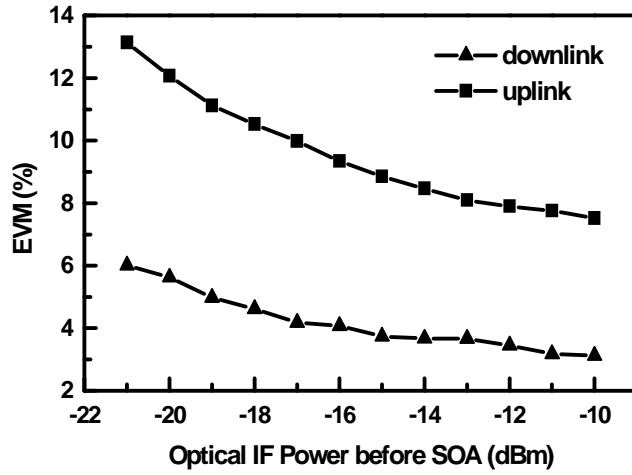


Figure 4-19. Measured EVMs as a function of SOA input optical IF signal power for downlink and uplink.

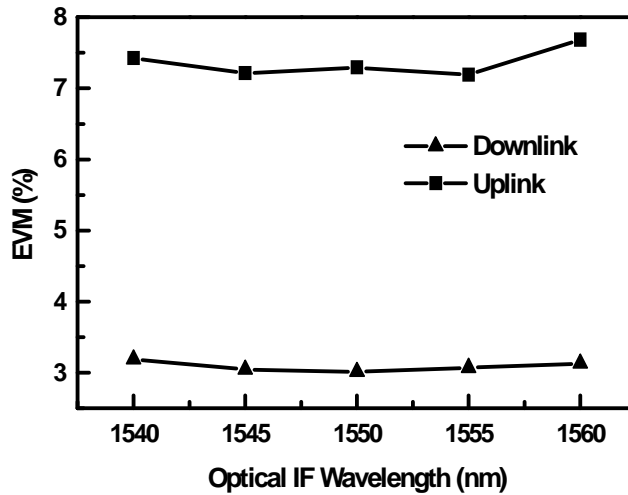


Figure 4-20. Measured EVMs as a function of optical IF signal wavelength for downlink and uplink.

## 5. Summary

Millimeter-wave wireless systems have been actively investigated for future broadband wireless systems. Especially, 60 GHz band, available as an unlicensed band, is attracting much attention due to wide bandwidth, frequency reusability, and high directivity. However, the high free-space propagation loss of 60 GHz signals demands many base stations covering small-sized cells. Consequently, simple and cost-effective base station design becomes very important for realizing 60 GHz wireless systems. For this, RoF systems are a very attractive solution due to low loss fiber transmission of radio signals, and centralization of expensive 60 GHz devices and equipment. Many 60 GHz RoF architectures have been proposed, and the remote frequency conversion scheme is a good candidate to realize 60 GHz RoF systems.

In this dissertation, 60 GHz RoF systems were demonstrated based on remote frequency conversion techniques. For downlink data transmission, the frequency up-conversion scheme using SOA XGM was proposed. The optical heterodyne 60 GHz signals and optical IF data signals are generated at the central station, and then transmitted to the base station, where two modes of optical heterodyne signals are cross-gain modulated by IF data signals, and then frequency up-converted signals at 60 GHz band are generated after photodetection of optical heterodyne signals. For uplink data transmission, the frequency down-conversion scheme using EAM was proposed. When 60 GHz band uplink RF signals modulate EAM along with the photodetection

of 60 GHz optical heterodyne signals in EAM, frequency down-converted IF signals are produced by EAM nonlinearity. At the same time, these signals modulate uplink optical signals delivered from the central station, and then are transmitted back to the central station. Therefore, uplink IF signals can be obtained after photodetection of optical IF signals. Because EAM can act as both optical modulator and photodetector, both frequency up- and down-conversion techniques can be combined to SOA-EAM configuration with which two functions simultaneously occur at the base station, resulting in the very simple base station for bi-directional RoF links.

In chapter 2, the frequency up-conversion method using SOA was investigated at first. The operation principles were explained, and then simple operation characteristics were analyzed based on the SOA simulation model using a TMM. The calculated results showed that high conversion efficiencies are possible at wide optical wavelength ranges. To demonstrate broadband operation of the proposed frequency up-converter, SOA XGM bandwidth was measured and also error-free 1.244 Gbps broadband data was transmitted. Less than 0.5 dB power penalty appears within 20 nm optical IF wavelength ranges.

Next, the frequency down-conversion method using EAM was investigated in chapter 3. After explaining simple operation principles, the conversion efficiency characteristics were examined based on measurement results as functions of EAM bias conditions, optical LO powers, and optical IF powers and wavelengths. For high conversion

efficiency, the EAM should be biased at around maximum modulation efficiency conditions, and high optical LO power was necessary. Within 30 nm wavelength ranges, very small efficiency fluctuation appears, which is good for WDM applications. Error-free 5 Msymbol/s QPSK uplink data transmission at 60 GHz band was also demonstrated.

Finally, the SOA-EAM configuration for both frequency up- and down-conversion was shown in chapter 4. The combined functions were explained, and then the conversion efficiencies as functions of EAM bias conditions, optical LO powers, and optical IF powers and wavelengths were measured and analyzed. The basic performances were similar to the individual up- and down-converter, however, it should be considered that both frequency up- and down-conversion efficiencies could not simultaneously be high at the same EAM bias condition. For up-conversion efficiency, high reverse bias of EAM gave high conversion efficiency. Conversely, the down-conversion efficiency was high at low reverse bias conditions. The dispersion insensitive signal transmission was proved by comparing measured results based on remote frequency conversion techniques with theoretical 60 GHz transmission results based on double-sideband signal modulation. Bi-directional data transmission at 60 GHz band was also demonstrated. For both downlink and uplink, high quality QPSK and 16QAM data transmission were succeeded. In addition, the demodulated data performances for both directions were not varied very much in wide operation wavelength ranges.

The RoF systems are very useful for 60 GHz wireless systems, and especially the remote optical/optoelectronic frequency conversion techniques can provide dispersion insensitive signal transmission as well as simple system architectures. In this dissertation, it was presented that frequency converters based on SOA and EAM are very useful for simplifying base stations and achieving flexible bi-directional RoF systems. Although further investigation is necessary, I believe that the proposed methods should be an important part in RoF system development.

## References

- [1] J. Mikkonen, C. Corrado, C. Evci, and M. Prögler, "Emerging wireless broadband networks," *IEEE Commun. Mag.*, pp. 112-117, Feb. 1998.
- [2] H. Izadpanah, "A millimeter-wave broadband wireless access technology demonstrator for the next-generation internet network reach extension," *IEEE Commun. Mag.*, pp. 140-145, Sep. 2001.
- [3] P. Smulders, "Exploiting the 60 GHz band for local wireless multimedia access: prospects and future directions," *IEEE Commun. Mag.*, pp. 140-147, Jan. 2002.
- [4] 이우용, "60GHz 밀리미터파 WPAN 기술 및 표준화," "*Ubiquitous 사회에 대비한 소출력 무선기기의 전파이용 정책 및 기술 workshop*", pp. 111-126, 2005.
- [5] S. E. Gunnarsson, C. Kärnfelt, H. Zirath, R. Kozhuharov, D. Kuylenstierna, A. Alping, and C. Fager, "Highly integrated 60 GHz transmitter and receiver MMICs in a GaAs pHEMT technology," *IEEE J. Solid-State Circuits*, vol. 40, no. 11, pp. 2174-2186, Nov, 2005.
- [6] Y. Shoji, K. Hamaguchi, and H. Ogawa, "Millimeter-wave remote self-heterodyne system for extremely stable and low-cost broad-band signal transmission," *IEEE Trans. Microw Theory Tech.*, vol. 50, no. 6, pp. 1458-1468, Jun. 2002.
- [7] M. Marcus, and B. Pattan, "Millimeter wave propagation: spectrum management implications," *IEEE Microwave Mag.*, pp. 54-62, Jun. 2005.
- [8] J. M. Payne, and W. P. Shillue, "Photonic techniques for local oscillator generation and distribution in millimeter-wave radio astronomy," *International Topical Meeting on Microwave Photonics*, pp.9-12, Nov. 2002.
- [9] A. J. Seeds, "Microwave photonics," *IEEE Trans. Microw Theory Tech.*, vol. 50, no. 3, pp. 877-887, Mar. 2002.

- [10] H. Ogawa, D. Polifko, and S. Banda, "Millimeter-wave fiber optics systems for personal radio communication," *IEEE Trans. Microw Theory Tech.*, vol. 40, no. 12, pp. 2285-2293, Dec. 1992.
- [11] L. Noël, D. Wake, D. G. Moodie, D. D. Marcenac, L. D. Westbrook, and D. Nasset, "Novel technique for high-capacity 60 GHz fiber-radio transmission systems", *IEEE Trans. Microw Theory Tech.*, vol 45, no. 8, pp. 1416-1423, Aug. 1997.
- [12] G. H. Smith, D. Novak, and C. Lim, "A millimeter-wave full-duplex fiber-radio star-tree architecture incorporating WDM and SCM," *IEEE Photon. Technol. Lett.*, vol 10, no. 10, pp. 1650-1652, Nov. 1998.
- [13] H. Harada, K. Sato, and M. Fujise, "A Radio-on-Fiber based millimeter-wave road-vehicle communication system by a code division multiplexing radio transmission scheme," *IEEE Trans. Intell. Transp. Syst.*, vol. 2, no. 4, DEC. 2001, pp. 165-179.
- [14] R. Hofstetter, H. Schmuck, and R. Heidemann, "Dispersion effects in optical millimeter-wave systems using self-heterodyne method for transport and generation," *IEEE Trans. Microw Theory Tech.*, vol. 43, no. 9, pp. 2263-2269, Sep. 1995.
- [15] U. Gliese, S. Nørskov, and T. N. Nielsen, "Chromatic dispersion in fiber-optic microwave and millimeter-wave links," *IEEE Trans. Microw Theory Tech.*, vol. 44, no. 10, pp. 1716-1724, Oct. 1996.
- [16] H. Sotobayashi, and K. Kitayama, "Cancellation of the signal fading for 60 GHz subcarrier multiplexed optical DSB signal transmission in nondispersion shifted fiber using midway optical phase conjugation," *J. Lightwave Technol.*, vol. 17, no. 12, pp. 2488-2497, Dec. 1999.
- [17] F. Ramos, J. Marti, and V. Polo, "Compensation of chromatic dispersion effects in microwave/milimeter-wave optical systems using four-wave-mixing induced in dispersion-shifted fibers," *IEEE Photon. Technol. Lett.*, vol. 11, no. 9, pp. 1171-1173, Sep. 1999.
- [18] H. Ogawa, and Y. Kamiya, "Fiber-optical microwave transmission using harmonic laser mixing, optoelectronic mixing and optically pumped

- mixing,” *IEEE Trans. Microw Theory Tech.*, vol. 39, no. 12, pp. 2045-2051, Dec. 1991.
- [19] E. Suematsu, and N. Imai, “A fiber-optic/millimeter-wave radio transmission link using HBT as direct photodetector and an optoelectronic upconverter,” *IEEE Trans. Microw Theory Tech.*, vol. 44, no. 1, pp. 133-143, Jan. 1996.
- [20] C.-S. Choi, H.-S. Kang, W.-Y. Choi, D.-H. Kim, and K.-S. Seo, “Phototransistors based on InP HEMT and their applications to millimeter-wave radio-on-fiber systems,” *IEEE Trans. Microw Theory Tech.*, vol. 53, no. 1, pp. 256-263, Jan. 2005.
- [21] C.-S. Choi, J.-H. Seo, W.-Y. Choi, H. Kamitsuna, M. Ida, and K. Kurishima, “60GHz bidirectional radio-on-fiber links based on InP-InGaAs HPT optoelectronic mixers,” *IEEE Photon. Technol. Lett.*, vol. 17, no. 12, pp. 2721-2723, Dec. 2005.
- [22] G. H. Smith, D. Novak, and Z. Ahmed, “Overcoming chromatic-dispersion effects in fiber-wireless systems incorporating external modulators,” *IEEE Trans. Microw Theory Tech.*, vol. 45, no. 8, pp. 1410-1415, Aug. 1997.
- [23] M. Tsuchiya, and T. Hoshida, “Nonlinear photodetection scheme and its system applications to fiber-optic millimeter-wave wireless downlinks,” *IEEE Trans. Microw Theory Tech.*, vol. 47, no. 7, pp. 1342-1350, Jul. 1999.
- [24] M. Ogusu, K. Inagaki, Y. Mizuguchi, and T. Ohira, “Carrier generation and data transmission on millimeter-wave bands using two-mode locked fabry-perot slave lasers,” *IEEE Trans. Microw Theory Tech.*, vol. 51, no. 2, pp. 382-391, Feb. 2003.
- [25] L. Chao, C. Wenyue, and J. F. Shiang, “Photonic mixers and image-rejection mixers for optical SCM systems,” *IEEE Trans. Microw Theory Tech.*, vol. 45, no. 8, pp. 1478-1480, Aug. 1997.
- [26] J. Park, M. S. Shakouri, and K. Y. Lau, “Millimetre-wave electro-optical upconverter for wireless digital communications,” *Electron. Lett.*, vol. 31, no. 13, pp. 1085-1086, Jun. 1995.

- [27] Q. Z. Liu, R. Davies, and R. I. MacDonald, "Experimental investigation of fiber optic microwave link with monolithic integrated optoelectronic mixing receiver," *IEEE Trans. Microw Theory Tech.*, vol. 43, no. 9, pp. 2357-2360, Sep. 1995.
- [28] N. J. Frigo, P. P. Iannone, P. D. Magill, T. E. Darcie, M. M. Downs, B. N. Desai, U. Koren, T. L. Koch, C. Dragone, H. M. Presby, and G. E. Bodeep, "A wavelength-division multiplexed passive optical network with cost-shared components," *IEEE Photon. Technol. Lett.*, vol. 6, no. 11, pp. 1365-1367, Nov. 1994.
- [29] R. B. Welstand, S. A. Pappert, C. K. Sun, J. T. Zhu, Y. Z. Liu, and P. K. L. Yu, "Dual-function electroabsorption waveguide modulator/detector for optoelectronic transceiver applications," *IEEE Photon. Technol. Lett.*, vol. 8, no. 11, pp. 1540-1542, Nov. 1996.
- [30] W. S. C. Chang, "RF photonic technology in optical fiber links," Cambridge Univ. Press, 2002.
- [31] L. D. Westbrook, L. Noël, and D. G. Moodie, "Full-duplex, 25km analogue fibre transmission at 120Mbit/s with simultaneous modulation and detection in an electroabsorption modulator," *Electron. Lett.*, vol. 33, no. 8, pp. 694-695, Apr. 1997.
- [32] A. Stöhr, K. Kitayama, and D. Jäger, "Full-duplex fiber-optic RF subcarrier transmission using a dual-function modulator/photodetector," *IEEE Trans. Microw Theory Tech.*, vol. 47, no. 7, pp. 1338-1341, Jul. 1995.
- [33] C. Rolland, K. L. Prosyk, C. M. Maritan, and N. Puertz, "High speed and low loss, bulk electroabsorption waveguide modulators at 1.3  $\mu\text{m}$ ," *IEEE Photon. Technol. Lett.*, vol. 3, no. 10, pp. 894-896, Oct. 1991.
- [34] D. A. B. Miller, T. C. Damen, A. C. Gossard, W. Wiegmann, T. H. Wood, and C. A. Burus, "Band-edge electroabsorption in quantum well structures: the quantum-confined Stark effect," *Phys. Rev. Lett.*, vol. 53, no. 22, pp. 2173-2175, Nov. 1984.
- [35] Y.-K. Seo, C.-S. Choi, and W.-Y. Choi, "All optical signal up-conversion for Radio-on-Fiber applications using cross-gain modulation in

- semiconductor optical amplifiers,” *IEEE Photon. Tech. Lett.*, vol. 14, no. 10, pp. 1480-1450, Oct. 2002.
- [36] Y.-K. Seo, J.-H. Seo, and W.-Y. Choi, “Photonic frequency up-conversion efficiencies in semiconductor optical amplifiers,” *IEEE Photon. Tech. Lett.*, vol. 15, no. 5, pp. 751-753, May 2003.
- [37] L. E. Richter, H. I. Mandelberg, M. S. Kruger, and P. A. McGrath, “Linewidth determination from self-heterodyne measurements with subcoherence delay times,” *IEEE J. Quantum Electron.*, vol. 22, no. 11, pp. 2070-2074, Nov. 1986.
- [38] L. Goldberg, H. F. Taylor, J. F. Weller, and D. M. Bloom, “Microwave signal generation with injection-locked laser diodes,” *Electron. Lett.*, vol. 19, no. 13, pp. 491-493, 1983.
- [39] S. Fukushima, C. F. C. Silva, Y. Muramoto, and A. J. Seeds, “10 to 110 GHz tunable opto-electronic frequency synthesis using optical frequency comb generator and uni-traveling-carrier photodiode,” *Electron. Lett.*, vol. 37, no. 12, pp. 780-781, Jun. 2001.
- [40] L. N. Langley, M. D. Elkin, C. Edge, M. J. Wale, U. Gliese, X. Huang, and A. J. Seeds, “Packaged semiconductor laser optical phase-locked loop (OPLL) for photonic generation, processing and transmission of microwave signals,” *IEEE Trans. Microwave and Techniques*, vol. 47, no. 7, pp. 1257-1264, 1999.
- [41] A. C. Bordonalli, B. Cai, A. J. Seeds, and P. J. Williams, “Generation of microwave signals by active mode locking in a gain bandwidth restricted laser structure,” *IEEE Photon. Tech. Lett.*, vol. 8, no. 1, pp. 151-153, Jan. 1996.
- [42] J. O’Reilly and P. Lane, “Remote delivery of video services using mm-waves and optics,” *J. Lightwave Technol.*, vol. 12, no. 2, pp. 369-375, Feb. 1994.
- [43] R. A. Griffin, P. M. Lane, and J. J. O’Reilly, “Dispersion-tolerant subcarrier data modulation of optical millimeter-wave signals,” *Electron. Lett.*, vol. 32, no. 24, pp. 2258-2260, Nov. 1996.

- [44] J. J. O'Reilly, P. M. Lane, M. H. Capstick, H. M. Salgado, R. Heidemann, R. Hofstetter, and H. Schmuck, "RACE R2005: microwave optical duplex antenna link," *J. IEE Proc.*, vol. 140, no. 6, pp. 385-391, Jun. 1993.
- [45] M. J. Connelly, "Semiconductor optical amplifiers," *Kluwer Academic Publishers*, 2002.
- [46] H. Ghafouri-Shiraz, "Fundamentals of laser diode amplifiers," *John Wiley & Sons*, 1996.
- [47] T. Durhuus, B. Mikkelsen, C. Joergensen, and K. E. Stubkjaer, "All-optical wavelength conversion by semiconductor optical amplifiers," *J. Lightwave Technol.*, vol. 14, no. 6, pp. 942-964, Jun. 1996.
- [48] M. Asghari, I. H. White, and R. V. Penty, "Wavelength conversion using semiconductor optical amplifiers," *J. Lightwave Technol.*, vol. 15, no. 7, pp. 1181-1190, Jul. 1997.
- [49] J.-H. Seo, Y.-K. Seo, and W.-Y. Choi, "Spurious-free dynamic range characteristics of the photonic up-converter based on a semiconductor optical amplifier," *IEEE Photon. Technol. Lett.*, vol. 15, no. 11, pp. 1591-1593, Nov. 2003.
- [50] H. Lee, H. Yoon, Y. Kim, and J. Jeong, "Theoretical study of frequency chirping and extinction ratio of wavelength-converted optical signals by XGM and XPM using SOA's," *IEEE J. Quantum Electron.*, vol. 35, no. 8, pp. 1213-1219, Aug. 1999.
- [51] T. Durhuus, B. Mikkelsen, and K. E. Stubkjaer, "Detailed dynamic model for semiconductor optical amplifiers and their crosstalk and intermodulation distortion," *J. Lightwave Technol.*, vol. 10, no. 8, pp. 1056-1065, Aug. 1992.
- [52] P. J. Annetts, M. Asghari, and I. H. White, "The effect of carrier transport on the dynamic performance of gain-saturation wavelength conversion in MQW semiconductor optical amplifier," *IEEE J. Select. Topics Quantum Electron.*, vol. 3, no. 4, pp. 320-329, Apr. 1997.

- [53] G. P. Agrawal and N. A. Olsson, "Self-phase modulation and spectral broadening of optical pulses in semiconductor laser amplifiers," *IEEE J. Quantum Electron.*, vol. 25, no. 11, pp. 2297-2306, Nov. 1989.
- [54] L. M. Zhang, S. F. Yu, M. C. Nowell, D. D. Marcenac, J. E. Carroll, and R. G. S. Plumb, "Dynamic analysis of radiation and side-mode suppression in a second-order DFB laser using time-domain large-signal traveling wave model," *IEEE J. Quantum Electron.*, vol. 30, no. 6, pp. 1389-1395, Jun. 1994.
- [55] A. E. Willner and W. Shieh, "Optimal spectral and power parameters for all optical wavelength shifting: single stage, fanout, and cascability," *J. Lightwave Technol.*, vol. 13, no. 5, pp. 771-781, May 1995.
- [56] G. P. Agrawal and N. K. Dutta, "Semiconductor lasers," *Van Nostrand Reinhold*, 1993.
- [57] J. Yao, G. Maury, Y. L. Guennec, and B. Cabon, "All-optical subcarrier frequency conversion using an electrooptic phase modulator," *IEEE Photon. Tech. Lett.*, vol. 17, no. 11, pp. 2427-2429, Nov. 2005.
- [58] Z. Jia, J. Yu, and G.-K. Chang, "All-optical 16×2.5 Gb/s WDM signal simultaneous up-conversion based on XPM in an MOLM in ROF systems," *IEEE Photon. Tech. Lett.*, vol. 17, no. 12, pp. 2724-2726, Dec. 2005.
- [59] P. N. Freeman, N. K. Dutta, and J. Lopata, "Semiconductor optical amplifier for wavelength conversion in subcarrier multiplexed systems," *IEEE Photon. Tech. Lett.*, vol. 9, no. 1, pp. 46-48, Jan. 1997.
- [60] D. Marcenac, and A. Mecozzi, "Switches and frequency converters based on cross-gain modulation in semiconductor optical amplifiers," *IEEE Photon. Tech. Lett.*, vol. 9, no. 6, pp. 749-751, Jun. 1997.
- [61] D. S. Shin, G. L. Li, C. K. Sun, S. A. Pappert, K. K. Loi, W. S. C. Chang, and P. K. L. Yu, "Optoelectronic RF Signal Mixing Using an Electroabsorption Waveguide as an Integrated Photodetector/Mixer," *IEEE Photon. Technol., Lett.*, vol. 12, no. 2, pp. 193-195, 2000.
- [62] K. Kitayama, A. Stöhr, T. Kuri, R. Heinzelmann, D. Jäger, and Y. Takahashi, "An approach to single optical component antenna base

- stations for broad-band millimeter-wave fiber-radio access systems,” *Trans. Microw Theory Tech.*, vol. 48, no. 12, pp. 2588-2595, Dec. 2000.
- [63] K. Kitayama, and R. A. Griffin, “Optical Downconversion from Millimeter-Wave to IF-Band Over 50-km-Long Optical Fiber Link Using an Electroabsorption Modulator,” *IEEE Photon. Technol. Lett.*, vol. 11, no. 2, pp. 287-289, Feb. 1999.
- [64] T. Kuri, K. Kitayama, and Y. Ogawa, “Fiber-Optic Millimeter-Wave Uplink System Incorporating Remotely Fed 60-GHz-Band Optical Pilot Tone”, *IEEE Trans. Microwave Theory Tech.*, vol. 47, no. 7, pp. 1332-1337, 1999.
- [65] D. A. B. Miller, D. S. Chemla, T. C. Damen, A. C. Gossard, W. Wiegmann, T. H. Wood, and C. A. Burrus, “Electrical field dependence of optical absorption near the band gap of quantum-well structures,” *Phys. Rev. Lett. B*, vol. 32, no. 2, pp. 1043-1060, Jul. 1985.
- [66] M. K. Chin, “A simple method using photocurrent and power transmission for measuring the absorption coefficient in electroabsorption modulators,” *IEEE Photon. Technol. Lett.*, vol. 4, no. 8, pp. 866-869, Aug. 1992.
- [67] J. Lim, Y.-S. Kang, K.-S. Choi, J.-H. Lee, S.-B. Kim, and J. Kim, “Analysis and characterization of traveling-wave electrode in electroabsorption modulator for radio-on-fiber application”, *J. Lightwave Technol.*, vol. 21, no. 12, pp. 3004-3010, Dec. 2003.
- [68] J. Kim, Y.-S. Kang, Y.-D. Chung, and K.-S. Choi, “Development and RF characteristics of analog 60-GHz electroabsorption modulator module for RF/optical conversion,” *IEEE Trans. Microwave Theory Tech.*, vol. 54, no. 2, pp. 780-787, 2006.
- [69] J.-H. Seo, C.-S. Choi, W.-Y. Choi, Y.-S. Kang, Y.-D. Chung, and J. Kim, “Remote optoelectronic frequency down-conversion using 60 GHz optical heterodyne signals and electroabsorption modulator”, accepted for publication in *IEEE Photon. Technol. Lett.* vol. 17, no. 5, May 2005.
- [70] D. M. Pozar, “Microwave and RF design of wireless systems,” *John Wiley and Sons, Inc.* 2001.

- [71] Agilent Technologies, "Testing and troubleshooting digital RF communications receiver design," *Application Note* 1314.
- [72] J.-H. Seo, C.-S. Choi, Y.-S. Kang, Y.-D. Chung, J. Kim, and W.-Y. Choi, "SOA-EAM frequency up/down-converters for 60-GHz bi-directional radio-on-fiber systems," *IEEE Trans. Microwave Theory Tech.*, vol. 54, no. 2, pp. 959-966, 2006.
- [73] K. Asaka, Y. Suzuki, Y. Kawaguchi, S. Kondo, Y. Noguchi, H. Okamoto, R. Iga, and S. Oku, "Lossless electroabsorption modulator monolithically integrated with a semiconductor optical amplifier and a passive waveguide," *IEEE Photon. Technol. Lett.*, vol. 15, no. 5, May 2003.
- [74] J. G. Proakis, "Digital Communications," *McGraw-Hill*, fourth edition, 2001.

## Publication Lists

### *International Journals*

- [1] **Jun-Hyuk Seo**, Young-Kwang Seo, Woo-Young Choi, "1.244Gbps data distribution in 60GHz remote optical frequency up-conversion systems," accepted for publication in *IEEE Photonics Technology Letters*.
- [2] **Jun-Hyuk Seo**, Chang-Soon Choi, Woo-Young Choi, Young-Shik Kang, Yong-Duk Jung, and Jeha Kim, "SOA-EAM frequency up/down-converters for 60-GHz bi-directional Radio-on-Fiber systems," *IEEE Transactions on Microwave Theory and Techniques*, vol. 4, no. 2, pp. 959-966, Feb. 2006.
- [3] Chang-Soon Choi, **Jun-Hyuk Seo**, Woo-Young, Choi, Hideki Kamitsuna, Minoru Ida, and Kenji Kurishima, "60GHz bidirectional Radio-on-Fiber links based on InP-InGaAs HPT optoelectronic mixers," *IEEE Photonics Technology Letters*, vol. 17, no. 12, pp. 2721-2723, Dec. 2005.
- [4] **Jun-Hyuk Seo**, Chang-Soon Choi, Woo-Young Choi, Young-Shik Kang, Yong-Duk Jung, and Jeha Kim, "Remote Optoelectronic Frequency Down-Conversion using 60 GHz Optical Heterodyne Signals and an Electroabsorption Modulator," *IEEE Photonics Technology Letters*, vol. 17, no. 5, pp. 1073-1075, May 2005.
- [5] **Jun-Hyuk Seo**, Young-Kwnag Seo, and Woo-Young Choi, "Spurious Free Dynamic Range Characteristics of the Photonic Up-Converter Based on a Semiconductor Optical Amplifier," *IEEE Photonics Technology Letters*, vol. 15, no. 11, Nov. 2003.
- [6] Young-Kwang Seo, **Jun-Hyuk Seo**, and Woo-Young Choi, "60-GHz Radio-On-Fiber Distribution of 2 x 622 Mb/s WDM Channels Using Remote Photonic-Frequency Upconversion," *Microwave and Optical Technology Letter*, vol. 39, no. 3, pp. 201-203, Nov. 2003.
- [7] Young-Kwang Seo, **Jun-Hyuk Seo**, and Woo-Young Choi, "Photonic Frequency-Upconversion Efficiencies in Semiconductor

Optical Amplifiers," *IEEE Photonics Technology Letters*, vol. 15, no. 5, pp. 751-753, May 2003.

[8] **Jun-Hyuk Seo**, Young-Kwang Seo, and Woo-Young Choi, "Nonlinear Distortion Suppression in Directly Modulated Distributed Feedback Lasers by Sidemode Optical Injection Locking," *Japanese Journal of Applied Physics*, vol.41, no.2A, pp. L136-L138, Feb. 2002.

### ***International Conferences***

[1] **Jun-Hyuk Seo**, and Woo-Young Choi, "Gigabit transmission in 60-GHz-band using optical frequency up-conversion by semiconductor optical amplifier and photodiode configuration," accepted for publication in *IEEE International Microwave Symposium*, 2006.

[2] Jae-Young Kim, **Jun-Hyuk Seo**, Woo-Young Choi, Hideki Kamitsuna, Minoru Ida, and Kenji Kurishima, "60GHz Radio-on-Fiber systems using optically injection-locked self oscillating optoelectronic mixers based on InP/InGaAs HPTs," *Conference on Optical Fiber Communications*, OWG6, 2006.

[3] **Jun-Hyuk Seo**, Chang-Soon Choi, Woo-Young Choi, Young-Shik Kang, Yong-Duk Jung, and Jeha Kim, "Conversion efficiency of EAM optoelectronic frequency down-converters," *General Assembly of International Union of Radio Science*, pp. 23-29, 2005.

[4] **Jun-Hyuk Seo**, Chang-Soon Choi, Woo-Young Choi, Young-Shik Kang, Yong-Duk Jung, and Jeha Kim, "Conversion efficiency characteristics of cascaded SOA-EAM frequency up/down-converters," *IEEE International Topical Meeting on Microwave Photonics*, pp. 107-110, 2005.

[5] Chang-Soon Choi, **Jun-Hyuk Seo**, Woo-Young, Choi, Hideki Kamitsuna, Minoru Ida, and Kenji Kurishima, "Radio-on-fiber downlink transmission systems based on optically controlled InP/InGaAs HPT oscillators," *IEEE International Topical Meeting on Microwave Photonics*, pp. 333-336, 2005.

- [6] **Jun-Hyuk Seo**, Chang-Soon Choi, Woo-Young Choi, Young-Shik Kang, Yong-Duk Jung, and Jeha Kim, "Bi-directional 60 GHz Radio-on-Fiber Systems using Cascaded SOA-EAM Frequency Up/Down-converters," *IEEE International Microwave Symposium*, pp. 3-6, 2005.
- [7] Chang-Soon Choi, **Jun-Hyuk Seo**, Woo-Young Choi, Hideki Kamitsuna, Minoru Ida, and Kenji Kurishima, "Radio-on-fiber downlink transmission systems based on optically controlled InP/InGaAs HPT oscillators," *IEEE International Microwave Symposium*, pp. 11-14, 2005.
- [8] **Jun-Hyuk Seo**, Chang-Soon Choi, Woo-Young Choi, Young-Shik Kang, Yong-Duck Chung, and Jeha Kim, "Cascaded SOA-EAM configuration for millimeter-wave frequency up/down-conversion," *The 8<sup>th</sup> Korea-Japan Joint Workshop on Microwave and Millimeter-wave Photonics*, pp. 35-38, 2005.
- [9] Chang-Soon Choi, **Jun-Hyuk Seo**, Dae-Hyun Kim, Kwang-Seok Seo, and Woo-Young Choi, "Radio-on-fiber downlink systems based on InP HEMT oscillators," *8<sup>th</sup> International Topical Workshop on Contemporary Photonic Technologies*, pp. 72-73, 2005.
- [10] **Jun-Hyuk Seo**, Chang-Soon Choi, Woo-Young Choi, Young-Shik Kang, Yong-Duk Jung, and Jeha Kim, "Frequency Conversion with Cascaded SOA-EAM for Bi-directional Radio-on-Fiber Systems," *IEEE International Topical Meeting on Microwave Photonics*, pp. 56-59, 2004
- [11] **Jun-Hyuk Seo**, Young-Kwang Seo, and Woo-Young Choi, "Nonlinear Characteristics of an SOA Photonic Frequency Up-Converter," *IEEE International Topical Meeting on Microwave Photonics*, pp.109-112, 2003.
- [12] Young-Kwang Seo, **Jun-Hyuk Seo**, Chang-Soon Choi and Woo-Young Choi, "WDM/Radio-on-Fiber Distribution Using Remote Photonic Frequency-Upconversion," *6<sup>th</sup> Int. Symposium on Contemporary Photonics Technology*, pp. 115-116, 2003.
- [13] Young-Kwang Seo, **Jun-Hyuk Seo**, Chang-Soon Choi, and Woo-Young Choi, "Remote Photonic Frequency-Upconversion using a

Semiconductor Optical Amplifier for WDM /Broadband Radio-on-Fiber Links," *The 4th Korea-Japan Joint Workshop on Microwave-Photonics*, pp. 201-205, 2003.

[14] Young-Kwang Seo, **Jun-Hyuk Seo**, and Woo-Young Choi, "All-Optical Frequency Up-conversion Using a Semiconductor Optical Amplifier," *IEEE International Topical Meeting on Microwave Photonics*, pp.117-120, 2002.

[15] Woo-Young Choi, Ki-Hyuk Lee, Hyun-Yong Choi, and **Jun-Hyuk Seo**, "Analysis and Suppression of Dynamic Nonlinear Distortions in Semiconductor Laser Diodes (Invited Paper)," *5<sup>th</sup> International Symposium on Contemporary Photonics Technology*, pp. 151-154, 2002.

[16] Young-Kwang Seo, **Jun-Hyuk Seo**, and Woo-Young Choi, "Enhancement of Locking Bandwidth in DFB Lasers by Side-Mode Injection-Locking," *OECC/IIOC 2001 Conference Incorporating ACOFT*, pp. 547-548, 2001.

[17] **Jun-Hyuk Seo**, Young-Kwang Seo, and Woo-Young Choi, "Nonlinear Distortion Suppression in Directly Modulated DFB Lasers by Sidemode Optical Injection," *IEEE International Microwave Symposium*, pp. 555-558, 2001.

[18] **Jun-Hyuk Seo**, Young-Kwang Seo and Woo-Young Choi, "Nonlinear Distortion Suppression in Directly Modulated DFB-LDs by Sidemode Optical Injection," *The 2<sup>nd</sup> Korea-Japan Joint Workshop on Microwave-Photonics*, pp. 59-62, 2001.

### ***Domestic Journals***

[1] **서준혁**, 최우영, "Microwave Photonics 연구실," *광학과 기술*, vol. 7, no. 4, pp.53-62, Oct. 2003.

[2] **서준혁**, 최우영, "헤테로다인 기법을 이용한 광 밀리미터파 신호 생성," *광학과 기술*, pp. 5-11, Jan. 2001.

## *Domestic Conferences*

- [1] 김재영, 서준혁, 최우영, Hideki Kamitsuna, Minoru Ida, and Kenji Kurishima, "InP HPT 기반 OIL-SOM 의 광전 주파수 상향변환 특성," *Photonics Conference*, pp. 15-16, 2005.
- [2] 서준혁, 최창순, 강영식, 정용덕, 김제하, 최우영, "Bi-directional millimeter-wave radio-on-fiber systems using SOA-EAM frequency converters," *광전자 및 광통신 학술회의*, vol. 12, no. 1, pp. 35-36, 2005.
- [3] 서준혁, 최창순, 최우영, 강영식, 정용덕, 김제하, "60GHz Uplink Radio-on-Fiber Systems using Frequency Down-Conversion of Electroabsorption Modulator," *Photonics Conference*, T2B4, 2004.
- [4] 안정환, 서영광, 서준혁, 최우영, "SOA 광학적 주파수 상향 변환기를 사용한 155Mbps 급 Radio-on-Fiber 시스템의 Bit Error Rate 특성," *광전자 및 광통신 학술회의*, pp.261-262, 2004.
- [5] 서준혁, 최창순, 최우영, 강영식, 정용덕, 김제하, "전계흡수 변조기를 이용한 광학적 주파수 상/하향 변환기," *광전자 및 광통신 학술회의*, pp.237-238, 2004.
- [6] 서준혁, 최우영, "Radio over fiber technology," *한국통신학회 하계종합학술발표회*, 2004.
- [7] 박성권, 서준혁, 서영광, 최우영, "SCM 신호의 SOA-XGM 파장변환에서의 상호변조왜곡 분석," *Photonics Conference*, pp.743-745, 2003.
- [8] 서준혁, 서영광, 최우영, "반도체 광 증폭기를 이용한 광학적 주파수 상향 변환기의 비선형 특성," *광전자 및 광통신 학술회의*, pp. 453-454, 2003.
- [9] 최창순, 강효순, 서영광, 서준혁, 최우영, 장경철, 김대현, 서광석, "60GHz Broadband Up-conversion using Metamorphic HEMT as a Harmonic Optoelectronic Mixer," *Photonics Conference*, pp. 83-84, 2002.

- [10] **서준혁**, 서영광, 최우영, "SOA 의 XGM 을 이용한 광학적 주파수 상향 변환 방법의 변환 효율 분석," *Photonics Conference*, pp. 227-228, 2002.
- [11] 서영광, **서준혁**, 최창순, 최우영, "Remote Photonic Frequency-Upconversion 을 이용한 WDM/Radio-on-Fiber Distribution," *Photonics Conference*, pp. 569-560, 2002.
- [12] **서준혁**, 서영광, 최창순, 최우영, "반도체 광 증폭기의 상호 이득 변조를 이용한 전광 주파수 상향 변환," *광전자 및 광통신 학술회의*, pp. 269-270, 2002.
- [13] 최우영, 이기혁, **서준혁**, "반도체 레이저의 비선형성 분석 (Analysis and Suppression of Dynamic Nonlinear Distortions in Semiconductor Laser Diodes) (Invited Paper)," *한국광학회 제 13 회 정기총회 및 동계학술발표회*, pp. 8-9, 2002.
- [14] **서준혁**, 최우영, "Optically Injection Locked 된 DFB 레이저에서 왜곡 성분 감소의 광 주입 파장 의존성," *Photonics Conference*, pp. 385-386, 2001.
- [15] **서준혁**, 서영광, 최우영, "Sidemode Optical Injection 을 이용한 직접 변조된 DFB 레이저의 Second Harmonic Distortion 의 억제," *Photonics Conference*, pp. 443-444, 2000.

## **Patents**

- [1] 최우영, 최창순, **서준혁**, 김재영, "광 검출 트랜지스터를 구비한 ROF 시스템/Radio on fiber system with photo detection transistor," 특허 출원번호 10-2006-0025937 호, 출원일: 2006.03.22.
- [2] **서준혁**, 최창순, 최우영, "양방향 광섬유기반 무선전송 시스템용 주파수 변환방법 및 장치/Frequency converting method and apparatus for bi-directional radio-on-fiber systems," 특허 출원번호 10-2004-0092391 호, 출원일 2004.11.12.

## *Awards*

[1] **우수 논문상: 서준혁**, 최창순, 강영식, 정용덕, 김제하, 최우영, "SOA-EAM 주파수 변환기를 이용한 양방향 밀리미터파 Radio-on-Fiber 시스템," 제 12 회 광전자 및 광통신 학술회의, 2005, 대구 EXCO.

[2] **First Place, Open Forum Presentations: Jun-Hyuk Seo** "Frequency Conversion with Cascaded SOA-EAM for Bi-directional Radio-on-Fiber Systems" *IEEE International Topical Meeting on Microwave Photonics* 2004, Ogunquit, Maine, USA.

[3] **우수 논문상: 서준혁**, 최우영, "Optically Injection Locked 된 DFB 레이저에서 왜곡 성분 감소의 광 주입 파장 의존성," *Photonics Conference* 2001, 설악한화리조트.